Title
Molecular Evolution of Adeno-associated Virus for Improved Retinal Gene Therapies

Author
Klimczak, Ryan Raymond

Publication Date
2010

Peer reviewed|Thesis/dissertation

Molecular Evolution of Adeno-associated Virus for Improved Retinal Gene Therapies

By

Ryan Raymond Klimczak

Dissertation submitted in partial fulfillment of the requirements for the degree of

Doctor of Philosophy

in

Molecular and Cell Biology

in the Graduate Division

of

University of California, Berkeley

Committee in charge:

Professor John G. Flannery, Chair
Professor David V. Schaffer
Professor Lu Chen
Professor Kristin Scott

Spring 2010

Abstract

Molecular Evolution of Adeno-associated Virus for Improved Retinal Gene Therapies

By

Ryan Raymond Klimczak

Doctor of Philosophy in Molecular and Cell Biology

University of California, Berkeley

Professor John Flannery, Chair

Current retinal gene therapies using adeno-associated viral (AAV) vectors are limited in their efficacy due to their dependence on an invasive subretinal delivery route to achieve sufficient gene delivery. Additionally, the genetic heterogeneity of inherited retinal degenerative diseases makes gene replacement and antisense therapeutic strategies impractical for treating a broad array of patients. This dissertation sought to address these limitations by creating intravitreally-permissive AAV vectors through directed evolution and examining their therapeutic potential using a mutation-independent approach.

Firstly, we examined natural barriers to intravitreal vector delivery. We identified the inner limiting membrane (ILM) as the main obstacle to efficient intravitreal gene delivery and found mild digestion with a nonspecific protease, Pronase E, substantially enhanced retinal transduction for several AAV serotypes, most notably for AAV serotype 5 (AAV5). Secondly, we evolved more efficient glial-permissive AAV vectors in the CNS and retina using an *in vitro* selection methodology. We isolated an AAV variant, ShH10, closely related to AAV6, capable of efficient, selective Müller cell infection through intravitreal injection. Thirdly, we utilized this variant to examine the efficacy of intravitreally targeting Müller cells to secrete glial-derived neurotrophic factor (GDNF) as a mutation-independent therapy for delaying photoreceptor degeneration in a rat model of retinitis pigmentosa (RP). We achieved functional and histological rescue in treated animals at five months post injection, with an average approximate rescue of 50% in ERG a and b-wave amplitudes. Lastly, we evolved AAV variants to intravitreally transduce photoreceptors using an *in vivo* selection approach in a transgenic line of mice bearing a rhodopsin-GFP fusion. We isolated an AAV variant, 7M8, derived from an AAV2 peptide display library, capable of significant intravitreal photoreceptor transduction relative to AAV2.

The creation of intravitreally-permissive AAV vectors as well as the development of mutation-independent gene therapies will enable safer and more effective therapies for treating inherited retinal degenerative diseases.

To the memory of my mother, Rhonda Klimczak, whose influence on me will reverberate throughout my life. She instilled in me the passion to learn, the tenacity to never give up, and the inspiration to pursue my dreams.

Acknowledgements

I would first like to thank my advisors, John Flannery and Dave Schaffer, for their scientific guidance, encouragement, and support. This dissertation would not have been possible without their mentorship. Their enthusiasm and passion for science was as motivating as it was inspiring and I am extremely fortunate to have been given the opportunity to collaborate between their labs.

I would also like to express my gratitude to my colleague and collaborator, Deniz Dalkara, whose persistance, patience, and hard work was truly indispensable in my research. Additionally, I would like to thank my collaborator, JT Koerber, for training me in all things related to AAV as well as my thesis committee for their guidance. Thank you to my lab mates Kate Kolstand, Karen Guerin, Meike Visel, Leah Byrne, and Kwang-il Lim, as well as undergraduate students Joshua Loya, Natalie Hoffman, and Christin Hong, for their assistance and friendship throughout my graduate work.

To the great friends I have made while living in Bay Area these past years, as well friends from old, I thank you for your support and good humor, without which I surely wouldn't be where I am today. I especially would like to thank my family: my mother and father Rhonda and Robert Klimczak, and my brothers Wesley and Dustin, for being there with me through it all.

Table of Contents

Abstract 1

Acknowledgements ii

Table of Contents iii

List of Figures and Tables v

Chapter 1. Introduction 2

Chapter 2. Inner Limiting Membrane Barriers to AAV-mediated Retinal Transduction From the Vitreous 12

Abstract 12

Introduction 13

Experimental Methods 14

Results 17

Discussion 27

Chapter 3. Directed Evolution of Glial-permissive AAV Variants 30

Chapter 3a. Molecular Evolution of Adeno-associated Virus for Enhanced Glial Gene Delivery 30

Abstract 30

Introduction 31

Experimental Methods 32

Results 34

Discussion 42

Chapter 3b. A Novel Adeno-associated Viral Variant for Efficient and Selective Intravitreal Transduction of Müller Cells 45

Abstract 45

Introduction....46

Experimental Methods....49

Results....50

Discussion....59

Chapter 4. Selective Secretion of hGDNF from Müller Cells via AAV-mediated Intravitreal Gene Delivery Leads to Functional Rescue in a Rat Model of Retinitis Pigmentosa 62

Abstract....62

Introduction....63

Experimental Methods....64

Results....67

Discussion....73

Chapter 5. Molecular Evolution of Adeno-associated Virus for Enhanced Intravitreal Photoreceptor Transduction 75

Abstract....75

Introduction....76

Experimental Methods....77

Results....79

Discussion....86

Chapter 6. Concluding Remarks....88

References....90

Supplementary Material....102

Figure and Table Legend

Chapter 1

Figure 1.1.....3

Figure 1.2.....4

Figure 1.3.....5

Figure 1.4.....10

Chapter 2

Figure 2.1.....17

Figure 2.2.....19

Figure 2.3.....20

Figure 2.4.....20

Figure 2.5.....21

Figure 2.6.....22

Figure 2.7.....24

Figure 2.8.....25

Figure 2.9.....26

Figure 2.10.....28

Chapter 3a

Figure 3a.1.....35

Figure 3a.2.....36

Table 3a.1.....37

Figure 3a.3.....38

Figure 3a.4.....40

Figure 3a.5.....41

Chapter 3b

Figure 3b.1.....48

Figure 3b.2.....52

Figure 3b.3.....53

Figure 3b.4.....54

Figure 3b.5.....55

Figure 3b.6.....56

Figure 3b.7.....57

Figure 3b.8.....58

Figure 3b.9.....59

Chapter 4

Figure 4.1.....67

Figure 4.2.....69

Figure 4.3.....70

Figure 4.4.....71

Figure 4.5.....72

Figure 4.6.....73

Chapter 5

Figure 5.1.....79

Table 5.1.....80

Figure 5.2.....80

Figure 5.3.....81

Figure 5.4.....82

Figure 5.5.....83

Figure 5.6.....84

Figure 5.7.....85

Figure 5.8.....85

Supplemental Material

Figure 3a.S1.....102

Figure 3a.S2.....104

Figure 3a.S3.....105

Figure 3a.S4.....105

Table 3a.S1.....106

Figure 3b.S1.....107

Chapter 1

Introduction

The Retina:

The retina is a thin, highly metabolically active layer of neurons and glia in the back of the eye. This tissue is the first in line in processing visual information, consisting of three main, stratified layers of neurons: the outer nuclear layer (ONL) composed of rod and cone photoreceptors, the inner nuclear layer composed of secondary neurons such as horizontal, bipolar, and amacrine cells, and the retinal ganglion cell (RGC) layer which sends axonal projections to the lateral geniculate nucleus for further cortical processing (Figure 1.1). The retinal pigment epithelium (RPE) is located above the ONL, overlying the outer segments of the photoreceptors. Amongst the supportive functions of these cells, some of their primary roles consist in phagocytosing the outer segment discs of photoreceptors as well as isomerizing all trans retinol to 11-cis retinal for phototransduction [1].

The simple architecture of the retina belies the complexity of the neuronal circuitry underlying visual processing. There are approximately 120 million rod cells and 6 million cone cells in the human retina, whereas there are about 1.3 million ganglion cells, denoting an overall level of convergence in signal processing [2]. At its fundamental level, photons entering the eye activate rhodopsin or iodopsin in the outer segment of the retina, causing the isomerization of retinal within the protein from a cis-form to a trans-form. The subsequent phototransduction signaling cascade results in the hyperpolarization of the photoreceptor cell membrane, triggering a reduction in the release of glutamate to postsynaptic bipolar cells [3]. However, bipolar cells may in turn depolarize (ON) or hyperpolarize (OFF) in response to the cessation of glutamate release, dependent upon whether they bear metabotropic or ionotropic receptors respectively.

These ON-center and OFF-center pathways are essential for analyzing rudimentary, but critical visual information such as contrast and edges. Horizontal cell processes in the outer plexiform layer help to mediate this phenomenon through lateral inhibition via connections with multiple photoreceptors. Amacrine cells located in the inner nuclear layer (INL) are thought to contribute in a similar fashion to center-surround circuitry through feedback at the bipolar and ganglion cell level in the inner plexiform layer (IPL). With at least 3 different types of horizontal cells [4], 11 different types of bipolar cells [5], 40 different types of amacrine cells [6], and 25 different types of RGCs currently identified in the human retina [7], the complexity of retinal processing and visual information segmentation becomes immediately apparent.

Apart from neurons, the retina is populated by three main types of glial cells: microglia, retinal astrocytes, and Müller cells. Microglia are of mesodermal origin and can engage in phagocytosis in the retina, commonly during conditions of retinal degeneration or trauma [8]. Retinal astrocytes are mainly localized to the nerve fiber layer of the retina, enveloping RGC axons and vasculature and forming part of the retinal

blood-brain barrier as well as serving other supportive functional roles similar to those played by astrocytes in the brain [9]. Müller glial cells are the most numerous and largest glial cell type in the retina, spanning the entire thickness of the tissue from the vitreous to the ONL. Like astrocytes in the central nervous system (CNS), they also assume a structural and supportive role in the retina, such as maintaining ionic homeostasis in the extracellular space and providing metabolic support to adjacent neurons [10]. Intriguingly, Müller cells have also been found to dedifferentiate into multipotent progenitor cells following retinal injury, supporting the hypothesis that they may have stem cell like qualities in the retina which may enable them to be used to generate new photoreceptors in degenerated retina [11]. Recent research has also implicated them as conduits for light transmission across the opaque retina, acting as optical fibers that may internally refract photons to rods and cones in the back of the eye [12].

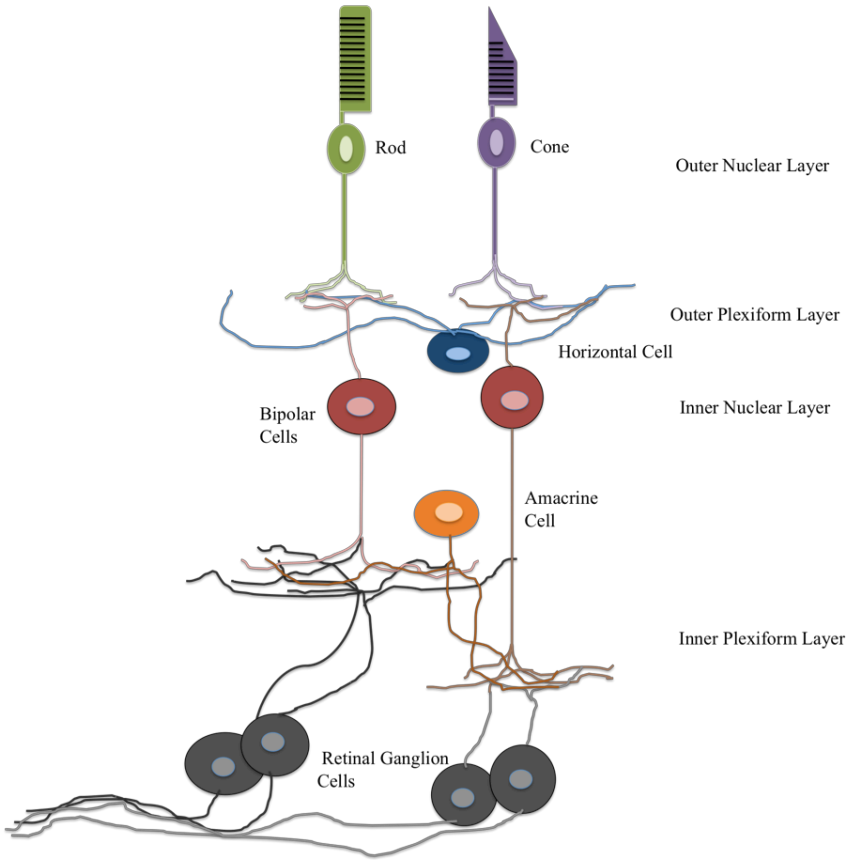

Figure 1.1 Diagram of the main retinal strata [13]. Photoreceptors in the ONL synapse onto bipolar cells and horizontal cells in the outer plexiform layer (OPL). In turn, bipolar cells synapse onto amacrine cells and retinal ganglion cells.

Retinal Degenerative Diseases:

The high metabolic activity of the retina lends itself to a greater vulnerability to neurodegeneration, as illustrated by the ubiquity of aquired and inherited retinal diseases.

The World Health Organization estimates that approximately 314 million individuals are visually impaired worldwide, while 45 million of them suffer from blindness.

In the United States, lifestyle diseases have become a major contributor to visual loss. Conditions such as hypertension can damage retinal blood vessels and cause them to thicken and leak, resulting in hypertensive retinopathy and decreases in vision. This retinal vasculature leakage can be even more severe in patients suffering from diabetic retinopathy. In the early, non-proliferative stages of this condition, high levels of blood sugar damage the microvasculature of the eye, compromising the blood-brain barrier and potentially leading to the development of macular edema [14, 15]. Ischemic conditions in latter stages of the disease can result in the proliferation of microvasculature as well as hemorrhaging that can occlude vision and ultimately destroy retinal tissue (Figure 1.2).

Figure 1.2 Simulation of major eye diseases (courtesy of the National Eye Institute, NIH -http://www.nei.nih.gov).

Glaucoma is another leading cause of blindness, often associated with increased pressure in the aqueous humor of the eye. The result of this increased pressure can lead to progressive loss of RGCs and subsequent damage to the optic nerve [16]. Individuals with familial histories of glaucoma are statistically more likely to suffer from this condition, although no clear underlying genetic cause has been attributed to this disease. On the other hand, studies have associated a sizeable genetic component to age-related macular degeneration (AMD) [17, 18]. This retinal degenerative condition leads to loss of vision in the center of the visual field and occurs in two varieties, a dry form and a wet form. In the dry form, cellular debris accumulates between the RPE and the choroid, called drusen, causing retinal detachement and subsequent atrophy of the RPE. This can result in photoreceptor cell loss in the macula. In the more severe wet form of AMD, choroidal neovascularization results in the disruption of Bruch's membrane and the leakage of blood and proteins below the macula, causing severe loss of vision. Amongst the genes associated with the development of AMD, loss of function mutations in the genes for the complement system proteins factor H (CFH), factor B (CFB), and factor 3 (C3) have been strongly implicated in the disease due to consequent increases in the inflammatory response within the macula [19]. Besides its high prevalence in older individuals, with up to 30% of individuals between 75 to 85 years of age having macular degeneration, there is also a strong familial correlation, with a four-fold higher risk for individuals with AMD-afflicted relatives [17].

One of the most common inherited retinal degenerative diseases is retinitis pigmentosa (RP), characterized by the progressive loss of rod cells in the retina. RP generally causes preliminary symptoms of night blindness, followed by a progressive narrowing of the field of vision leading to tunnel vision and potentially complete blindness in the final stages of the disease (Figure 1.2). The progression and severity of RP is largely dictated by the underlying causal mutations. To date, over 50 genes have been implicated in the disease [20, 21]. In the opsin gene alone, there have been more than a hundred different mutations identified as being associated with RP. A predominant cause of the disease results from the misfolding and / or aggregation of rhodopsin, causing toxicity within photoreceptors and ultimately triggering apoptotic pathways, resulting in progressive retinal degeneration [21]. RP can be inherited in an autosomal dominant, autosomal recessive, or x-linked manner. Overall, the abundance of mutations and diversity of mechanisms underlying this disease underscores the difficulty in treating and curing RP. This impediment also applies to the large array of other inherited retinal diseases that require targeted therapeutic approaches, but potentially lack market size and commercial viability for the development of therapies by industry.

Treatment and Therapies:

Conventional therapies for treating retinal degenerative conditions have generally involved surgical intervention. For instance, in diabetic retinopathy, laser photocoagulation can be used to burn away abnormal, proliferative blood vessels that

form in the retina [22]. In the case of blood hemorrhaging in the vitreous, a vitrectomy may be performed, in which opaque vitreous is replaced with a clear saline solution. In treating glaucoma, a number of medicinal and surgical options are available for decreasing intraocular pressure. The most common surgical technique involves a trabeculectomy, in which a portion of the trabecular meshwork, an area of the eye which normally drains vitreal fluid, is removed [23]. A loosely sutured scelral flap is made to overlie this, allowing a drainage outlet for excess vitreal fluid. Although there are no FDA-approved treatments for individuals with dry AMD, besides nutritional supplements and dietary changes, similar surgical techniques as those used in individuals with diabetic retinopathy can be used on patients with wet AMD [24]. Recently, new medicinal therapies have proven more effective in treating this disease by focusing on preventing neovascularization, the damaging component of wet AMD [25]. Drugs such as Avastin, Lucentis, and Macugen help to preserve remaining vision by inhibiting vascular endothelial growth factor (VEGF), a protein that promotes the growth of abnormal blood vessels in the retina.

The pathophysiology of retinitis pigmentosa has presented unique challenges in treating this disease. Currently there is no FDA approved therapy for RP and recent results in phase I clinical trials using encapsulated cells bearing RPE cells producing ciliary neurotrophic factor (CNTF) have been mixed [26]. CNTF, as well as other neurotrophic factors such as glial derived neurotrophic factor (GDNF), and fibroblast growth factor (FGF) have been shown to mediate rescue in animal models of RP through suppression of apoptotic pathways that mitigates the loss of photoreceptors [27-29]. When surgically implanted in the patient eye, progressive secretion of CNTF resulted in increased ONL thickness relative to control, however functional rescue was inconsistent [26, 30]. Intriguing results have been seen through the use of phototransducing chips placed on the retinal ganglion cell layer of the retina [31]. With the use of an external camera placed on a patient's eyeglasses, selective stimulation of RGC's enabled one patient with no light perception from RP to see and localize a flashlight following implantation. Although the technology still remains in its infancy, it may offer the most substantive hope to individuals with severely depleted ONL.

Recent clinical results in patients with another inherited form of retinal degenerative disease, leber's congential amaurosis (LCA), show the most significant promise for retinal gene therapy [32, 33]. LCA is a rare autosomal recessive disorder caused by the abnormal development of photoreceptors. Although several genes have been implicated in LCA, *RPE65* has been the target for current gene therapy trials. The RPE65 protein is a retinal isomerase localized in the RPE that converts all-trans retinol to 11-cis retinal, the phototrasducable form of retinal utilized by opsin [34]. For individuals with loss of function mutations in *RPE65*, introduction of a functional version through the use of a recombinant adeno-associated viral vector has led to significant and sustained gains in visual function for all treated patients [35]. The clinical success of these trials bodes well for the use of gene-delivery approaches towards other inherited degenerative diseases in the eye. However, in seeking a cure for RP, an effective therapy would need to introduce a functional version of a gene for a recessive condition or knockdown a dominant mutant, a gargantuan task for a disease with 50 known loci, and hundreds, if

not thousands of causative mutations [21]. A mutation-independent neuroprotective strategy may then be the most practical solution for clinical treatment. Therefore, there is a strong need for a simple, safe, and broad-based ocular gene delivery strategy that provides sustained production of a neuroprotective therapeutic for these conditions.

Gene Delivery in the Retina:

Several viral and non-viral vectors exists for delivering therapeutic genes to the retina. The eye represents a strong candidate for gene therapy because of its easy accessibility relative to other organs in the human body, enabling localized delivery through needle injection through the scelera into the vitreous or the subretinal space, avoiding the complicated requirements necessitated by systemic vector administration. Non-viral vectors are advantageous for gene delivery in that they offer less toxicity and immunogenicity relative to viruses, while also theoretically allowing for unlimited sizes of DNA to be delivered to cell nuclei. Two main systems have been used to deliver DNA in this manner: liposomes and polymers. Liposomes are a self-assembly of amphiphilic molecules and cationic lipids, such as TMAG (N-(α-trimethylammonioacetyl)-didodecyl-D-glutamate), which are used to bind negatively charged DNA to form stable lipoplexes for gene delivery [36]. In one *in vivo* study, intravitreal injection of plasmid DNA complexed in these liposomes in the rabbit retina resulted in transient gene expression throughout the eye, peaking at three days [37]. Cationic polymers, such as polyethylenimine (PEI) and poly-L-lysine (PLL) have also been used to condense and deliver DNA to retinal tissue. For instance, PEI was used to deliver shRNA targeting melanopsin to RGCs via intreavitreal injection, resulting in a knockdown of expression to undetectable levels following administration [37].

However non-viral vectors face two key issues for use in clinical gene therapy: they are inefficient in retinal gene delivery due to an inability to overcome numerous physical and electrostatic barriers in the eye and they display a limited duration of expression due to the transient nature of their delivery. Importantly, viral vector mediated gene delivery overcomes these barriers as viruses have selectively evolved over a billion years to deliver their genomes to host cell nuclei. In exploiting this fact, native genomes of viruses can be altered so as to replace genes necessary for viral replication with therapeutic genes of interest. Thus, when these transgenes are encapsidated in their corresponding viral shells, their capsid-dependent infective pathways are retained, enabling them to be used as gene delivery vehicles. Additionally, in the case of viral-mediated genomic integration, gene expression will occur over the lifetime of the cell.

The most commonly employed viral vector systems for ocular gene therapy are adenoviral, lentiviral, and adeno-associated viral (AAV) vectors. Adenoviral vectors are capable of infecting neurons and glial in the CNS and retina, however their practicality in the clinic is limited due to their inducement of strong inflammatory responses and their lack of long-term gene expression [38-40]. Lentiviral vectors have proved efficient in transducing retinal tissue with sustained expression via subretinal injection [41]. However, due to the size of the viral capsid, they are physically unable to penetrate the inner limiting membrane (ILM) of the retina from the vitreous, and thus are impractical

for intravitreal-mediated gene delivery. Vectors based on adeno-associated virus hold the most promise for gene therapy in terms of safety, stability, and efficiency and are now the most commonly employed vectors in the lab and the clinic for ocular gene delivery [42, 43]. AAV is a nonpathogenic parvovirus composed of a 4.7kb linear single stranded DNA genome enclosed within a 25nm icosahedral capsid (Figure 1.3) [44]. AAV's single-stranded DNA genome has two open reading frames, including *cap*, which encodes for the structural proteins VP1-3 that assemble into the viral capsid [45]. AAV was first isolated as a contaminant in laboratory adenovirus stocks, however numerous serotypes and over 100 AAV variants have been isolated from human/nonhuman primate tissues to date [46]. In the development of recombinant vectors for transgene delivery, AAV2 was the first AAV isolate to be employed, but the addition of new serotypes and variants to the known AAV repertoire has led to the rapid development and use of new rAAV vectors with novel tissue tropisms.

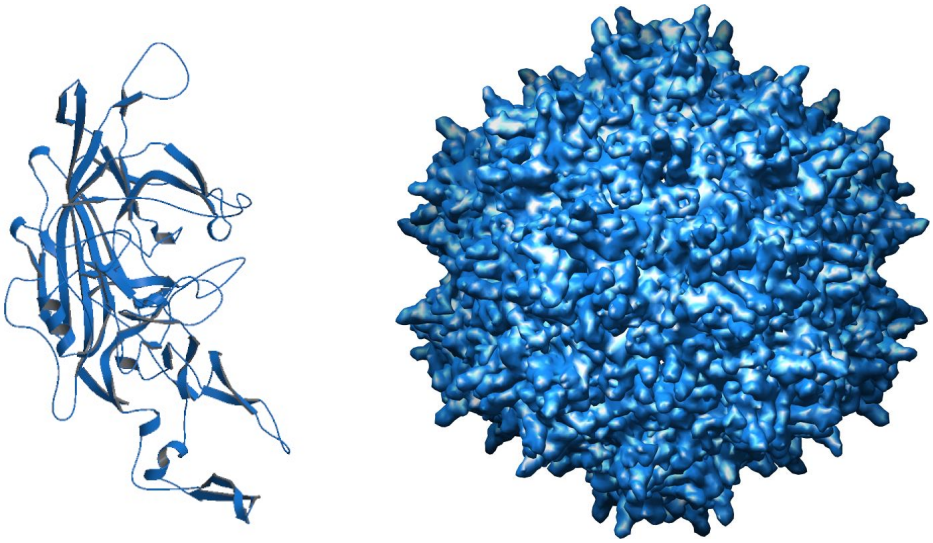

Figure 1.3. Ribbon structure of an AAV capsid subunit VP1 (left) and structure of a full AAV viral particle (right) form VIPER database (http://viperdb.scripps.edu).

Efficient infection with AAV is initiated by binding to cell surface glycosaminoglycan receptors and coreceptors and followed by receptor-mediated endocytosis through clathrin-coated pits in a dynamin dependant process [47]. Heperan sulfate proteoglycans (HSPGs) have been implicated as primary attachment receptors for serotypes 2 and 3 while sialic acid has been implicated for serotypes 1, 4, 5, and 6 [48]. However, for most newly discovered AAV serotypes, the specific attachment receptors and coreceptors remain uncharacterized. Once internalized within the cell, virions are vesicularly trafficked and processed within the endosome, escaping by a low pH-dependant process to the cytosol [47]. Subsequently, it is believed virions translocate to the nucleus prior to uncoating whereby the ss genome is converted into a double-stranded (ds) molecular form capable of expressing transgenes, either through *de novo* strand synthesis or through the annealing of complementary plus and minus ss molecules [49].

Importantly, each of these biological barriers functionally represents potential rate-limiting steps in AAV transduction, and in a varying degree, is capsid-dependant. Therefore, the use of novel AAV serotypes and viral capsid manipulation presents a powerful, multi-faceted approach to altering cellular tropism and enhancing infection efficiency.

Subretinal administration of AAV is the injection route employed by current clinical therapies to achieve sufficient transduction for rescue. However, this surgical approach requires creating a retinotomy (a hole through the neurosensory retina) and mechanically detaching the photoreceptor layer from its underlying supportive epithelium (RPE) through injection of an AAV fluid suspension, generating a "bleb". The resulting retinal detachment has had documented damaging effects, triggering cellular stress response pathways, reactive gliosis, retinal disorganization, photoreceptor degeneration, and functional losses in vision [50, 51]. In retinas compromised by degeneration, the effects of this detachment would only be further magnified [52]. Additionally, as degeneration occurs throughout the retina in most retinal diseases, use of a focal delivery and treatment strategy via subretinal injection into a specific region is not optimal because only cells within the "bleb" are transduced [35,53,54]. An intravitreal injection technique, whereby virus is administered directly into the vitreous of the eye, presents a more innocuous and simple approach for gene delivery to the retina, and it allows for a broader area of retinal transduction since the vitreous contacts the entire underlying retinal surface. However, intravitreal injection of conventional AAV serotypes cannot mediate sufficient transgene expression within or in proximity to the photoreceptors undergoing degeneration in the outer nuclear layer of the retina to achieve effective rescue of retinal function. This is in large part due to the unique diffusional barriers posed by intravitreal injections, namely the need for AAV to cross the meshwork of proteoglycans that compose the inner limiting membrane (ILM) of the retina, and in the case of photoreceptor transduction, the need to surpass the retinal strata underlying the ONL [55]. Therefore, there exists the need to create more efficacious AAV vectors capable of efficiently infecting photoreceptors or cells in proximity to photoreceptors, such as Müller cells.

Directed Evolution:

Several potential strategies exist in engineering AAV capsids to overcome physiological barriers to transduction and/or to increase tropism specificity. These techniques include: peptide insertion into discrete capsid locations, the use of mosaic or chimeric AAV vectors generated from multiple different serotypes, and the use of directed evolution using combinatorial AAV vector libraries generated from DNA shuffling and error-prone PCR (Figure 1.4) [56]. Just as Darwinian evolution has shaped the natural world through billions of year of natural selection, recursive cycles of mutagenesis and selection can be employed to direct evolution of macromolecules, including viral capsid proteins, towards desired properties. This black box approach enables the exploration of a large numbers of sequence permutations without the requirement of rationally tailoring proteins against a backdrop of innumerable and enormously complex variables.

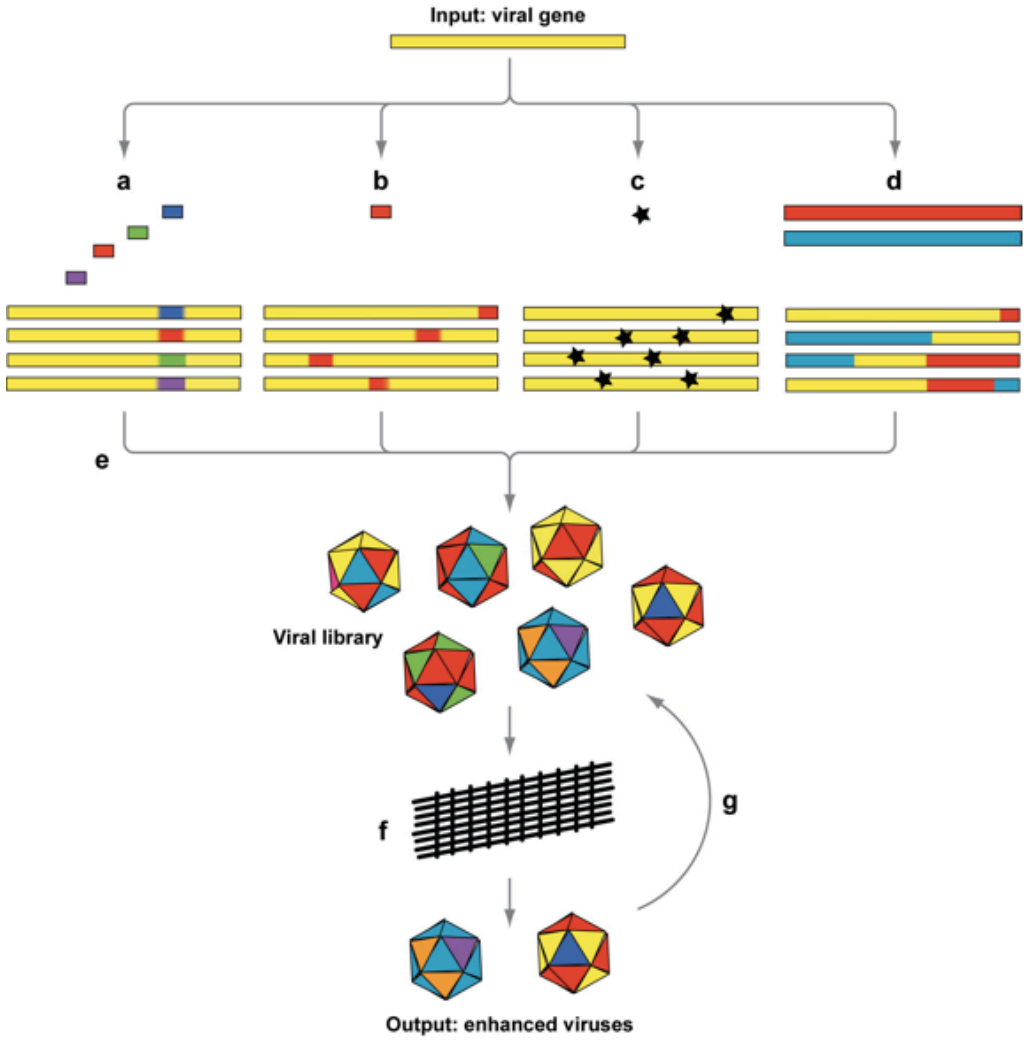

Figure 1.4. AAV viral libraries may consist of (a) a display of a random oligomer in a defined location, (b) random insertional mutagenesis, (c) random point mutagenesis through error-prone PCR, or (d) shuffling of semi-homologous genes. After generating a diverse library (e), a selection may be performed (f) to screen for variants with desired properties. Recovered variants (g) can be further selected (f) or further mutagenized (a-d). Image modified from Schaffer DV, Koerber JT, Lim KI (2008) Molecular engineering of viral gene delivery vehicles. Annu Rev Biomed Eng. 10:169-94.

This technique has already been employed to optimize numerous enzymes in terms of such properties as thermostability, substrate specificity, and enantioselectivity [57-60]. Given the capsid-dependent nature of AAV transduction, the AAV cap gene is a natural candidate for directed evolution to alter viral properties. Much success in the AAV field has already been attained using this approach, such as the generation of novel AAV2 viral variants that can escape neutralizing antibodies through the positive selection of random permissive mutations in the AAV2 capsid gene [61]. Additionally, AAV

variants have recently been evolved for improved CFTR delivery to human ciliated airway epithelium *in vitro*, an important advance for individuals afflicted with cystic fibrosis, as well as novel AAV variants that more efficiently cross the seizure-compromised blood-brain barrier in mice [62]. The accessibility of the retina facilitates an *in vivo* selection strategy for performing directed evolution, potentially enabling the creation of AAV variants with properties that can overcome the physiological barriers to intravitreal transduction of Müller cells, photoreceptors, and other retinal cells.

Summary:

This dissertation characterizes the barriers to intravitreal transduction and describes an artificial method for reducing them. Additionally, a Müller cell specific AAV variant is generated, characterized, and further used to deliver a GDNF transgene to these cells, secretion of which was found to rescue vision loss in an animal model of retinitis pigmentosa. Finally, results from an AAV directed evolutionary study to intravitreally target photoreceptors are provided. We are confident the data presented in this dissertation will contribute to the development of efficient and selective AAV variants for intravitreal retinal transduction to enable the creation of safer and more effective therapies for treating retinal degenerative diseases.

Chapter 2

Inner Limiting Membrane Barriers to AAV-mediated Retinal Transduction From the Vitreous

Preface:

This work was done in collaboration with Dr. Deniz Dalkara, a post-doctoral fellow in the Flannery and Schaffer Labs at UC Berkeley, as well as Dr. Kate Kolstad, a former graduate student in the Flannery lab. Natalie Hoffman and Meike Visel provided technical assistance. Natalia Caporale, a post-doctoral fellow in Dr. Yang Dan's lab at UC Berkeley, conducted the cortical experiment. Jessie Lee provided technical assistance for TEM experiments.

This chapter has been published in the journal *Molecular Therapy*. Dalkara D, Kolstad KD, Caporale N, Visel M, Klimczak RR, et al. (2009) Inner limiting membrane barriers to AAV-mediated retinal transduction from the vitreous. Mol Ther 12: 2096-102.

Abstract:

Adeno-associated viral gene therapy has shown great promise in treating retinal disorders, with three promising clinical trials in progress. Numerous adeno-associated virus (AAV) serotypes can infect various cells of the retina when administered subretinally, but the retinal detachment accompanying this injection induces changes that negatively impact the microenvironment and survival of retinal neurons. Intravitreal administration could circumvent this problem, but only AAV2 can infect retinal cells from the vitreous, and transduction is limited to the inner retina. We therefore sought to investigate and reduce barriers to transduction from the vitreous. We fluorescently labeled several AAV serotype capsids and followed their retinal distribution after intravitreal injection. AAV2, 8, and 9 accumulate at the vitreoretinal junction. AAV1 and 5 show no accumulation, indicating a lack of appropriate receptors at the inner limiting membrane (ILM). Importantly, mild digestion of the ILM with a nonspecific protease enabled substantially enhanced transduction of multiple retinal cell types from the vitreous, with AAV5 mediating particularly remarkable expression in all retinal layers. This protease treatment has no effect on retinal function as shown by electroretinogram (ERG) and visual cortex cell population responses. These findings may help avoid limitations, risks, and damage associated with subretinal injections currently necessary for clinical gene therapy.

Introduction:

Adeno-associated virus (AAV) has become the most promising ocular gene delivery vehicle over the past 10 years [33, 63, 64]. Its low immunogenicity, ability to infect the majority of retinal cells, and long-term transgene expression following a single treatment make the virus a very efficient gene delivery vector [65]. AAV is a nonpathogenic virus composed of a 4.7-kb single-stranded DNA genome enclosed within a 25-nm capsid[66]. In recombinant vectors, genes encoding replication (*rep*) and capsid (*cap*) proteins from the wild-type AAV genome are replaced by a promoter and therapeutic transgene cassette flanked by the AAV inverted terminal repeats that are required for packaging and replication. To date, hundreds of AAV variants have been identified [67, 68], and their tissue tropism and transduction efficiency are controlled by the capsid, which mediates initial receptor attachment, cellular entry, and trafficking mechanisms and thereby determines selectivity for particular cells or tissues. In particular, receptor-binding specificity is a key determinant of viral tropism. Specific glycan motifs have been identified as primary receptors for some AAV serotypes, and AAV2 uses heparan sulfate for cell recognition and entry whereas AAV1 and AAV5 bind to glycans with a terminal sialic acid [69]. In addition, AAV2, 8, and 9 bind to the 37/67-kDa laminin receptor [70], likely as their secondary receptor.

AAV is particularly promising for gene therapy in the retina [33, 63, 64], where mutations in genes expressed in photoreceptors and retinal pigment epithelia (RPEs) comprise the great majority of defects underlying inherited blindness. Because AAV is unable to reach these cells via intravitreal administration, the subretinal route of delivery is necessary. However, subretinal administration of AAV requires the surgeon to perform a vitrectomy, *i.e.*, create a needle hole through the retina (retinotomy) and detach the photoreceptors from the RPE with the injection of fluid. This retinal detachment causes series of macromolecular and structural modifications that are damaging to visual processing [71]. Also, in most retinal diseases, the degeneration is not uniform across the retina [35, 54], making identification of where to introduce the subretinal "bleb" difficult. Furthermore, the degenerating retina is often extremely fragile and poses a high risk of creating a retinal tear or macular hole [72]. Thus, in clinical settings it would be advantageous to introduce AAV vectors capable of outer retinal transduction from the vitreous.

It has been shown that after intravitreal injection, the AAV transduction profile of retinal cells differs significantly between neonatal and adult rats [73]. Injection of AAV2 at P0 results in photoreceptor, amacrine, and bipolar cell transduction, whereas the vast majority of transduced cells in adults are retinal ganglion cells (RGCs). The inner limiting membrane (ILM)—a basement membrane that contains 10 distinct extracellular matrix proteins [74] and histologically defines the border between the retina and the vitreous humor [75] —may pose a barrier for penetration of AAV into the retina from the vitreous in adults, whereas a less-differentiated ILM or increased extracellular space may results in fewer barriers in the developing retina. Importantly, the ILM is essential for normal eye development [76, 77]; however, it is dispensable in adults, and its removal is

considered beneficial for patients undergoing macular hole surgery [78].

We have investigated the localization and retinal transgene expression profile of five relevant AAV serotypes following intravitreal administration. In addition, we identified the ILM as a barrier to AAV-mediated retinal transduction by digesting it with Pronase E, a group of proteolytic enzymes from *Streptomyces griseus* previously shown to digest monkey ILM [79]. Specifically, coadministration of Pronase and AAV into the vitreous resulted in high-efficiency transduction of several retinal cell types, including photoreceptors and RPE. We anticipate this finding may greatly enhance AAV-mediated retinal gene therapy with intravitreal administration.

Materials and Methods:

Generation of rAAV vectors. AAV vectors containing sm.CBA promoter (which has the shortened hybrid chicken β–actin/rabbit β–globin intron) followed by enhanced GFP were produced by plasmid cotransfection into 293 cells[80]. The resulting clarified cell lysate was subjected to iodixanol density gradient purification, and the interface between 54 and 40% iodixanol fraction, along with the lower three-quarters of the 40% iodixanol fraction, was extracted after ultracentrifugation and diluted with an equal volume of phosphate-buffered saline (PBS) with 0.001% Tween-20. An Amicon Ultra-15 Centrifugal Filter Unit was preincubated with 5% Tween in PBS for 20 minutes, then washed once with PBS + 0.001% Tween. The diluted iodixanol fractions were loaded onto the centrifugal buffer exchange unit and spun until 250 µl of concentrated vector remained. Fifteen milliliters of sterile PBS + 0.001% Tween was added, and the concentration step was repeated three times with fresh sterile PBS + 0.001% Tween. A final viral concentrate of ~200 µl, devoid of iodixanol, was ultimately obtained. The vector was then titered for DNase-resistant vector genomes by quantitative PCR using diluted plasmid DNA as a standard. Finally, the purity of the vector was validated by silver-stained sodium dodecyl sulfate–polyacrylamide gel electrophoresis.

Cy3 labeling of rAAV vectors. Purified and concentrated rAAV was labeled as previously described[81]. Briefly, amine-reactive Cy3 dye (GE Healthcare Biosciences, Uppsala, Sweden) was resuspended in a 0.2 mol/l $NaCO_3$/$NaHCO_3$ buffer at pH 9.3. Viral stock was mixed at a ratio of 1:1 with the dye suspension to a total volume of 400 µl. The reaction was allowed to take place for 2 hours at room temperature and quenched by the addition of 4 µl of 1 mol/l Tris–HCl at pH 8.0. Buffer exchange and concentration were then conducted using Amicon Ultra-5 Centrifugal Filter Units (Millipore, Billerica, MA).

Intraocular administration routes. Adult wild-type Sprague-Dawley rats were used for all studies, and animal procedures were conducted according to the Association for Research in Vision and Ophthalmology statement for the use of animals and the National Institutes of Health guidelines for the use of laboratory animals, as approved by the Office of Laboratory Animal Care at the University of California at Berkeley. Before vector administration, rats were anesthetized with ketamine (72 mg/kg) and xylazine (64

mg/kg) by intraperitoneal injection. An ultrafine 30 1/2-gauge disposable needle was passed through the sclera, at the equator and next to the limbus, into the vitreous cavity. Injections were made with direct observation of the needle in the center of the vitreous cavity. The total volume delivered was 5 µl, containing $2–5 \times 10^{12}$ vg/ml of AAV-Cy3. In addition, where indicated, 5×10^{12} vg/ml of AAV encoding enhanced GFP driven by the ubiquitous chicken β–actin promoter was mixed at a ratio of 4:1 with 0.001% Pronase E and injected.

Fundus photography. *In vivo* retinal imaging was performed 2–4 weeks after injections with a fundus camera (RetCam II; Clarity Medical Systems, Pleasanton, CA) equipped with a wide angle 130° retinopathy of prematurity lens to monitor enhanced GFP expression in live, anesthetized rats. Pupils were dilated before imaging with tropicamide (1%).

Electroretinography. Sprague-Dawley rats were injected with 5 µl of AAV5 encoding enhanced GFP mixed at a ratio of 4:1 with 0.0002% Pronase E in the vitreous of one eye and 5 µl of PBS in the contralateral eye, $n = 8$. This was repeated with the middle-dose (0.001%, final concentration, $n = 6$) and high-dose (0.002%, final concentration, $n = 8$) Pronase E concentrations. One-week postinjection, animals were dark-adapted for 4 hours and anesthetized, and their pupils were then dilated. Animals were placed on a heating pad, and contact lenses were positioned on the cornea. Reference electrodes were inserted subcutaneously in the cheeks, and a ground electrode was inserted in the tail. ERGs were recorded (Espion ERG system; Diagnosys, Littleton, MA) in response to seven light flash intensities from 0.0001 to 3.16 cd-s/m^2 presented in series of three. Light flash intensity and timing were elicited from a computer-controlled Ganzfeld flash unit. Data were analyzed with MatLab (v7.7; The MathWorks, Natick, MA). After correction for oscillatory potentials, scotopic A-wave values were measured from the baseline to the minimum ERG peak whereas scotopic B-waves were measured from the minimum to maximum ERG peaks. Statistical differences between Pronase E and PBS-injected eyes were calculated using paired Student's *t*-test.

Cryosections. Two to four weeks after vector injection, rats were humanely euthanized, the eyes were enucleated, a hole was made in the cornea, and tissue was fixed with 10% neutral buffered formalin for 2–3 hours. The cornea and lens were removed. The eyecups were washed in PBS followed by 30% sucrose in PBS overnight. Eyes were then embedded in optimal cutting temperature embedding compound (Miles Diagnostics, Elkhart, IN) and oriented for 5–10-µm thick transverse retinal sections.

Immunolabeling and histological analysis. Tissue sections were rehydrated in PBS for 5 minutes followed by incubation in a blocking solution of 1% bovine serum albumin, 0.5% Triton X-100, and 2% normal donkey serum in PBS for 2–3 hours. Slides were incubated overnight at 4 °C with commercial mouse monoclonal antibodies against intact capsids of AAV1, 2, or 5 (American Research Products, Belmont, MA) at 1:100, rabbit monoclonal antibody raised against the GFP (Invitrogen, Carlsbad, CA) at 1:400, or in anti-laminin antibody (L9393; Sigma, St Louis, MO) at 1:100 in blocking solution. The sections were then incubated with Alexa 488–conjugated secondary anti-rabbit antibody (Molecular Probes, Grand Island, NY) at 1:1,000 in blocking solution for 2 hours at room

temperature. The results were analyzed by fluorescence microscopy using an Axiophot microscope (Zeiss, Thornwood, NY) equipped with X-Cite PC200 light source and QCapture Pro camera, or by confocal microscopy (LSM5; Carl Zeiss Microimaging, Thornwood, NY).

Transmission electron microscopy. A generic processing protocol was used to prepare samples for transmission electron microscopy. Briefly, glutaraldehyde-fixed, osmocated retinas were treated with uranyl acetate at 4 °C overnight. Samples were then dehydrated with 35–100% water/acetone steps on ice. After Epon–Araldite resin infiltration, samples were left in a polymerization oven for 2 days. Sections of 70–100-nm thickness were cut from Epon–Araldite resin–embedded samples with a Reichert–Jung Ultra E microtome (Leica, Heerbrugg, Switzerland). They were collected on 0.6% Formvar-coated slot grids and poststained in 2% aqueous uranyl acetate and Reynold's lead citrate. Sections were imaged on a FEI Tecnai 12 TEM (FEI, Eindhoven, The Netherlands) with an UltraScan 1000 CCD camera (Gatan, Pleasanton, CA).

Visually evoked potentials. A week prior to recordings, Sprague-Dawley rats were injected with 5×10^{13} vg/ml of AAV5 mixed at a ratio of 4:1 with 0.001% Pronase E (n = 6) or 5×10^{13} vg/ml of AAV5 mixed at a ratio of 4:1 with 0.01% Pronase E (n = 6) and injected in the vitreous of one eye and 5 μl of PBS in the contralateral eye. One week postinjection, animals were anesthetized using ketamine (72 mg/kg intraperitoneally) and xylazine (64 mg/kg intraperitoneally) and pupils dilated. Animals were restrained in a stereotaxic apparatus (David Kopf Instruments, Tujunga, CA), and body temperature was maintained at 36–37 °C via a heating blanket (Harvard Apparatus, Holliston, MA). Anesthesia was supplemented with 0.5–1% isoflurane as needed during the recordings. A small craniotomy and durotomy (~1 mm^2) were performed over the primary visual cortex (2–3 mm lateral to the midline, 1 mm anterior to λ). A glass micropipette (resistance ~0.5–3 MΩ) containing saline solution was lowered to 0.5–0.6 mm below the surface of the cortex and contralateral to the side of the stimulated eye. Visual stimulation consisted of 10-ms pulses of light (white LED, 1 cm from eye) presented at 0.2 Hz for 40–50 repeats. Sweeps were filtered at 2 kHz, sampled at 10 kHz by a 12-bit digital acquisition board (National Instruments, Austin, TX), and analyzed with custom software running in MatLab (The MathWorks).

Results:

Labeling and characterization of AAV serotypes 1, 2, 5, 8, and 9

To assess the localization of viral particles in the retina after intravitreal injection, we labeled each AAV serotype by covalently linking a Cy3 amine–reactive dye to lysine residues exposed on the viral capsid surface [81]. Labeled virus was incubated with 293T cells to visualize particle localization before proceeding with *in vivo* studies (Figure 2.1a–c,g,h). To confirm that fluorescent signal observed at the cell surface and in endosomal/lysosomal compartments was associated with intact viral particles, we employed immunocytochemistry. Antibodies against AAV1, 2, and 5 colocalized with the Cy3 dye (Figure 2.1d–f), confirming Cy3 labeling is an appropriate means of monitoring viral dispersion in and among cells.

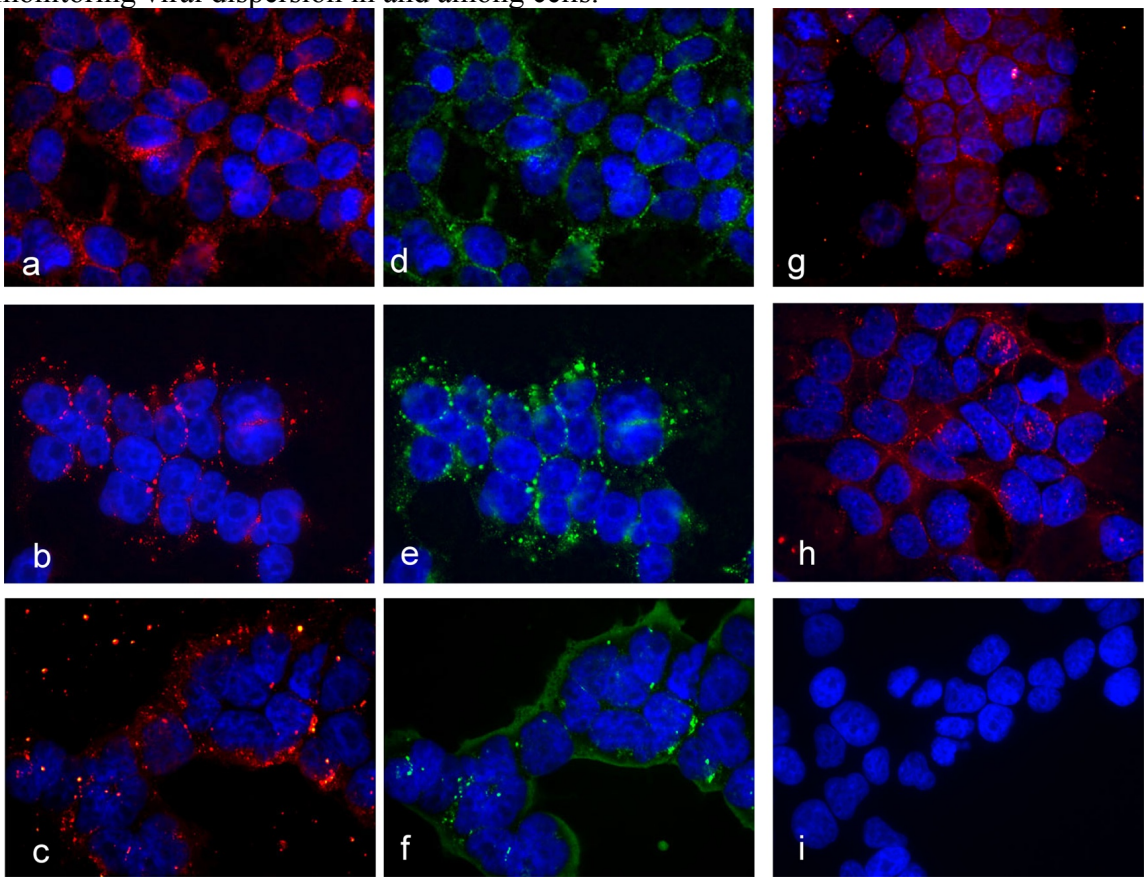

Figure 2.1. Cy3-labeled AAV particles at a MOI of 10^4 were observed at the cell surface and in the endosomal/lysosomal compartments after a 20 min incubation with cells at 37ºC: a) AAV1-Cy3 b) AAV2-Cy3 c) AAV5-Cy3. In parallel, the Cy3-labeled viral particles were immunostained with antibodies directed against conformational epitopes of intact AAV capsids: d) AAV1-Cy3 with anti-AAV1 (green), e) AAV2-Cy3 with anti-AAV2 (green) f) AAV5-Cy3 with anti-AAV5 (green), g) AAV8-Cy3, h) AAV9-Cy3, and i) an equivalent quantity of unconjugated Cy3 dye.

Retinal penetration of Cy3-labeled viral particles following intravitreal injection

Localization of the different AAV serotypes after intravitreal injection was assessed by visualization of direct fluorescence resulting from the labeled capsids (Figure 2.2b,e,h,k,m) and by immunostaining the same cryosections with anti-AAV capsid antibodies when available (Figure 2.2c,f,i). The cryosections of retinas treated with AAV1-Cy3 did not exhibit any significant fluorescence (Figure 2.2b,c).

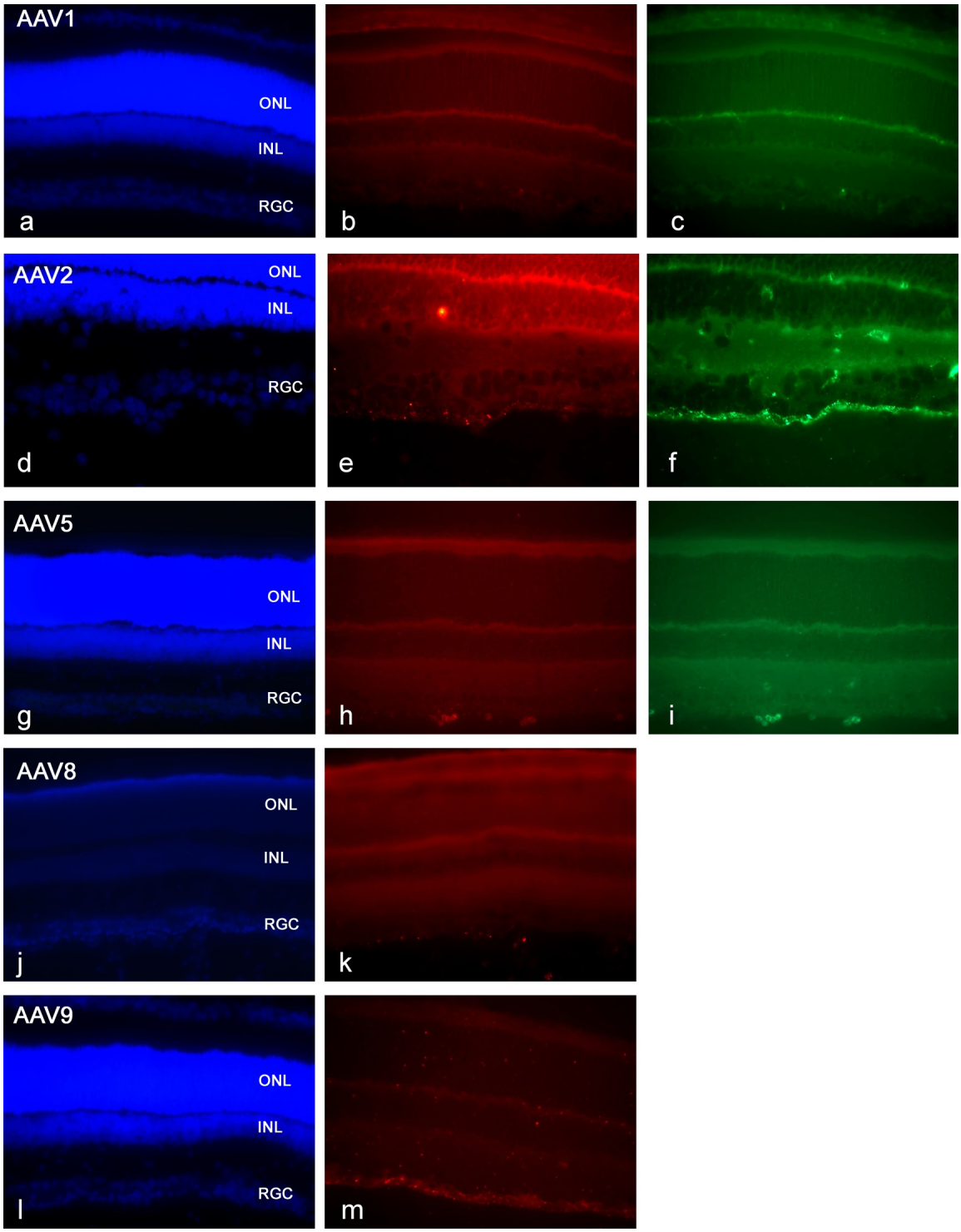

Figure 2.2. Localization of Cy3-labeled AAV particles in the retina of p30 rats. DAPI fluorescence (left panel), Cy3 fluorescence corresponding to the viral particles (middle panel), and green immunofluorescence (right panel) from anti-AAV intact capsid antibodies against AAV1, AAV2 and AAV5 capsids (c, f, and i).

AAV5-Cy3 showed only very localized signal in displaced ganglion cells. To confirm that these results were not due to the difficulty of visualizing the Cy3 capsid label over tissue autofluorescence, AAV5-Cy3 was injected subretinally, and robust fluorescence was observed in the RPE and photoreceptors at the region of injection (Figure 2.3). Cy3-AAV2 and nine injected retinas showed viral accumulation at the vitreoretinal junction (Figure 2.2e,m), as indicated by punctate fluorescence on the ILM, at the RGCs, on the nerve fibers associated with RGCs, and at the Müller cell endfeet. AAV8 could also be detected at the vitreoretinal junction, though to a lesser extent (Figure 2.2k). Although AAV2 and 9 showed strikingly similar localization patterns, only AAV2 resulted in green fluorescent protein (GFP) expression in the retina 1 month after intravitreal injection (Figure 2.4), consistent with prior reports with AAV2.

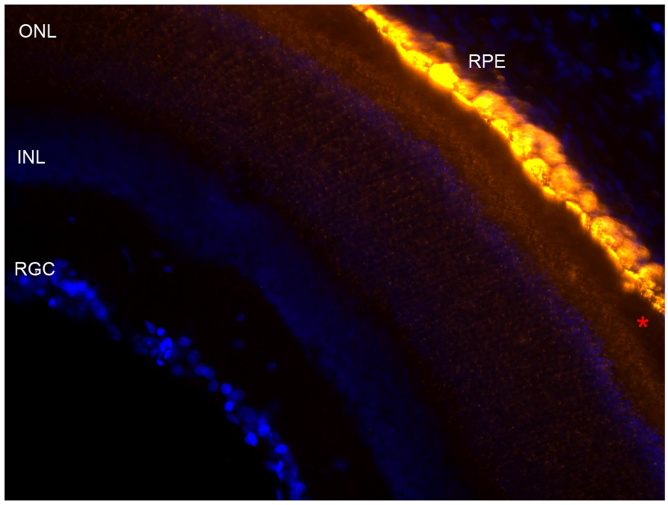

Figure 2.3. Retinal cryosection showing spreading of Cy3-labeled AAV5 particles following subretinal injection.

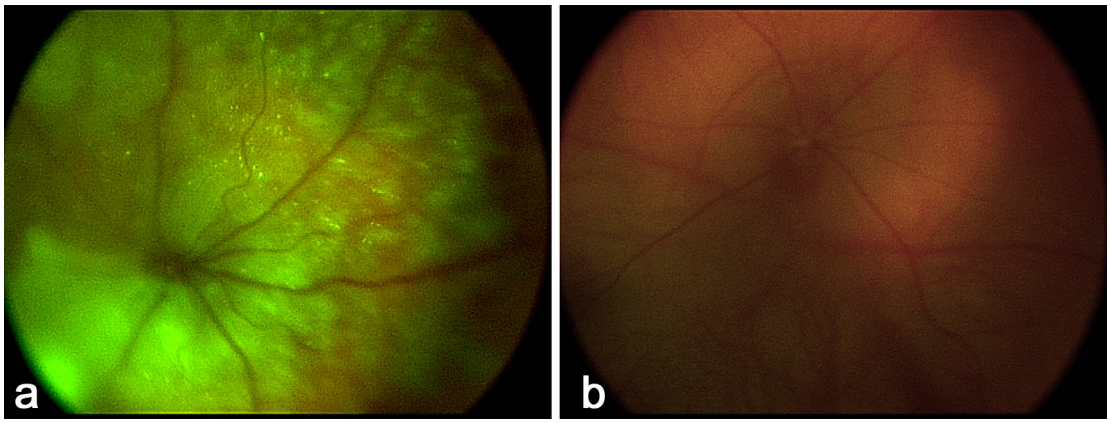

Figure 2.4. Representative fundus image of eyes injected with a) AAV2.smCBA.hGFP and b) AAV9.smCBA.hGFP.

Mild digestion of the ILM with Pronase E, a nonspecific protease

The localization of AAV2 and AAV9 at the vitreoretinal junction, where the ILM separates the vitreous from the retina, suggests that this anatomical feature may play a major role in initial viral attachment and subsequent penetration into the retina. It had been shown by Heegaard *et al*. that various enzymes can be used to disrupt the macaque monkey ILM [79]. After testing multiple glycosaminoglycases and proteases, the nonspecific protease, Pronase E, was shown to be the most successful agent in digesting the ILM. Pronase is a mixture of at least 10 proteases, including serine-type proteases, zinc endopeptidases, zinc leucine aminopeptidases, and a zinc carboxypeptidase [82]. We hypothesized that using Pronase E would disrupt the ILM, thereby enabling vector access to receptor-binding sites and potential cells that were previously unavailable to viral serotypes such as AAV1 and AAV5.

AAV is resistant to digestion by enzymes such as trypsin [83], but we first confirmed that the AAV serotypes we used are also resistant to Pronase by performing *in vitro* tests. AAV was incubated with 0.01 and 0.05% Pronase E at 37 °C overnight, and DNase-resistant viral genomes were then quantified by quantitative PCR. We found that Pronase treatment did not degrade the viral capsid at the concentrations relevant for intraocular use (data not shown). Therefore, enzyme was mixed with AAV prior to all intravitreal injections to obviate the need for multiple injections into the same eye. As a control, virus was injected into the contralateral eye without the enzyme. Various doses of Pronase were used to permeabilize the ILM (0.01, 0.005, 0.001, and 0.0002% total) and revealed that enzyme levels were very important. At high doses, the disruptive effect of the enzyme on the ILM could be readily visualized by antilaminin immunohistochemistry on cryosections of treated retinas (Figure 2.5).

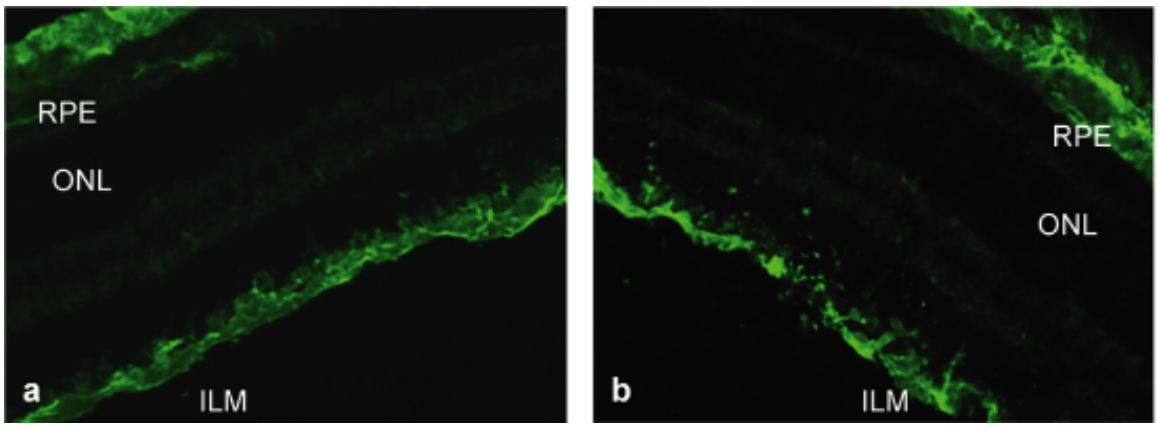

Figure 2.5. Morphological effects of Pronase E on the inner limiting membrane (ILM). (a) Untreated retina stained with anti-laminin antibody shows immunoreactivity at the ILM and at the choroid, whereas (b) laminin immunolabeling after treatment with 0.01% Pronase E exhibits a disintegrated ILM structure. ONL, outer nuclear layer; RPE, retinal pigment epithelium.

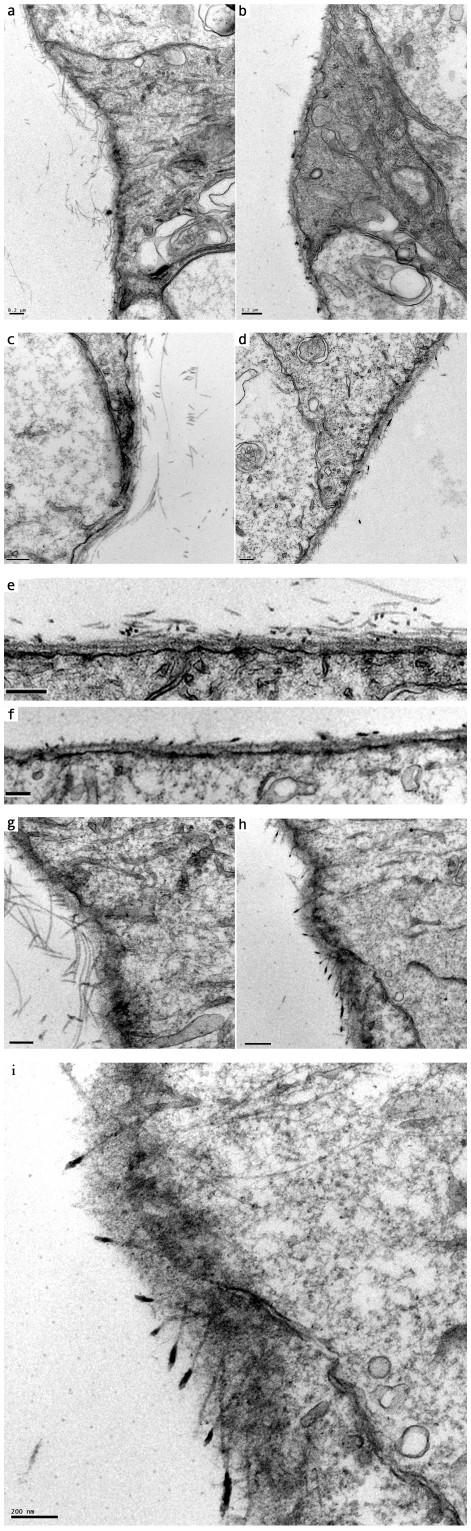

Figure 2.6. Comparative images of naïve and Pronase-treated retinas by TEM.
a,c) non-treated and b,d) 0.002% A Pronase-treated rat retina cross section comparing

ILM structure at the Müller cell endfoot. Scale bars are 200 nm. A stretch of ILM from c) non-treated and d) 0.002% Pronase treated retinas. Scale bars are 200 nm. Higher magnification image of g) non-treated and h) 0.002% Pronase treated retinal ILM. Scale bars are 200 nm and 500 nm respectively. i) Further magnification of h), where the scale bar is 200 nm.

Interestingly, we have also observed some changes in the Pronase-treated ILM using transmission electron microscopy (Figure 2.6), where retinas treated with Pronase showed a reduction in loose collagen fibrils and the appearance of dark aggregates along the ILM, which we hypothesize to be degraded proteins that have aggregated after enzymatic digestion. In contrast, at lower doses (≤0.001%) the effect of the enzyme on laminin immunohistochemistry was not pronounced.

We next analyzed whether these morphological changes corresponded to retinal functional changes and found that Pronase doses of ≤0.0002% did not alter electroretinograms (ERG) compared to the untreated eye (Figure 2.7a). Dosages >0.0002% are deleterious to the retina, as shown by a reduction in ERG A-wave and B-wave amplitudes (Figure 2.7b,c). As Pronase E is a nonselective protease, once it had disrupted the ILM, it likely perturbed the underlying nerve fiber layer and RGCs, which are essential components for vision. However, considering that only radial currents, and not RGC activity, are reflected in the ERG, we also recorded local field potential responses in V1 in animals treated with Pronase. These animals were only treated with enzyme in one eye, allowing the contralateral eye visual input to serve as an internal control. Interestingly, our data show that visually evoked potentials are more robust to enzymatic treatment compared to ERGs (Figure 2.8). A reduction was observed only at the highest concentration (Figure 2.8, right panel), yet this was not statistically significant (n = 4 out of 6). It is thus likely that the cortex is compensating for the reduction in signal.

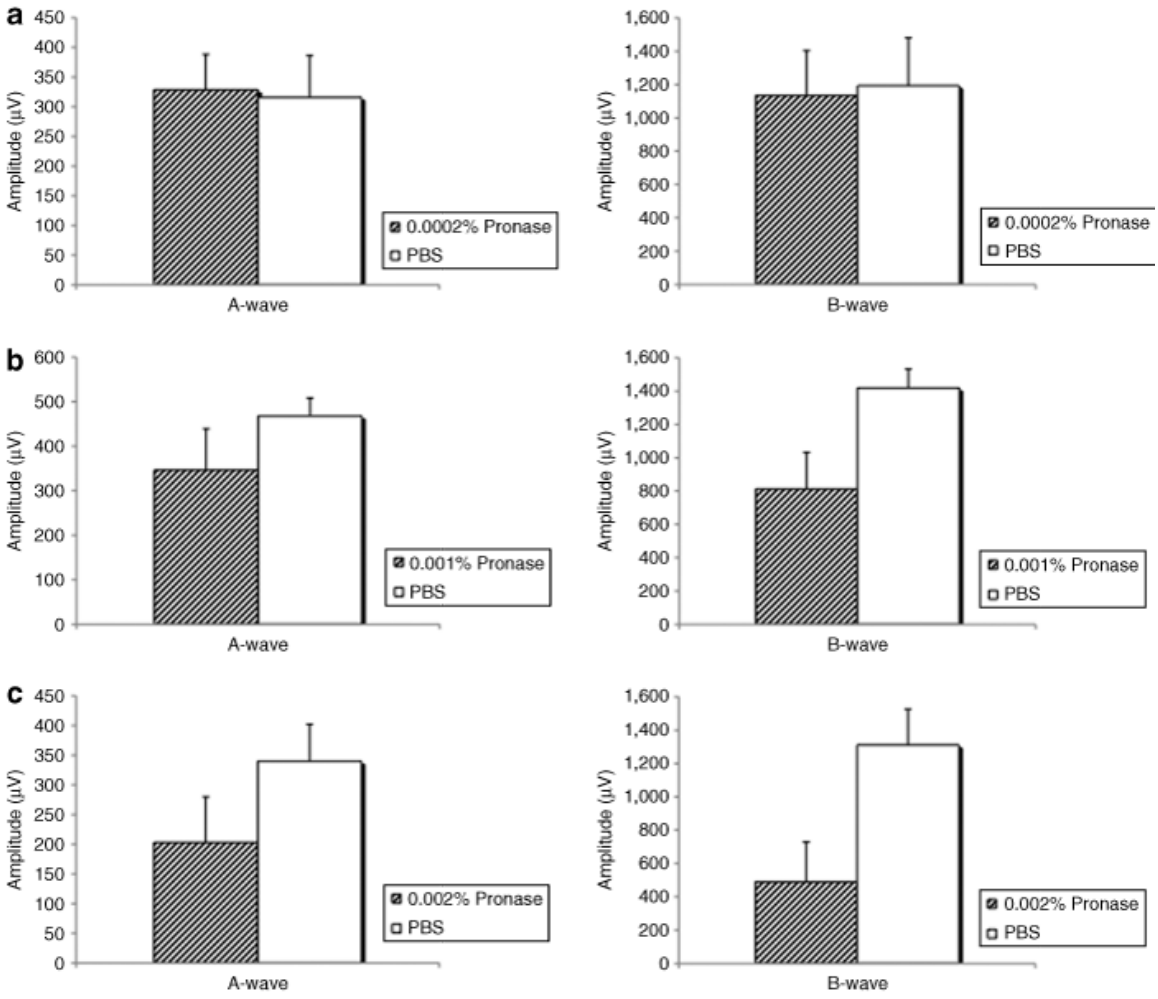

Figure 2.7. The electroretinogram of animals injected with 0.0002% (n = 8), 0.001% (n = 6), and 0.002% (n = 8) Pronase E was analyzed to assess toxicity of mild enzymatic cleavage of the inner limiting membrane (ILM). Each animal was injected with the enzyme in the vitreous of one eye and phosphate-buffered saline (PBS) in the contralateral eye. Pronase E concentrations are (a) 0.0002%, (b) 0.001%, and (c) 0.002%. Pronase E injection exhibited no significant change in A- or B-wave amplitude compared to control PBS-injected eyes. Statistical differences between Pronase E and PBS-injected eyes were calculated by Student's *t*-test.

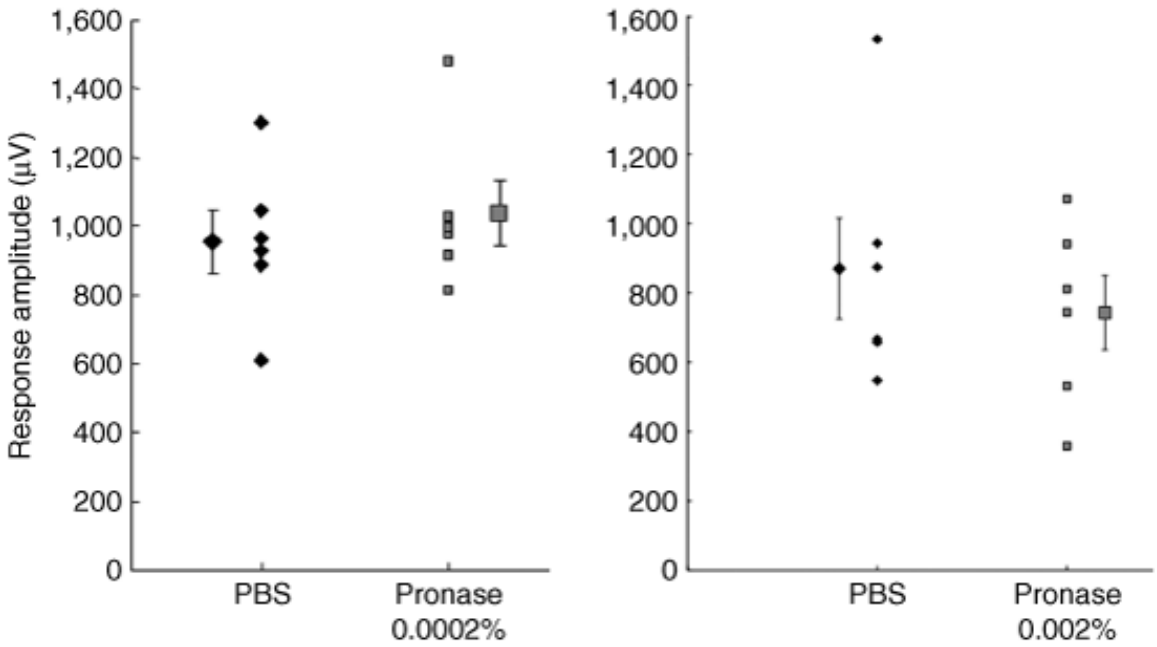

Figure 2.8. Peak amplitude of visually evoked potentials in response to full-field stimulation of eyes injected with phosphate-buffered saline (PBS) (diamonds) or Pronase (squares) at the low dose, $n = 6$, and high dose, $n = 6$. Recordings were performed on the contralateral visual cortex. Means for each data set are shown laterally displaced. Error bars indicate SEM. The two data sets for each dose were not significantly different ($n = 6$, $P > 0.6$, Wilcoxon signed-rank test).

GFP expression following AAV/Pronase E co-injection

All AAV serotypes injected intravitreally with Pronase (0.0002%) showed robust GFP expression in various cell types throughout the retina 3 weeks after injection (Figure 2.9a-d). In stark contrast, when AAV alone was injected intravitreally, only AAV2 led to gene expression in the inner retina, consistent with prior reports [44]. The strongest transduction was achieved with Pronase and AAV5 (Figure 2.9e-h), which mediated strong GFP expression in RGCs, Müller cells, photoreceptors, and RPE. The proportion of cells transduced varied throughout the extent of the retina (Figure 2.9f-h), potentially due to nonhomogeneous diffusion of the enzyme through the vitreous and a resulting higher concentration of the enzyme at the site of injection.

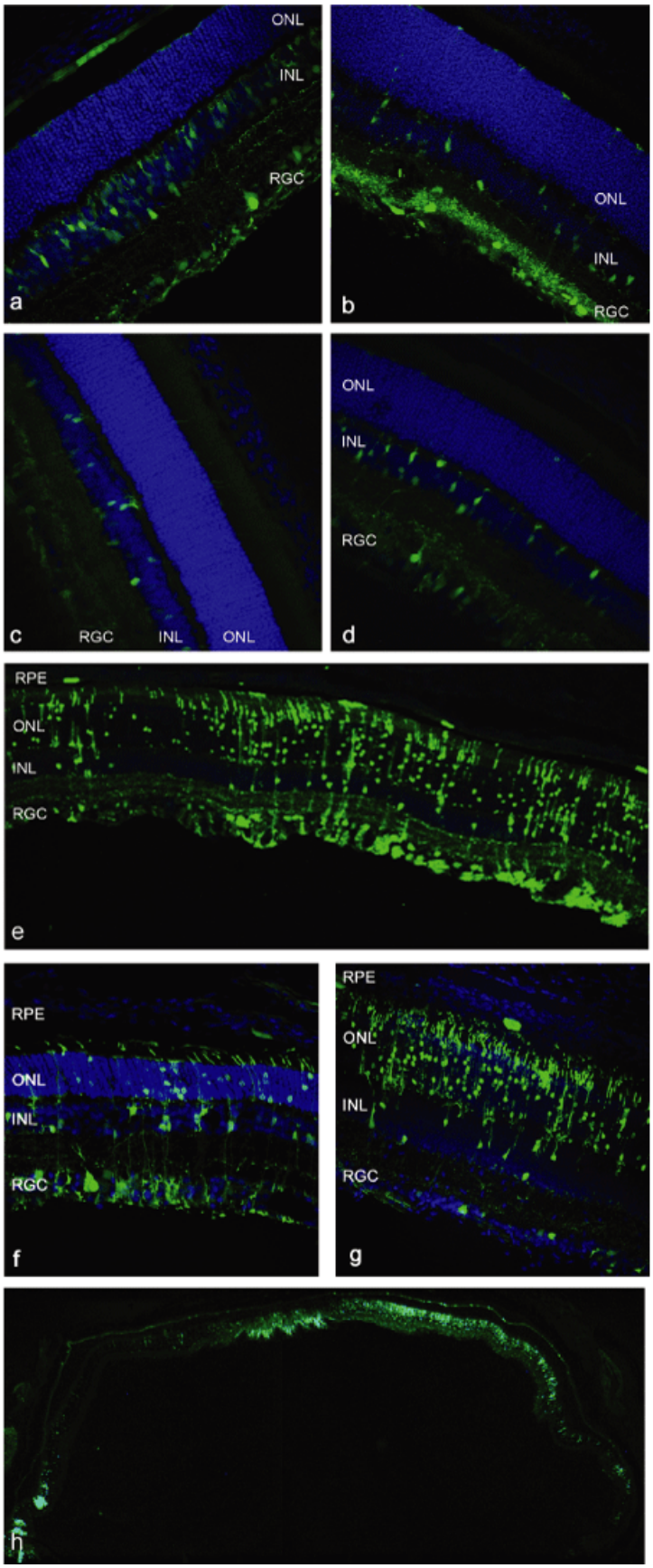
ONL
INL
RGC
a
ONL
INL
RGC
b
c
RGC
INL
ONL
ONL
INL
RGC
d
RPE
ONL
INL
RGC
e
RPE
ONL
INL
RGC
f
RPE
ONL
INL
RGC
g
h

Figure 2.9. Green fluorescent protein (GFP) expression in cryosections of rat retina after intravitreal delivery of 10^{11} vector genomes of adeno-associated virus (AAV) vectors carrying smCBA.hGFP in the presence of 0.0002% Pronase, 3 weeks after injection. Nuclei are stained with 4′,6-diamidino-2-phenylindole, shown in blue. (a) AAV1, (b) AAV2, (c) AAV8, (d) AAV9, and (e–h) AAV5. A representative area shows robust GFP fluorescence in all retinal layers in e. The proportion of transduced cells shows variability from one part to the other ($n = 6$) with strong expression in retinal ganglion cells (RGCs) and Müller cells in f and predominantly photoreceptors with weaker RGC with some expression in the RPE in g. An entire cryoslice is shown in h.

AAV vectors traverse a complex pathway during the process of gene delivery. At the cellular level, viral binding to cell surface receptors, internalization, nuclear accumulation, capsid uncoating, and single- to double-stranded genome conversion can all represent barriers to gene transfer [84, 85]. For *in vivo* delivery, however, the virus–host interaction begins at the site of administration, and the virus needs to bypass extracellular barriers such as basal membranes before reaching the target tissue and cells.

The tropism of AAV serotypes 1 through 9 has previously been studied in the retina [86, 87]. Following subretinal delivery, AAV serotypes 1 and 4 primarily infect and mediate expression in RPE cells [87, 88]; AAV2, 5, 7, 8, and 9 transduce RPE and photoreceptors [86]; and AAV8 and 9 also infect Müller glia. Interestingly, AAV5, 7, 8, and 9 also exhibit more efficient transduction and faster transgene expression than type 2 after subretinal injection. However, only AAV2 has been found to efficiently transduce the inner retina after intravitreal injection [84], indicating that the vitreoretinal junction represents a tissue barrier to AAV gene delivery. Studies showing that physically larger viruses like Pseudorabies Virus are capable of RGC transduction from the vitreous seem to indicate that the nature or this barrier is not diffusional or purely physical [89]. In rodents, this feature of the retina is relatively thin and homogeneous; however, in larger animals such as dogs and monkeys, the ILM is significantly thicker and varies in thickness from one region of the retina to the other. This may have important consequences for translational studies relying on the intravitreal delivery of AAV.

Discussion:

In this study, we investigated and sought to overcome this barrier. After fluorescently labeling several relevant AAV serotype capsids, we visualized their localization in retinal tissue upon intravitreal injection. Serotypes 2, 8, and 9 were able to find attachment sites at the ILM and accumulate to various degrees at the vitreoretinal junction, and AAV2 and 9 in particular exhibited very similar localization patterns. However, the highly interdigitated nature of the components of the vitreoretinal junction (Figure 2.10) prevented us from clearly identifying the specific sites where viral particles had bounded and accumulated. AAV8 showed a weaker fluorescent signal at the ILM,

indicating less robust attachment. It has been shown that the laminin receptor is involved in viral transduction by all three serotypes and could thus partially account for the attachment observed at the ILM, as laminin receptors are abundant at the vitreoretinal junction, the Müller cell endfeet, and RGCs[90]. In addition, AAV2 binds to heparan sulfate proteoglycan, also present at the ILM[91]. This binding may assist in viral accumulation at the ILM and thereby contributes to the intravitreal permissivity of this serotype. Interestingly, AAV2 and 9 seemed to show very similar fluorescent localization and signal intensity, yet AAV9 leads to no detectable expression after intravitreal injection (Figure 2.4). Cell surface and intracellular trafficking barriers are likely to be responsible for this difference. A recent discovery shows that phosphorylation of surface-exposed capsid tyrosines target the AAV viral particles for ubiquitination and proteasome-mediated degradation, and mutations of these tyrosine residues lead to substantially increased vector transduction[92]. This finding has been used successfully to manipulate AAV retinal transduction profiles, and mutant AAV2, 8, and 9 displayed strong and widespread transgene expression in the inner retina after intravitreal delivery compared to their wild-type counterparts[93]. This finding, together with our localization results, clearly indicates that AAV serotypes 2, 8, and 9 are all able to bind to the vitreoretinal junction, but subsequent cellular barriers limit the transduction of inner retinal cells by AAV8 and 9.

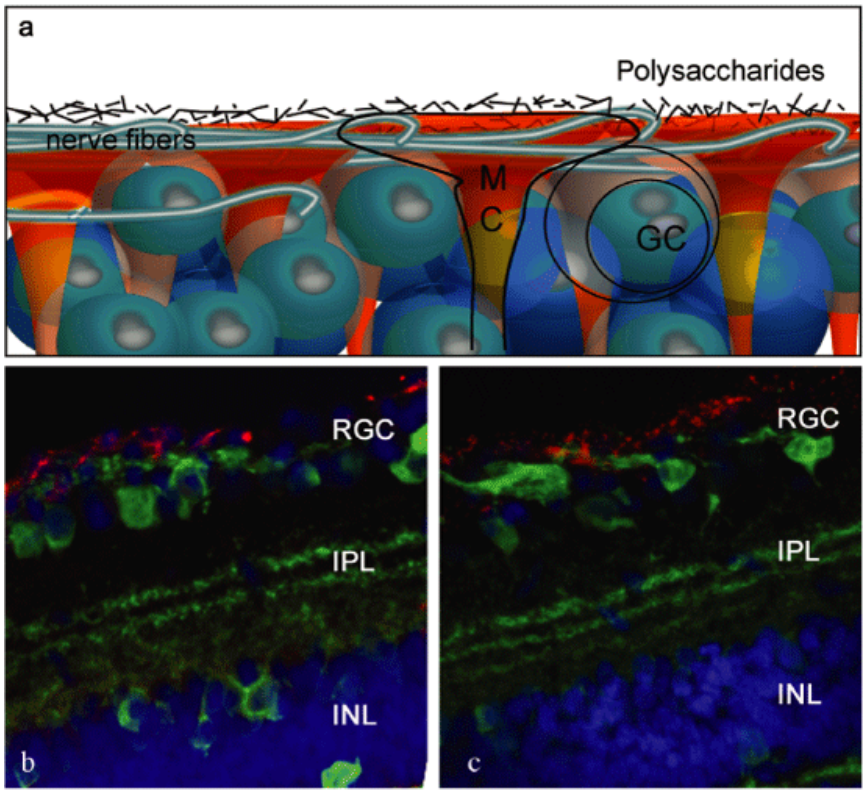

Figure 2.10. AAV particle localization at the vitreoretinal junction. (a) Schematic representation of the overlapping structures of the vitreoretinal junction. (b) Confocal images of AAV2-Cy3 and (c) AAV9-Cy3 accumulation at the vitreoretinal junction (red). The cryosections are counterstained with an antibody against calbindin (green), which

labels the retinal neurons.

In contrast to AAV2, 8, and 9, we find that AAV serotypes 1 and 5 are unable to find attachment sites at the vitreoretinal junction. It is known that both serotypes depend on sialic acid[94] for initial binding and that this monosaccharide is absent at the ILM[95]. Disruption of the ILM, a dispensable structure for the adult retina, using a nonspecific protease apparently resolves the access barrier to retinal transduction by sialic acid–dependent AAV serotypes 1 and 5[69]. In particular, our results show that intravitreal injection of AAV5 in combination with Pronase E leads to robust gene expression in various cells of the retina, including the RPE and photoreceptors. To our knowledge, this is the first time RPE transduction has been achieved by an intravitreally injected AAV vector. Interestingly, AAV5 is apparently the only serotype to date that is capable of packaging genomes larger than 4,700 nucleotides[96]; therefore, ILM digestion in conjunction with AAV5 delivery may allow for targeting of outer retinal cells without the need for subretinal injection and offers the capacity to deliver large genes to these cells[96]. Finally, a cell-specific promoter can be used to limit and control the levels of transgene expression in a cell type of choice.

Collectively, our data point to the importance of both extracellular and intracellular determinants of viral transduction in the retina. For intravitreal injections, viral binding and accumulation at an intact ILM may be necessary for the virus to access and infect the retina. By contrast, viral particles that lack binding sites at the ILM do not undergo concentration at this site, remain diffuse within the vitreous humor, and do not lead to gene expression. The ILM thus represents an important barrier to retinal gene delivery from the vitreous.

Chapter 3

Directed Evolution of Glial-permissive AAV Variants

Chapter 3a

Molecular Evolution of Adeno-associated Virus for Enhanced Glial Gene Delivery

Preface:

This work was done in collaboration with Dr. James T. Koerber, a graduate student in the Schaffer Lab at UC Berkeley, as well as Dr. Deniz Dalkara and Dr. Jae-Hyung Jang, post-doctoral fellows in the Flannery and Schaffer Labs, respectively. Kate Kolstad, a graduate student in the Flannery lab, and Karen Guerin, a post-doctoral fellow in the Flannery lab, assisted with retinal injections.

This chapter has been published in the journal *Molecular Therapy*. Koerber JT, Klimczak RR, Jang JH, Dalkara D, Flannery JG, and Schaffer DV (2009) Molecular evolution of adeno-associated virus for enhanced glial gene delivery. Mol Ther 12: 2088-95.

Abstract:

The natural tropism of most viral vectors, including adeno-associated viral (AAV) vectors, leads to predominant transduction of neurons and epithelia within the central nervous system (CNS) and retina. Despite the clinical relevance of glia for homeostasis in neural tissue, and as causal contributors in genetic disorders such as Alzheimer's and amyotrophic lateral sclerosis, efforts to develop more efficient gene delivery vectors for glia have met with limited success. Recently, viral vector engineering involving high-throughput random diversification and selection has enabled the rapid creation of AAV vectors with valuable new gene delivery properties. We have engineered novel AAV variants capable of efficient glia transduction by employing directed evolution with a panel of four distinct AAV libraries, including a new semi-random peptide replacement strategy. These variants transduced both human and rat astrocytes *in vitro* up to 15-fold higher than their parent serotypes, and injection into the rat striatum yielded astrocyte transduction levels up to 16% of the total transduced cell population, despite the human astrocyte selection platform. Furthermore, one variant exhibited a substantial shift in tropism toward Müller glia within the retina, further highlighting the general utility of these variants for efficient glia transduction in multiple species within the CNS and retina.

Introduction:

Glia play a number of critical roles in the central nervous system (CNS) and peripheral nervous system, including providing structural and nutritional support for neurons, maintaining tissue homeostasis, and participating in signal transmission in neural tissue [97, 98]. Given these natural roles, glia are an attractive therapeutic target, particularly because many regions of the brain possess significantly more glia than neurons [99], and since it is unlikely that neurons severely afflicted by disease or injury are the optimal source of secreted neuroprotective factors. Furthermore, dysfunction of astrocytes likely plays a significant role in the pathology of genetic diseases, including Alzheimer's [100] or amyotrophic lateral sclerosis [101], and reactive astrogliosis has been implicated as detrimental for neuroregeneration. Müller cells, the radial glial cells of vertebrate retina, react similarly to astrocytes in many ocular injuries, including retinal detachment and retinal neovascular disease.

To date, the use of viral vectors including adeno-associated virus (AAV) to transduce glia *in vivo* has met with limited success [86, 102-104], even when combined with glial-specific promoters[105]. AAV, a nonpathogenic virus in humans, is capable of robust systemic delivery [106] and exhibits a strong clinical safety profile [32, 72, 107]. Therefore, we sought to engineer an AAV variant for highly efficient gene delivery to glia.

AAV's single-stranded DNA genome has two open reading frames, including *cap*, which encodes for the structural proteins VP1-3 that assemble into the icosahedral viral capsid [45]. AAV vectors based on the capsids of the natural variants [67] mediate efficient gene delivery in a range of tissues [103, 108, 109]. However, within the brain and retina, natural AAV variants predominantly exhibit neuronal tropism [93, 96, 103, 110, 111], potentially due to inefficient uptake by astrocytes [112]. Some level of astrocyte transduction *in vivo* has been reported for AAV4 and AAV5 [103, 104, 110, 113], though AAV4 transduces astrocytes only within the subventricular zone, and reports of AAV5 transduction of astrocytes have been highly variable, potentially due to differences in vector production and promoter usage [111, 114]. Recently, AAV9 has been shown to transduce astrocytes via intravenous injection, though expression was observed in other tissues including heart and muscle [115].

Engineering the AAV capsid for targeted delivery based on the rational insertion of defined peptide sequences into the capsid has enjoyed some success [116-119]. As a complementary approach, we recently reported that directed evolution can successfully create AAV vectors with novel gene delivery properties [120], and this approach has since been extended to generate highly chimeric AAV variants by family shuffling [62, 121-123]. Here, we successfully merged numerous AAV library strategies to engineer novel AAV vectors for CNS and retinal gene therapy.

A panel of highly diverse ($>10^7$ members each) AAV libraries—generated by random mutagenesis, DNA shuffling, AAV peptide display, and a new semi-random loop replacement method—were selected via multiple evolutionary cycles, or genetic diversifications followed by selection on primary human astrocytes. In addition to

enhanced properties *in vitro*, several resulting variants efficiently transduced astrocytes at levels up to 5.5-fold greater than the parental serotypes in the rat striatum, and one vector additionally exhibited enhanced tropism for Müller cells in the retina. These novel vectors further demonstrate the utility of directed evolution for creating novel viruses and may enhance gene therapies for the treatment of numerous neurological disorders.

Materials and Methods:

Cell lines and viral production. Cell lines were cultured at 37 °C and 5% CO_2, and unless otherwise mentioned were obtained from the American type culture collection (Manassas, VA). Primary human astrocytes from the cerebral cortex (ScienCell, San Diego, CA) were cultured according to the manufacturer's instructions. AAV293 cells (Stratagene, La Jolla, CA), rat astrocytes (primary cells derived from adult rat brain), and the human glioblastoma cell line U87MG were cultured in Dulbecco's modified Eagle's medium. SHSY-5Y, a human neuroblastoma cell line, was cultured in minimum essential medium, alpha modification (αMEM) (Sigma-Aldrich, St Louis, MO). All media were supplemented with 10% fetal bovine serum (Invitrogen, Carlsbad, CA) and 1% penicillin/streptomycin (Invitrogen).

Library generation and viral production. Random mutagenesis libraries were generated by subjecting *cap* genes from AAV2 to error-prone PCR using CAP For and CAP Rev as forward and reverse primers, respectively, as previously described [120]. All primer sequences are provided in Supplementary Table 3a.S2. Peptide display libraries were generated similar to previous reports [118] [119]. Briefly, a unique *Avr*II was introduced into pSub2Cap2 between amino acid 587 and 588 by PCR mutagenesis. A random 21 nucleotide insert, 7mer For, was used to synthesize dsDNA inserts, along with the antisense primer 7mer Rev. The resulting dsDNA inserts were cloned into the *Avr*II site of pSub2Cap2 after digestion with *Nhe*I. A previously generated AAV library constructed by DNA shuffling of *cap* genes from AAV1, 2, 4–6, 8, and 9 was also used [121].

The novel random loop replacement libraries were constructed as follows (Figure 3a.2). First, sequences of 130 AAV *cap* genes were obtained from the GenBank database and aligned with BioEdit (www.mbio.ncsu.edu/BioEdit/bioedit.html). Positions within each wtAAV2 loop (Table 3a.1) were then analyzed for several characteristics: amino acid identity, charge, polarity, and hydrophobicity. Any feature contained within >90% of the sequences was then encoded into the new AAV2 loop sequence using defined or restricted codons. All other positions were then replaced by a random codon (NNK). Next, site-directed mutagenesis was used to introduce a stop codon (TAA) into each of the loops of interest within the AAV2 *cap* gene to generate four template plasmids and prevent carryover of wtAAV2 sequences into the final viral library. Spliced overlap extension was performed using two partial *cap* products: P1, which contains fully wtAAV2 sequence (using flanking forward and loop reverse primers), and P2, which contains a wtAAV2 anchor sequence to anneal with the 3′-end of P1 followed by the semi-randomized loop sequence and the remainder of the wtAAV2 sequence (using loop forward and flanking reverse primers). The resulting products were gel purified, and various molar ratios were used as templates for a second PCR using the flanking primers.

Primers used for the mutagenesis are provided in Supplementary Table 3a.S2. Finally, the resulting *cap* genes were cloned into pSub2 for replication competent AAV production [120].

The rcAAV libraries and rAAV vectors expressing GFP under a CMV promoter were packaged as previously described [120, 121]. DNase-resistant genomic titers were obtained via quantitative PCR, and transduction titers were obtained by flow cytometry.

Library selection and evolution. Primary human astrocytes (5×10^5) were infected with each viral library at a genomic multiplicity of infection of 10^3. Twelve hours after infection, the media were changed, and cells were infected with wt adenovirus to amplify successful AAV variants. Forty-eight hours later, cells were harvested and lysed to yield the viral pool for the next selection round. After four such rounds of selection, successful *cap* genes were recovered by PCR. The resulting pool of *cap* genes was subjected to DNA shuffling and EP PCR to generate a new library for the next selection rounds [120, 121]. In total, the AAV2 EP/7mer library and chimeric AAV library were subjected to two evolutionary cycles (*i.e.*, mutagenesis plus selection steps), and the random loop libraries were subjected to one evolutionary cycle.

In vitro transduction and cell-binding analysis. Transduction studies using rAAV CMV-GFP were performed with 5×10^4 cells (primary human astrocytes, rat astrocytes, U87MG, CHO, pgsD, and SHSY-5Y) in 12-well plates. Cells were transduced with rAAV GFP vectors at a genomic multiplicity of infection of 10^3–10^5 ($n = 3$), and the percentage of GFP-expressing cells was determined by flow cytometry 48 hours after infection. Viral-binding assays were performed as previously described[62].

In vivo characterization. ds rAAV vectors expressing GFP under a CAG promoter—composed of the CMV enhancer, chicken β-actin promoter, and rabbit β-globin intron[105]—were packaged with capsids from AAV2, AAV6, ShH13, ShH19, and L1-12 and purified using iodixanol gradient ultracentrifugation followed by heparin column purification as previously described[120]. rAAV vectors were stereotaxically injected into the striatum of the rat brain (AP, +0.2; ML, ±3.5; DV, −4.5 from skull) of adult female Fischer 344 rats (100 g, 6 weeks). The animals were anesthetized with ketamine (90 mg/kg animal) and xylazine (10 mg/kg animal) prior to injection, and 3 µl of high-titer AAV vectors (5×10^8 vg/µl) were injected using Hamilton syringe as described[124]. After 3 weeks, animals ($n = 4$ per vector) were transcardially perfused with 4% paraformaldehyde in phosphate- buffered saline, and the retrieved brains were postfixed by immersing in 4% paraformaldehyde overnight at 4 °C, with subsequently stored in 30% sucrose for cryoprotection before sectioning.

Coronal sections (40 µm) were cut using a freezing, sliding microtome. Cell phenotype was identified by the primary antibodies mouse-anti NeuN (1:200; Chemicon, Billerica, MA) and guinea pig-anti GFAP (1:1,000; Advanced ImmunoChemical, Long Beach, CA), and GFP expression was amplified using primary rabbit anti-GFP (1:2,000; Invitrogen). Corresponding secondary antibodies (labeled with AlexaFluor 488, 546, and 633) were used for detection. For nucleus staining, some sections were counterstained using TO-PRO-3 (1:2,000; Invitrogen). Animal protocols were approved by the UCB

Animal Care and Use Committee and conducted in accordance with National Institutes of Health guidelines.

rAAV6 and ShH13 were also injected subretinally into adult wt Sprague Dawley rats. Before vector administration, rats were anesthetized with ketamine (72 mg/kg) and xylazine (64 mg/kg) by intraperitoneal injection. An ultrafine 30½-gauge disposable needle was inserted through the sclera to create an entryway for a Hamilton syringe for subsequent injection of 3 µl of high-titer AAV vector (1×10^{12} vg/ml) between the retinal pigment epithelium and photoreceptor layer. Three weeks after vector injection, the eyes were enucleated, a hole was made in the cornea, and eyes were fixed in 10% neutral buffered formalin for 2–3 hours. The cornea and lens were removed, and the resulting eyecups were stored in 30% sucrose overnight. Eyes were then embedded in optimal cutting temperature embedding compound (OCT; Miles Diagnostics, Elkhart, IN) and oriented for making 5–10-µm thick transverse retinal sections using a freezing, sliding microtome. Müller glia were visualized using the primary antibody rabbit anti-glutamine synthetase (1:2,500; Sigma, St Louis, MO), and the corresponding Cy3-conjugated secondary antibody was used for detection. All procedures were handled according to the ARVO Statement for the Use of Animals and approved by the UCB Animal Care and Use Committee.

Results

Barriers in AAV gene delivery to astrocytes

We first determined the relative gene delivery efficiencies of seven AAV serotypes (1, 2, 4–6, 8, and 9) on primary human astrocytes (Figure 3a.1). Iodixanol-purified, high-titer recombinant AAV (rAAV) cytomegalovirus (CMV) –green fluorescent protein (GFP) vectors [121]were generated, and we found that the transduction efficiencies of the serotypes varied considerably, over a 500-fold range, with the following order: AAV2 > 1 = 6 = 9 > 5 > 4 > 8. Because high genomic multiplicity of infections ($>10^4$) were required to transduce >50% of the astrocytes even for the more efficient natural serotypes, and because all AAV variants are reportedly inefficient on glia *in vivo*[86, 93, 103, 110, 111], we next probed potentially limiting steps in AAV gene delivery to human astrocytes.

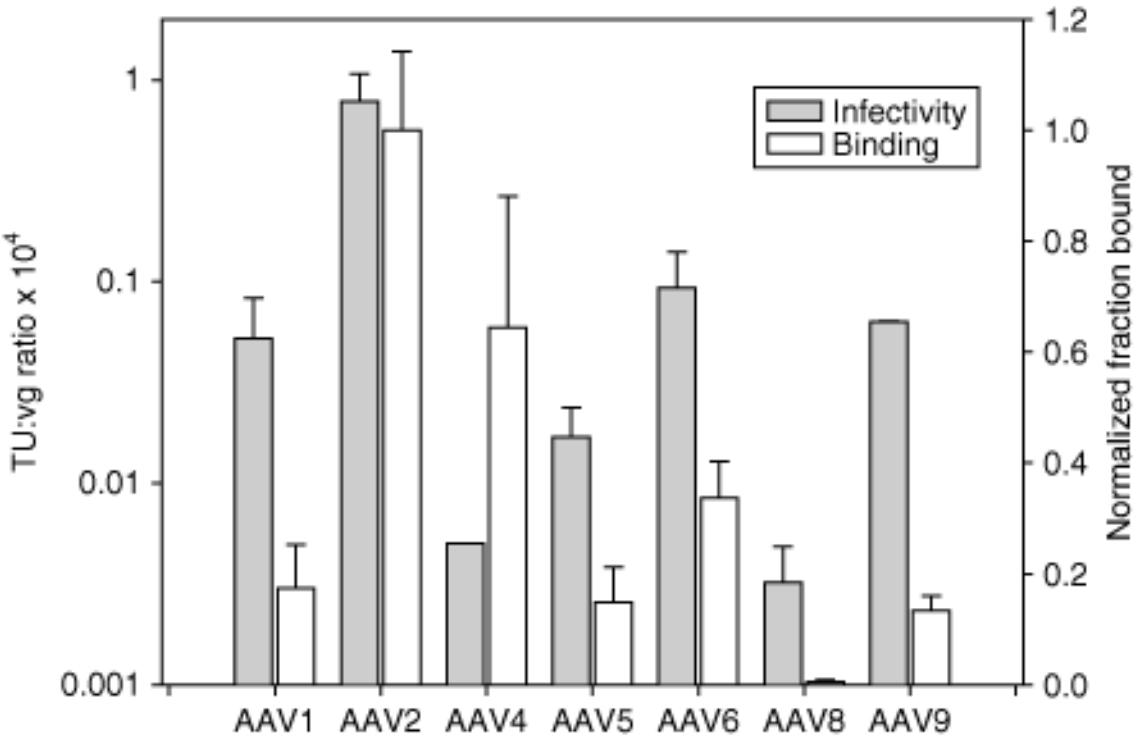

Figure 3a.1. Characterization of natural AAV serotypes. rAAV CMV-GFP vector transduction efficiencies (gray bars) on primary human astrocytes (gMOI = 10^3–10^5) using seven AAV serotypes (1, 4–6, 8, and 9) varied significantly (n = 3, error bars represent SD). Binding levels (white bars) of each serotype to primary human astrocytes matched the relative transduction efficiencies, except for surprisingly high binding levels of AAV4, which transduced primary human astrocytes poorly (n = 3, error bars represent SD). AAV, adeno-associated virus; CMV, cytomegalovirus; GFP, green fluorescent protein; gMOI, genomic multiplicity of infection.

We first quantified the relative-binding ability of several viral serotypes to astrocytes (Figure 3a.1). Intriguingly, the trend in viral binding (AAV2 > 4 > 6 > 1 = 5 = 9 > 8) closely matched that of viral transduction, except that AAV4 which bound almost as well as AAV2, was extremely poor in transducing astrocytes. The low transduction efficiency observed for AAV4 is thus due to a later step in viral infection, such as internalization or inefficient unpackaging [125]. Interestingly, treatment of astrocytes with the proteasome inhibitor MG132 or the genotoxic agent hydroxyurea—which reportedly overcome barriers in vector degradation and genome processing in some systems such as lung epithelium [126] —resulted in only modest (<1.5-fold) increases in GFP+ cells for all serotypes (data not shown). The data indicate that vector engineering may be required to achieve efficient transduction of astrocytes because even serotypes that bind efficiently to astrocytes (AAV2 and 4) fail to achieve high levels of gene delivery (Figure 3a.1).

Library construction

We conducted directed evolution of the AAV capsid to enhance astrocyte gene delivery using a panel of highly diverse (>10^7) viral libraries: an AAV2 random mutagenesis library (AAV2-EP) [120], a chimeric AAV library (ShH) [121], and an AAV2 peptide display library (AAV2 7mer) [118, 119]. In addition, we generated new AAV2-based libraries via a bioinformatics-based surface loop replacement strategy. Previously, peptide-based AAV2 capsid engineering studies have predominantly manipulated the surface loop containing the heparan sulfate proteoglycan (HSPG)–binding site (*i.e.*, ~^{585}RGNR~) [116-119]; however, recent studies of the AAV2 capsid have highlighted several other regions that significantly influence the transduction properties of AAV2 [121, 122, 127]. Therefore, we chose to engineer four important surface loops [128] (Table 3a.1 and Figure 3a.2).

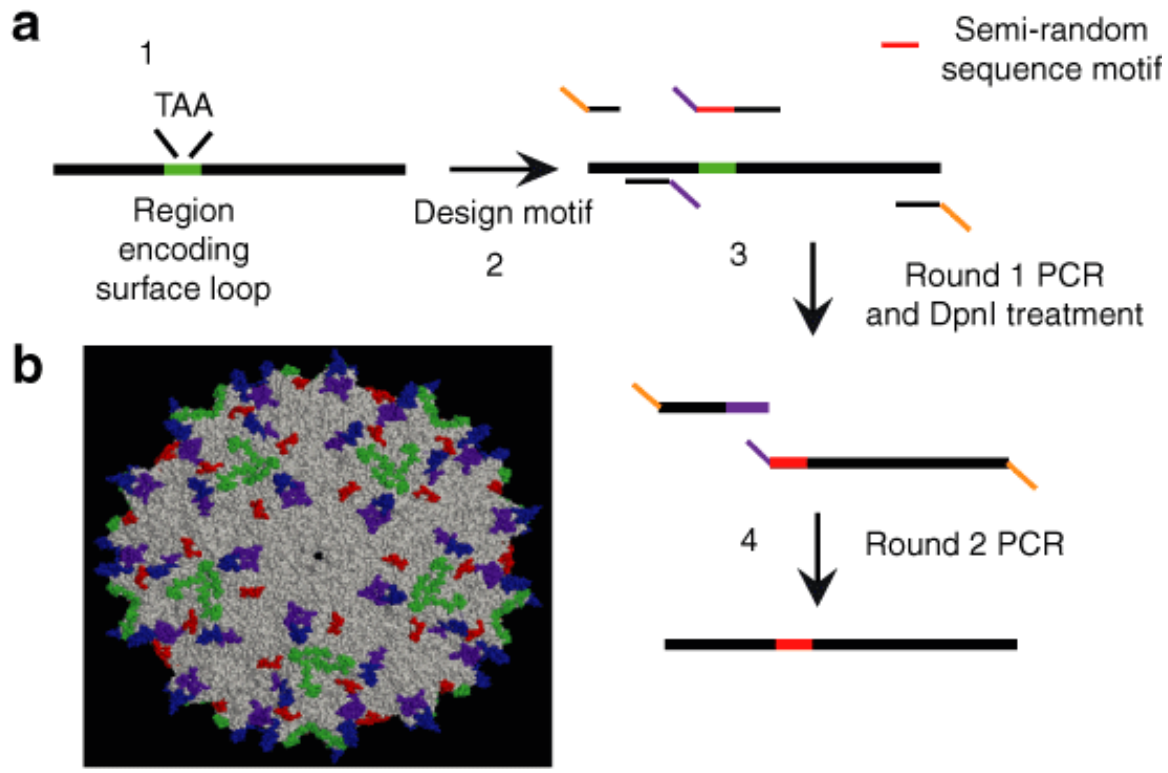

Figure 3a.2. Design of novel loop replacement library. (a) Library design consisted of introduction of a stop codon within the target loop sequence (1), semi-random motif design (2), an initial PCR round to amplify two overlapping fragments (3), and a final PCR to assemble the full-length *cap* gene containing the semi-random motif (4). (**b**) Four separate AAV2 libraries containing semi-random loops [L1, ~^{262}SQSGASN~ (purple); L2, ~^{446}SRTNTPSGTTTQSR~ (blue); L3, ~^{545}QGSEKTNVDIEK~ (red); and L4, ~^{585}RGNRQAATADVNT~ (green)] were constructed, with sequences determined through a bioinformatics analysis of AAV VP1 protein sequences. AAV, adeno-associated virus.

Clone	Loop sequence	Clone	Loop sequence
AAV2	~^{262}SQSGASN~	AAV2	~^{446}SRTNTPSGTTTQSR~
Motif	~$^{262}X_8$~	motif	~$^{446}XXTX_3(S/G)GX_6$~
L1-12	~^{262}SQDTQASN~	L2-14	~^{446}GSTLNSSGGNSKPF~
		L2-17	~^{446}SDTSRTGGDSASGS~
		L2-18	~^{446}SRTTICSGVGKCEG~
		L2-23	~^{446}GRTMVASGSGGLAQ~
AAV2	~^{545}QGSEKTNVDIEK~	AAV2	~^{585}RGNRQAATADVNT~
Motif	~$^{545}XX(A/S/T)X_3(N/D)XX(I/L)XX$~	motif	~$^{585}X_5(A/P)X_4VNX$~
L3-1	~^{545}EWTGCSDADIDE~	L4-2	~^{585}KGVRQATCDAVNT~
L3-6	~^{545}EWTGCSDDDIDE~	L4-3	~^{585}TYRKPADTDLVNT~
L3-7	~^{545}SGSSTSDLDIDS~	L4-7	~^{585}CKSAPPDWRAVNS~
L3-11	~^{545}DGATQRDRDLGE~	L4-9	~^{585}RNMRGPQSEEVNT~
L3-13	~^{545}AASGRDDVDLEG~	L4-23	~^{585}GLRRGPLAESVNC~
L3-20	~^{545}CTTGVGDLDLED~		

Abbreviation: AAV, adeno-associated virus.

Table 3a.1. Summary of loop regions within clones selected from AAV random loop libraries after a single round of evolution.

We replaced the wild-type (wt) AAV2 sequence with a semi-random sequence determined by bioinformatics analysis of 130 AAV *cap* genes obtained from the GenBank database. These loops include L1 (~^{262}SQSGASN~, purple in Figure 3a.2), L2 (~^{446}SRTNTPSGTTTQSR~, blue in Figure 3a.2), L3 (~^{545}QGSEKTNVDIEK~, red in Figure 3a.2), and L4 (~^{585}RGNRQAATADVNT~, green in Figure 3a.2). Specifically, the VP1 protein sequences were aligned to identify positions within these loops highly conserved either in amino acid identity or in chemical properties (*e.g.*, charge, polarity, hydrophobicity, etc.). For each loop, residues that were conserved in >90% of sequences were fixed, whereas amino acids whose identity was limited to one of several residues in >90% of the sequences were encoded with a restricted codon (*e.g.*, RGC for serine and glycine). Finally, all other residues were replaced with a random amino acid, encoded by an NNK codon. The resulting semi-random sequences (Table 3a.1) were introduced into the AAV2 *cap* gene using spliced overlap extension PCR. This library, which builds upon work conducted with the HSPG-binding site [116-119], is the first to explore and exploit the modular nature of numerous additional surface loops and to engineer highly

diverse libraries guided by bioinformatic analysis of many (>100) serotypes.

Selection and *in vitro* characterization of successful viral variants

One round of evolution consisted of initial library diversification followed by four or five selection steps. An *in vitro* selection approach with primary astrocytes from the adult human cerebral cortex was implemented. Briefly, 5×10^5 primary human astrocytes were infected with iodixanol-purified, replication-competent AAV libraries [120, 121] at a genomic multiplicity of infection of 10^3, and successful virions were amplified by the later addition of wt adenovirus type 5 to complete one round of selection. After five rounds of selection, preliminary characterization of individual rAAV CMV-GFP generated with capsid clones from the AAV2 EP, AAV2 7mer, and chimeric AAV libraries failed to reveal variants with enhanced gene delivery. Therefore, the *cap* genes from the AAV2 libraries (EP and 7mer) and the chimeric AAV library were pooled and further diversified using DNA shuffling and random mutagenesis. The resulting library was then subjected to four additional selection steps. Subsequent analysis of the mutants selected in this second round of evolution revealed several clones related to AAV2 and/or AAV6 that exhibited enhanced transduction of primary human astrocytes (two- to fivefold higher than wtAAV2 and tenfold higher than wtAAV6) (Figure 3a.3, Supplementary Figures 3a.S2 and 3a.S3). ShH13 was closely related to AAV6, whereas the others were based on AAV2 (Supplementary Figure 3a.S2). Some variants (ShH7, ShH14, ShH21, and 2H22) differ from the parent serotype by up to five mutations, whereas several variants (ShH13, ShH18, ShH19, and ShH22) are viral chimeras with capsid regions from several serotypes swapped into either AAV2 (ShH18, ShH19, and ShH22) or AAV6 (ShH13) scaffolds. Interestingly, no variants from the AAV2 7mer were found after the second evolutionary cycle.

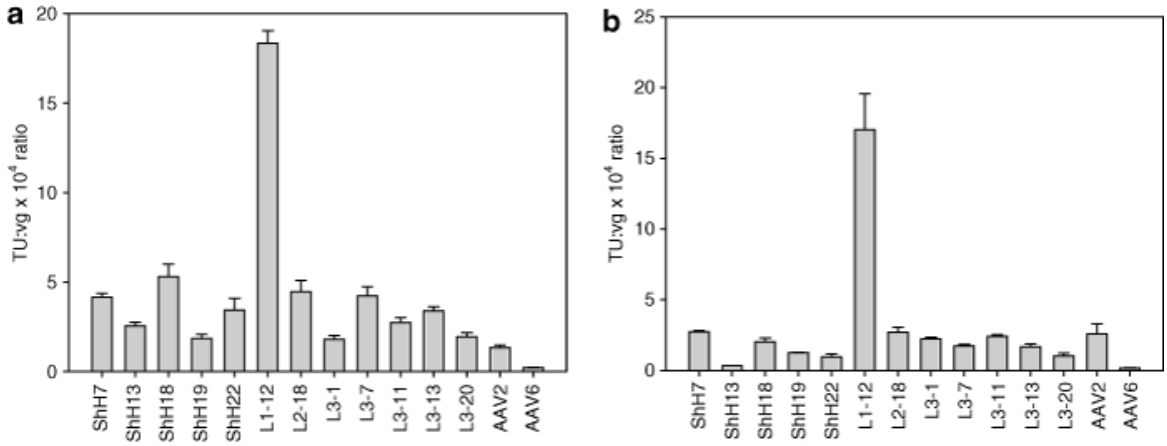

Figure 3a.3. Enhanced transduction of primary human astrocytes by novel AAV variants. (a) Transduction of primary human astrocytes by rAAV CMV-GFP vectors with capsids selected from the AAV EP, chimera, and random loop libraries demonstrated enhanced gene delivery by numerous viral variants ($n = 3$, error bars represent SD). (**b**) Transduction of SHSY-5Y neuroblastoma cells with rAAV CMV-GFP vectors revealed a decrease in transduction for most EP, chimera, and random loop variants, except for L1-

12 (*n* = 3, error bars represent SD). AAV, adeno-associated virus; CMV, cytomegalovirus; GFP, green fluorescent protein.

Clones isolated after a single round of evolution with the loop replacement libraries contained new L1, L2, or L3 regions and were more efficient on astrocytes (2- to 15-fold) relative to wtAAV2 (Figure 3a.3a, Supplementary Figure S3, and Table 3a.1). Furthermore, most of these new functional loops possessed very low sequence similarity to wtAAV2, demonstrating that these regions of the AAV2 capsid are highly modular. Intriguingly, some variants (L2-17, L3-6, L4-7, L4-9, and L4-23) exhibited considerable reductions in viral infectivity (more than tenfold), potentially due to the loss of important complementary interactions between some residues within these loops and structurally adjacent regions of the capsid.

To characterize the gene delivery properties of the selected variants further, we analyzed their relative transduction efficiencies on SHSY-5Y (a human neuroblastoma cell line). Interestingly, efficiencies for most of the viral variants were significantly less (two- to fivefold) than that of wtAAV2 (Figure 3a.3b), perhaps implying potential astrocytic selectivity compared to AAV2's strong neuronal tropism [103, 112]. Gene delivery efficiencies of these novel variants varied on other glial cells, including rat astrocytes (where ShH19 exhibited highest transduction levels) and U87MG glioblastoma cells (Supplementary Figure 3a.S4). Importantly, all of the AAV2-based variants exhibited HSPG dependencies similar to wtAAV2, except for two (L1-12 and L3-7) that were more dependent on HSPG than wtAAV2 (Supplementary Figure 3a.S5). Therefore, the enhanced transduction efficiencies of these AAV2-like mutants are likely due to improvements in either secondary receptor interactions or later stages of viral infection.

In vivo gene delivery of selected viral mutants

To further demonstrate the potential of these novel variants for *in vivo* gene delivery to astrocytes, we generated double-stranded (ds) AAV vectors expressing GFP under the control of the hybrid CAG (CMV early enhancer/chicken β-actin) promoter, which has been shown to mediate more robust gene expression within the CNS, and in particular within astrocytes, than the CMV promoter [105, 110, 111]. Capsids from the most efficient human astrocyte variant (L1-12), the most efficient rat astrocyte variant (ShH19, Supplementary Figure 3a.S4), the AAV6-like variant (ShH13), and the corresponding control parent serotypes AAV2 and AAV6 were analyzed. High-titer rAAV dsCAG-GFP vectors were purified via the same method (iodixanol gradient ultracentrifugation followed by heparin affinity chromatography), to avoid differences in vector purity that have been implicated in altering astrocyte transduction *in vivo* [111].

A volume of 3 µl DNase-resistant genomic particles (5×10^8 vg) were stereotactically injected into striatum of female rats, and all AAV variants and control serotypes exhibited robust GFP expression 3 weeks after injection (Figure 3a.4). For all variants and serotypes, >99.5% of the GFP+ cells were either NeuN+ or GFAP+, with minimal transduction of other cell types, such as microglia (data not shown). Similar to previous reports utilizing the CAG promoter [110, 114], wtAAV2 transduced astrocytes

infrequently (2.7 ± 1.8%), whereas wtAAV6 mediated somewhat higher gene delivery to astrocytes (8.4 ± 1.6%). ShH13 transduction of astrocytes was not significantly higher than wtAAV6. In contrast, the AAV2-like variants ShH19 and L1-12 transduced 5.5-fold (14.9 ± 3.0%) and 3.3-fold (9.0 ± 3.0%) greater numbers of astrocytes, respectively, compared to wtAAV2. Furthermore, these enhanced transduction levels may further increase when utilized in a human, as the selections were performed with primary human cells. To explore further the utility of these variants in glia *in vivo*, we injected recombinant variants into the subretinal space in rat eyes to observe their efficiency in infecting a glial subtype within the retina, Müller cells. Three weeks after injection, observation of GFP expression revealed that ShH13 exhibited the most pronounced shift in tropism toward glia, with expression localized predominantly to Müller cells and retinal pigment epithelium, while its parent vector AAV6 showed much lower GFP expression and primarily within photoreceptors and the retinal pigment epithelium (Figure 3a.5).

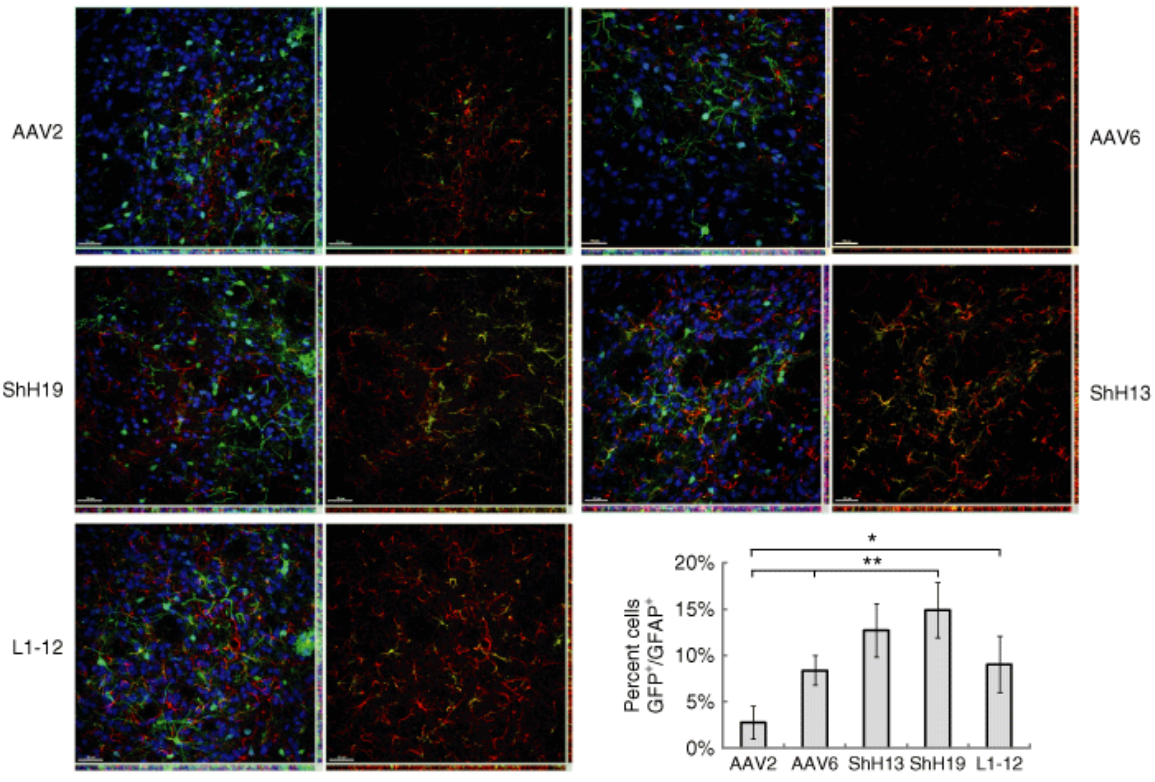

Figure 3a.4. Enhanced *in vivo* astrocyte tropism of evolved AAV variants. Representative images of coronal brain sections 3 weeks after injection with dsCAG-GFP vectors using capsids from AAV2, AAV6, ShH13, ShH19, and L1-12 show robust levels of GFP expression (green). Representative images (original magnification ×25) of cell types reveal enhanced astrocyte transduction levels by ShH19 ($P < 0.01$ compared to AAV2/6), and L1-12 ($P < 0.02$ compared to AAV2) compared to the parent AAV2 and AAV6 vectors: GFP+ cells (green), NeuN+ neurons (blue), and GFAP+ astrocytes (red). For each variant, the image on the right indicates areas of colocalization between GFP

and GFAP (yellow). The corresponding x-z and y-z planes are shown on the bottom and on the right side, respectively, for each image. Bar = 50 µm. Quantified percentage of astrocytes transduced (GFP+/GFAP+) within the total GFP+ cell population (n = 4, error bars represent SD). For each vector, over 950 GFP+ cells were counted and analyzed for costaining with either NeuN (neuron) or GFAP (astrocytes). AAV, adeno-associated virus; GFP, green fluorescent protein.

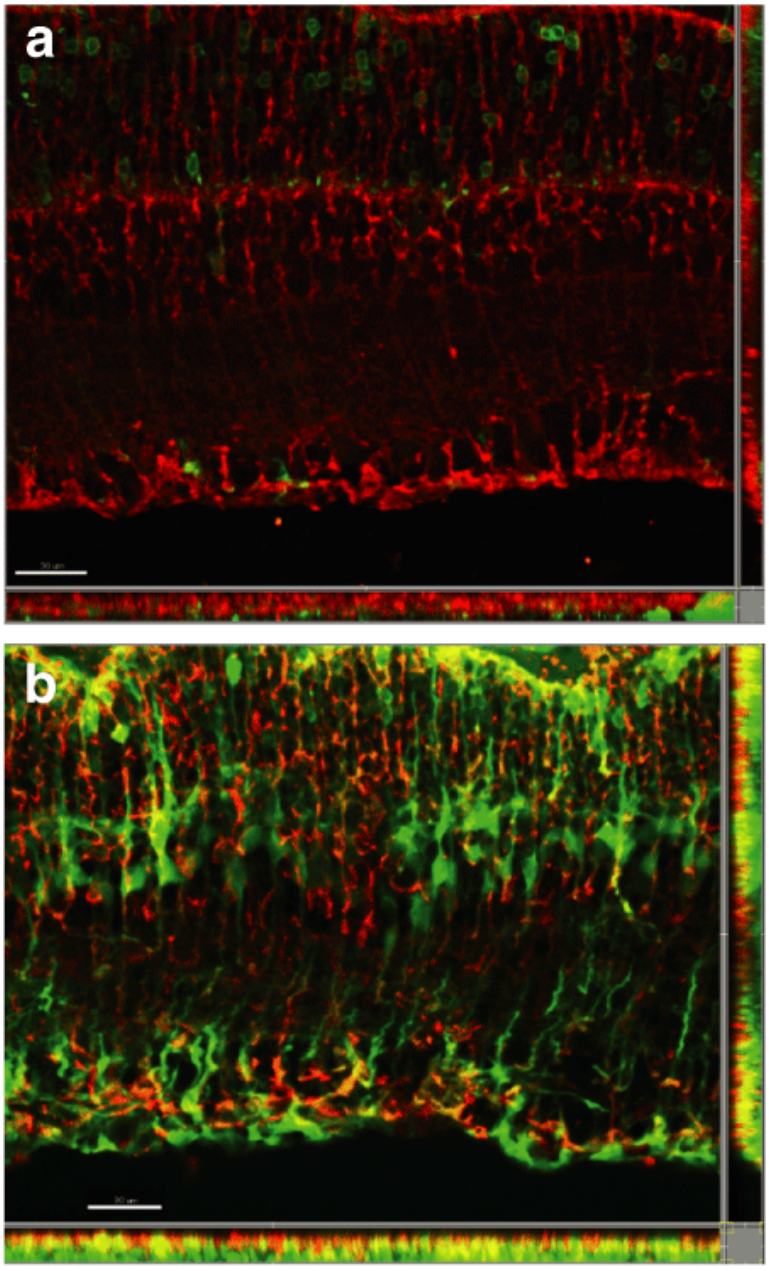

Figure 3a.5. Enhanced transduction of retinal Müller glia *in vivo* by ShH13. Representative images (original magnification ×25) of subretinal injections with dsCAG-GFP vectors with capsids from ShH13 and AAV6 reveal a pronounced shift in viral tropism toward Müller glia in the ShH13 variant compared to the parent AAV6 vector:

GFP expression (green), overlay with GS+ Müller glia (red), isolation of areas of colocalization (yellow). The corresponding x-z and y-z planes are shown on the bottom and on the right side, respectively, for each image. Bar = 30 μm. (a) AAV6 expression is predominantly seen in photoreceptors and RPE (not shown), whereas (b) ShH13 shows robust expression in Müller glia and RPE (not shown). AAV, adeno-assocaited virus; RPE, retinal pigment epithelium.

Discussion

Glia are a potentially important therapeutic target within the CNS and retina, either to counteract disease pathology directly involving these cells or to harness them to secrete therapeutic proteins and thereby protect neighboring neurons from injury or disease. Most current AAV serotypes fail to efficiently transduce astrocytes or Müller glia *in vivo*, and even serotypes such as AAV4 and AAV5 that can infect astrocytes either transduce only a subset within a specific brain region (the subventricular zone for AAV4) [104]or exhibit variable efficiencies (AAV5) [103, 110]. Additionally, recent work in the retina utilizing AAV vectors that are more resistant to proteasome-mediated degradation resulted in greatly improved efficiencies, yet still relatively low gene delivery to Müller glia [93]. Accordingly, we have employed directed evolution to engineer a novel AAV vector capable of efficient gene delivery to astrocytes and potentially other glia cells. Furthermore, while the selections were performed on human cell *in vitro*, the resulting variants exhibited enhanced infection of astrocytes upon injection into the rat striatum (ShH19 and L1-12) (Figure 3a.4) or Müller glia within the rat retina (ShH13) (Figure 3a.5), making them attractive candidates for future studies in disease models. These results suggest that directed evolution coupled with stringent selections can engineer novel capsid variants that can effectively transduce related cells across multiple species.

Barriers to efficient AAV gene delivery—such as poor binding, proteasome degradation, and genome processing—vary greatly among cell types [116, 118, 119, 126]. Our results indicate that while efficient cell binding is likely one such barrier present within astrocytes, downstream barriers may also play a significant role as evidenced by the binding results for AAV4 (Figure 3a.1) and the improved efficiencies of numerous AAV2- and AAV6-based variants with similar HSPG dependencies as their parents (Supplementary Figure 3a.S5). Of particular note, a previous study using fluorescently labeled AAV2 failed to detect any significant viral uptake in astrocytes [112], reflecting poor internalization of AAV2, potentially due to inefficient interactions with secondary protein receptors that facilitate receptor-mediated endocytosis [127]. Importantly, while a lack of detailed mechanistic knowledge of specific gene delivery barriers in this and other cases can preclude rational design strategies to improve vector properties, a broader “black box” approach to engineer efficient AAV vectors through random diversification and high-throughput selection can still succeed.

Recent efforts in AAV capsid engineering [121, 122, 129] have suggested that certain loop regions may be highly modular and may therefore enable functional loop swapping methods among various serotypes. Based on these observations, we developed

a new semi-random loop replacement strategy for the engineering of novel vectors. Strikingly, after four rounds of selection, many of these variants, which contained new loop sequences of up to 14 amino acids in length, demonstrated enhanced levels of gene delivery (Figure 3a.3a). For example, replacement of loop 2 (L1, ~^{262}SQSGASN~) of wtAAV2 (shown in purple in Figure 3a.2b) with an octamer sequence, analogous to the size of wtAAV6, yielded clones with improved gene delivery efficiencies on a panel of cell types (Figure 3a.3, Supplementary Figures 3a.S4 and 3a.S5). This loop—whose length in natural serotypes varies from four (AAV4, AAV11, and AAV12) to eight (AAV1, AAV5, AAV6, and AAV9) amino acids—modulates the tropism of AAV vector, potentially via interactions with secondary protein receptors [121,127].

Our loop-engineering strategy focused on identifying residues that are conserved among the serotypes. However, it does not detect amino acid positions that may have coevolved with other positions within a given serotype, due for example to physical contact between a loop and another region in the tertiary or quaternary structure of the capsid, but whose identity may not be strictly conserved from serotype to serotype. For instance, this approach initially considered amino acid 553 within L3 as random; however, all six selected clones retained the aspartic acid of wtAAV2 at this location. Within the AAV2 capsid structure [128], D553 (within L3) forms an ionic interaction with R459 (within L2), which may help stabilize these two capsid loops and ensure proper capsid assembly. Similar analysis of the selected L2 sequences revealed the retention of a hydrogen bond acceptor (serine) or basic residue (arginine) at the randomized amino acid position 447 (R for wtAAV2), which interacts with both E499 and N551. Future refinement in this approach may incorporate information regarding key structural contacts [128, 130, 131] to aid the engineering of novel AAV vectors with customized gene delivery properties.

Analysis of the novel AAV2 and AAV6 variants yields several interesting insights. Within the AAV2-like clones, mutations N496H, located at the apex of the threefold axis of symmetry, and Q598L, located within the crater at the threefold axis, may play a role in the enhanced transduction (Figure 3a.3, Supplementary Figures 3a.S2 and 3a.S3). These sites may thus represent new targets for vector engineering. Interestingly, none of the mutations in the AAV6-based mutant ShH13 is predicted to be surface-exposed, and these changes may thus indirectly alter receptor binding via modulating the surface structure of the viral capsid, or alter later infection steps such as intracellular trafficking or vector unpackaging. For example, one such interior mutation (F129L) lies within the VP1-unique region but does not overlap with previously identified functional domains within VP1[132]. In a recent directed evolution study, we demonstrated that changes within this region can significantly enhance the gene delivery properties of the evolved variant, potentially due to changes in endosomal escape of the virus [62]. Finally, the most efficient AAV variants *in vivo* (ShH19 and L1-12) acquired very similar loop 2 sequences (SQDTQASN and SASTGASN for L1-12 and ShH19, respectively, compared to SQSGASN for wtAAV2, shown in purple in Figure 3a.2b) through distinct methods (*i.e.*, shuffling for ShH19 and loop replacement for L1-12) [121, 127]. Together, these results highlight how exploring complementary yet distinct libraries can reveal key common features (*i.e.*, capsid regions) that may be exploited in future directed evolution experiments.

The ability of ShH13 to transduce two glia cell types, astrocytes and Müller cells, suggests a common mechanism for the improved gene delivery. Müller glia possess apical-basal polarity, and many astrocytes also retain some features of this polarity [133]. In epithelial cells, cell polarity has previously been shown to result in inefficient trafficking of AAV to the nucleus [126], and an analogous nonproductive infection may occur within some glia. ShH13, which contains only mutations on the interior of the capsid and within the VP1-unique region, may exhibit enhanced transport through the cytoplasm through altered PLA_2 activity [62, 132]. Alternatively, the variant could utilize a receptor more highly expressed in astrocytes and Müller cells relative to the surrounding neuronal cells, such as epidermal growth factor receptor or fibroblast growth factor receptor 3 [134, 135].

In summary, by employing directed evolution with a diverse array of novel AAV libraries including a new peptide loop replacement library, we engineered novel AAV vectors capable of highly efficient delivery to astrocytes *in vitro* and importantly to astrocytes and Müller glia *in vivo*. These AAV capsids in conjunction with cell-specific promoters, such as GFAP, and other recently identified capsid mutations [93] may yield further enhancements in the targeted gene delivery to astrocytes and Müller glia to treat a variety of genetic diseases. For example, modulating mutant superoxide dismutase-1 expression within astrocytes may reduce neuronal cell death in amyotrophic lateral sclerosis [101], or therapeutic gene delivery may prevent the accumulation of amyloid β-plaques in Alzheimer's disease [100]. Furthermore, because Müller cells span the entire retina and surround every class of neuron present within this tissue, transduction of Müller cells would permit spread of neurotrophic factors throughout all layers of this tissue to significantly augment existing therapies for retinitis pigmentosa, age-related macular degeneration and neovascularization [32, 41, 107]. These novel capsids may thus endow AAV vectors with the capacity to treat a variety of neurodegenerative disorders in disease models and ultimately in the clinic.

Chapter 3b

A Novel Adeno-associated Viral Variant for Efficient and Selective Intravitreal Transduction of Müller Cells

Preface:

This work was done in collaboration with Dr. James T. Koerber, a graduate student in the Schaffer Lab at UC Berkeley, as well as Dr. Deniz Dalkara, a post-doctoral fellow in the Flannery lab. Kate Kolstad, a graduate student in the Flannery lab, and Karen Guerin, a post-doctoral fellow in the Flannery lab, assisted with retinal injections. Joshua Loya and Christin Hong, undergraduates at UC Berkeley, assisted with immunostaining and quantitative analysis. Murine data was generated in collaboration with Dr. Lucie Pellissier, a post-doctoral fellow in Dr. Jan Wijnhold's lab at the Netherlands Institute for Neuroscience (NIN).

This chapter has been published in the journal *PLoS ONE*. Klimczak RR, Koerber JT, Dalkara D, Flannery JG, Schaffer DV (2009) A novel adeno-associated viral variant for efficient and selective intravitreal transduction of rat Müller cells. PLoS ONE 10: e7467.

Abstract:

The pathologies of numerous retinal degenerative diseases can be attributed to a multitude of genetic factors, and individualized treatment options for afflicted patients are limited and cost-inefficient. In light of the shared neurodegenerative phenotype among these disorders, a safe and broad-based neuroprotective approach would be desirable to overcome these obstacles. As a result, gene delivery of secretable-neuroprotective factors to Müller cells, a type of retinal glia that contacts all classes of retinal neurons, represents an ideal approach to mediate protection of the entire retina through a simple and innocuous intraocular, or intravitreal, injection of an efficient vehicle such as an adeno-associated viral vector (AAV). Although several naturally occurring AAV variants have been isolated with a variety of tropisms, or cellular specificities, these vectors inefficiently infect Müller cells via intravitreal injection. We have previously applied directed evolution to create several novel AAV variants capable of efficient infection of both rat and human astrocytes through iterative selection of a panel of highly diverse AAV libraries. Here, in vivo and in vitro characterization of these isolated variants identifies a previously unreported AAV variant ShH10, closely related to AAV serotype 6 (AAV6), capable of efficient, selective Müller cell infection through intravitreal injection. Importantly, this new variant shows significantly improved transduction relative to AAV2 (>60%) and AAV6. Our findings demonstrate that AAV is a highly versatile vector capable of powerful shifts in tropism from minor sequence changes. This isolated variant represents a new therapeutic vector to treat retinal degenerative diseases through secretion of neuroprotective factors from Müller cells as well as provides new opportunities to study their biological functions in the retina.

Introduction:

As a therapeutic device, adeno-associated viral (AAV) mediated ocular gene therapy holds tremendous promise for treating and potentially curing a variety of inherited retinal degenerative diseases, such as glaucoma, age-related macular degeneration (AMD), retinitis pigmentosa, and other blinding diseases. The therapeutic potential of AAV-mediated gene delivery to the retina has best been illustrated by the positive results from three phase I clinical trials for Leber's Congenital Amaurosis (LCA), a rare autosomal recessive blinding disease caused by loss of function mutations in the visual cycle enzyme retinol isomerase (RPE65) required to synthesize 11-cis retinal [32, 72, 107]. Gene-replacement therapy employing an AAV vector (rAAV) bearing a functional copy of the RPE65 gene in patients afflicted with the null mutant RPE65 resulted in significant improvements in visual function with no observable toxicity. These clinical trials clearly lay the foundation for AAV in retinal gene therapy, providing the first example of successful gene therapy with long-term safety and amelioration in visual function. Moreover, these results set the stage for the application of AAV-mediated gene delivery towards other retinal degenerative diseases.

Importantly, genetic heterogeneity is a key feature of retinal degeneration conditions, and to date, over 130 genes with mutations causing one or more forms of inherited orphan retinal degenerative diseases have been cloned, and over 50 more have been identified based on candidate gene studies or linkage mapping (http://www.sph.uth.tmc.edu/retnet). This large genetic heterogeneity, leading to a common phenotype of photoreceptor cell death, suggests that a mutation-independent neuroprotective strategy may be the most practical solution to a clinical treatment. Therefore, there is a strong need for a simple, safe, and broad-based ocular gene delivery strategy that provides sustained production of a neuroprotective or anti-angiogenic therapeutic for these conditions.

Several viral vector systems have been evaluated for ocular gene delivery; however, AAV offers distinct advantages in safety, stability, and efficiency. AAV belongs to the *Parvoviridae* family and Dependovirus genus, whose members require co-infection with a helper virus such as adenovirus to promote replication, and AAV establishes a latent infection in the absence of a helper [66]. Virions are composed of a 25 nm icosahedral capsid encompassing a 4.9 kb single-stranded DNA genome [128] with two open reading frames: *rep* and *cap*. The non-structural *rep* gene encodes four regulatory proteins essential for viral replication, whereas *cap* encodes three structural proteins (VP1–3) that assemble into a 60-mer capsid shell. This viral capsid mediates the ability of AAV vectors to overcome many of the biological barriers of viral transduction– including cell surface receptor binding, endocytosis, intracellular trafficking, and unpackaging in the nucleus [112, 136, 137]. In addition, the capsid diversity found among natural AAV variants, or serotypes, isolated from human and nonhuman primate tissues accounts for its diverse tropisms, as AAV has been shown in animal models to deliver genes to cells in numerous tissues including the retina, brain, muscle, and lung [81, 138-140]. As some AAV serotypes bind to glycans for receptor-mediated cellular entry, this variety is in part based on the varying glycan dependences found among AAV serotypes. AAV2 shows strong dependence on heparan sulfate proteoglycans (HSPG) for

transduction, whereas AAV1, 5, and 6 are dependent on N-linked sialic acids [66, 69, 128].

Subretinal administration of many of these AAV variants has led to efficient gene expression in a number of retinal neurons and epithelia, including photoreceptors and RPE [93, 141], and it is thus the injection route employed by current clinical therapies to achieve sufficient transduction for rescue [32]. However, this surgical approach requires creating a retinotomy (a hole through the neurosensory retina) and mechanically detaching the photoreceptor layer from its underlying supportive epithelium (RPE) through injection of an AAV fluid suspension, generating a "bleb". The resulting retinal detachment has had documented damaging effects, triggering cellular stress response pathways, reactive gliosis, retinal disorganization, photoreceptor degeneration, and functional losses in vision [50, 51]. In retinas compromised by degeneration, the effects of this detachment would only be further magnified [142]. Additionally, as degeneration occurs throughout the retina in most retinal diseases, use of a focal delivery and treatment strategy via subretinal injection into a specific region is not optimal because only cells within the "bleb" are transduced [35, 53, 54]. An intravitreal injection technique, whereby virus is administered directly into the vitreous of the eye, presents a more innocuous and simple approach for gene delivery to the retina, and it allows for a broader area of retinal transduction since the vitreous contacts the entire underlying retinal surface. Intravitreal injection is already routinely used clinically to administer anti-vascular endothelial growth factor (anti-VEGF) antibody for the treatment of AMD [143].

Despite these benefits, intravitreal injections pose significant challenges. First, dilution of vector into the vitreal fluid leads to lower vector concentrations compared to subretinal injections, a particular concern for larger mammals. However, intravitreal vector administration into macaque eyes showed that AAV is still able to overcome this challenge and lead to retinal transduction [144]. An additional consideration is that the increase in vitreous viscosity in humans above the age of 40 could impair the diffusion of the virus in older patients' vitreous, though this concern is potentially offset by an increase in liquid vitreous localized directly in front of the retina [145]enabling one to inject into this fluid region and avoid the more viscous vitreous gel. In addition to these vitreal fluid barriers, treating photoreceptor degeneration in early stages of disease progression using gene delivered neurotrophic factors requires high efficiency vectors, but intravitreal injection of conventional AAV serotypes cannot mediate sufficient expression of these factors in proximity to the photoreceptors undergoing degeneration in the outer nuclear layer of the retina to achieve effective rescue of retinal function [146]. Infecting Müller glia, a cell that is accessible from the vitreous and transverses the entire thickness of the retina, would be ideal to mediate expression of secreted neurotrophic or anti-angiogenic factors throughout all layers of the retina (Figure 3b.1).

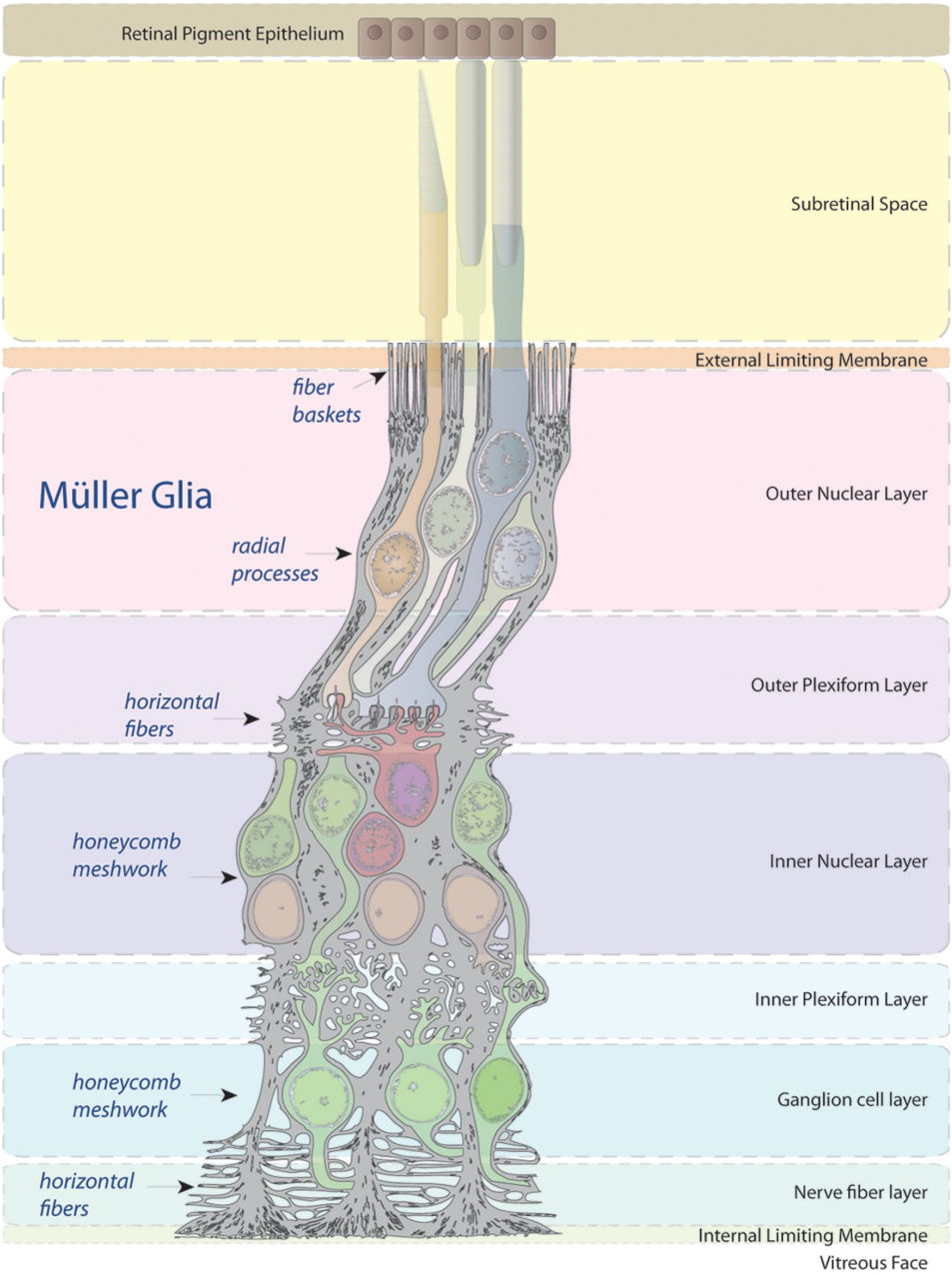

Figure 3b.1. Müller glia in the retina. Illustration of Müller glia spanning the entire retina, where they ensheath all neuronal types from retinal ganglion cells (RGC) (bottom) to the photoreceptors. Modified from Histology of the Human Eye, an Atlas and Textbook. Hogan, Michael J., Jorge A. Alvarado, Joan Esperson Weddell. Philadelphia: W. B. Saunders, 1971.

Müller cells serve numerous, significant physiological functions in the retina including but not limited to: metabolic support of neurons, K^+ and water homeostasis, free radical scavenging and oxidative protection, neurotrophic secretion, and neurotransmitter and retinoid uptake and recycling [147]. They are thus in many ways analogous to astrocytes in the central nervous system (CNS), sharing many of the same cellular properties [148, 149]. Moreover, because Müller cells can survive under

neurodegenerative conditions, they may mediate independent protection of the entire retina for a more extended period compared to a transduced damaged or dying neuron impacted by one of these diseases. As such, they represent an ideal candidate for viral gene therapy for secretion of neuroprotective factors.

Recently, the efficiency of this approach has been demonstrated as Müller cell secretion of neurotrophin-4 (NT-4) was shown to protect photoreceptors from oxidative stress in a mouse model of neovascularization through intravitreal injection [150]. However, the therapeutic effect of this approach can be enhanced using a more efficient AAV variant, as current AAV serotypes are limited in their efficiency and specificity for intravitreal Müller transduction [146, 150]. An AAV variant with greater Müller cell specificity would also allow the use of fewer viral particles to achieve the desired levels of expression and reduce the potential for ectopic transfection, important considerations to minimize the immune response to capsid proteins [93, 151].

Recently, we applied directed evolution to select variants from combinatorial libraries that demonstrate a diverse range of cellular tropisms *in vitro* and *in vivo* relative to their parent serotypes as well as variants with enhanced permissivity to astrocytes *in vivo* through selection in primary human astrocytes [141, 121]. Here, we further explore the utility of these astrocyte-permissive variants for intravitreal administration in the retina and identify a new AAV variant with enhanced and specific intravitreal Müller cell transduction *in vivo*. Efficient and specific intravitreal transduction of Müller cells by this vector will permit the development of more innocuous and effective treatments for retinal degenerative conditions through panretinal secretion of neuroprotective or anti-angiogenic factors, as well as new approaches to investigate fundamental questions in the biological role of this cell type in the retina.

Materials and Methods:

Generation of rAAV vectors Vectors were produced by the plasmid co-transfection method [141], and the resulting lysates were purified via iodixanol gradient ultracentrifugation as previously described [121]. This fraction was then passed through a heparin column, which was washed with 5 mL PBS and eluted with 5 mL of a 1 M NaCl solution. The resulting viral fractions were desalted and concentrated with Amicon Ultra-15 Centrifugal Filter Units to a final volume of 200 µl. Vector was then titered for DNase-resistant vector genomes by real time PCR relative to a standard.

Intraocular administration routes Adult wild type Spaque Dawley rats were used for all studies. All animal procedures were conducted according to the ARVO Statement for the Use of Animals and the guidelines of the Office of Laboratory Animal Care at the University of California, Berkeley. Before vector administration, rats were anesthetized with ketamine (72 mg/kg) and xylazine (64 mg/kg) by intraperitoneal injection. An ultrafine 30 1/2-gauge disposable needle was passed through the sclera, at the equator and next to the limbus, into the vitreous cavity. Injection of 5 µl, containing $1-5\times10^{12}$ vg/ml of AAV dsCAG-GFP, was made with direct observation of the needle in the center of the

vitreous cavity.

Fundus photography Fundus imaging was performed one to eight weeks after injection with a fundus camera (Retcam II; Clarity Medical Systems Inc., Pleasanton, CA) equipped with a wide angle 130° retinopathy of prematurity (ROP) lens to monitor eGFP expression in live, anesthetized rats. Pupils were dilated for fundus imaging with phenylephrine (2.5%) and atropine sulfate (1%).

Cryosections One to eight weeks after vector injection, rats were humanely euthanized, the eyes were enucleated, a hole was introduced in the cornea, and tissue was fixed with 10% neutral buffered formalin for 2–3 hours. The cornea and lens were removed. The eyecups were washed in PBS followed by 30% sucrose in the same buffer overnight. Eyes were then embedded in optimal cutting temperature embedding compound (OCT; Miles Diagnostics, Elkhart, IN) and oriented for 10 µm thick transverse retinal sections.

Immunolabeling and histological analysis Tissue sections were rehydrated in PBS for 5 min, followed by incubation in a blocking solution of 1% BSA, 0.5% Triton X-100, and 2% normal donkey serum in PBS for 2–3 hours. Slides were then incubated with commercial monoclonal antibodies raised against glutamine synethetase in rabbit (Sigma G2781) at a 1:3000 dilution, calbindin (Abcam ab11426-50) in rabbit at a 1:1000 dilution, vimentin in mouse (Dako M0725) at a 1:1000 dilution, or laminin in rabbit (Sigma, L9393) at 1:100 in blocking solution, overnight at 4°C.

The sections were then incubated with Cy3-conjugated secondary anti-rabbit or anti-mouse antibody (Molecular Probes) at a 1:1000 dilution in blocking solution for 2 hours at room temperature. The results were examined by fluorescence microscopy using an Axiophot microscope (Zeiss, Thornwood, NY) equipped with a Xcite PC200 light source and QCapturePro camera or a confocal microscope (LSM5; Carl Zeiss Microimaging). Transduction profiles were analyzed by counting individual cells from whole retinas in 15 µm cryosections (n = 6) using fluorescence microscopy. Efficiencies were calculated by dividing the total number of these transduced Müller cells by the total number of Müller cells in the retinal slice (mm) in which these cells were present (n = 6).

***In Vitro* Transduction Analysis** Transduction studies using rAAV CMV-GFP were performed with 5×10^4 cells (CHO, pgsA, Pro5, and Lec1) in 12-well plates. Cells were transduced with rAAV GFP vectors at a gMOI of 10^3–10^5 (n = 3), and the percentage of GFP-expressing cells was determined by flow cytometry 48 hours post-infection.

Results:

In vivo characterization of Müller cell permissive variants

We recently evolved several novel AAV capsids that efficiently transduced both primary human astrocytes *in vitro* and rat astrocytes *in vivo* using highly diverse AAV

libraries (>10^7) [141]. These variants were generated via multiple evolutionary rounds (i.e. diversification followed by positive selection for enhanced astrocyte transduction *in vitro*) with several distinct libraries: (1) an AAV2 random mutagenesis library generated via error prone PCR [120], (2) a random chimera AAV library generated by shuffling the *cap* genes of 7 natural human and non-human AAV serotypes [121], and (3) a novel AAV2 library with surface-exposed loops of the capsid library diversified based on a bioinformatics approach[141].

Due to the shared properties between astrocytes and Müller cells, we decided to explore the utility of these variants for intravitreal transduction of Müller cells. Here, the eight isolated mutants that demonstrated the greatest *in vitro* astrocyte infectivity (Supplemental Figure 3b.1, [141]) were individually analyzed for the ability to transduce the rat retina from the vitreous using double-stranded (ds) AAV CAG-GFP vectors purified via iodixanol gradient ultracentrifugation and heparin affinity chromatography. Intravitreal injections of 2.5×10^{10} genomic particles revealed one previously unreported variant named ShH10, derived from an AAV6 parent serotype from the shuffled (ShH) library, that showed a dramatic increase in specificity and efficiency for Müller cells relative to controls at three weeks post-injection (Figures 3b.2, 3b.3). Interestingly, no other mutants demonstrated visible expression as determined by GFP fundus imaging and immunohistochemistry (data not shown).

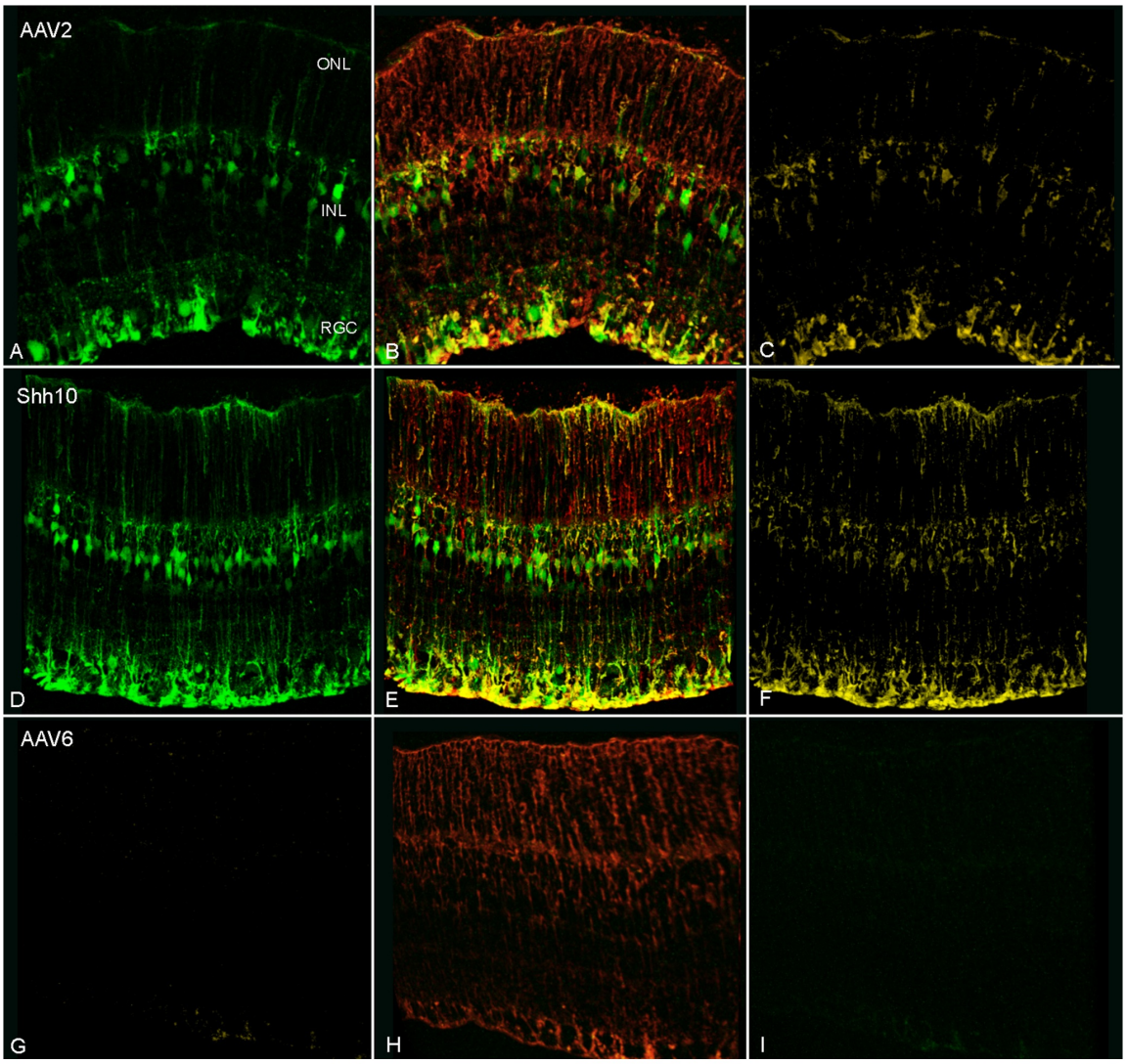

Figure 3b.2. rShH10 expression following intravitreal injection in the adult rat retina. Confocal imaging of immunostained transverse retinal sections 3 weeks post-injection of 2.5×10^{10} viral particles (vector genomes) of dsCAG-GFP vectors with capsids from AAV2 (A–C), ShH10 (D–F), and AAV6 (G–I) (n = 6). Glutamine synthetase (GS) staining (red) (B,E,H) and visualization of colocalization (C,F,I) reveals more robust Müller cell expression by ShH10 (E, F) relative to AAV2 (B,C), whereas AAV6 shows no visible expression (G–I). Additionally, GFP expression shows specific transduction of Müller cells by ShH10 (D) compared to AAV2 (A), which exhibits considerably more transduction of retinal ganglion cells and interneurons.

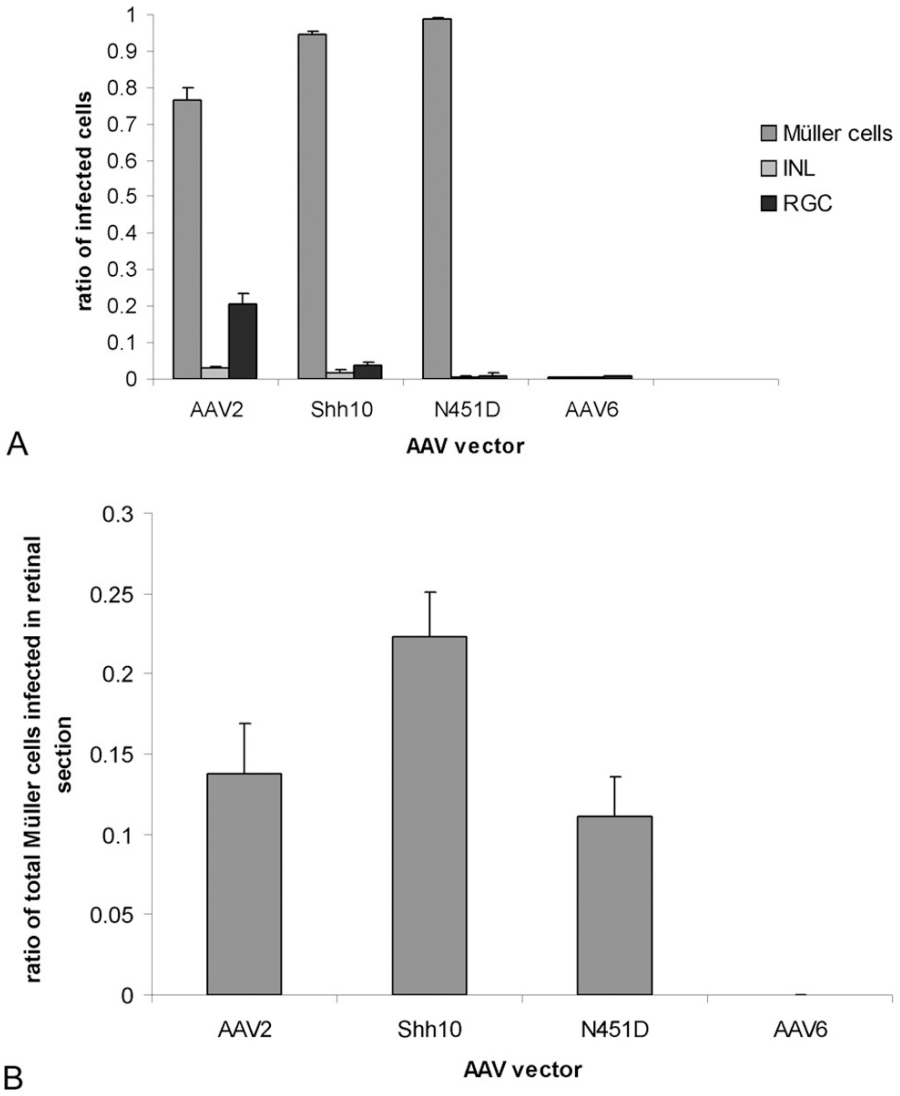

Figure 3b.3. Transduction specificity and efficiency of ShH10. Representative retinal slices from injected eyes were quantified for the number of each cell type that was infected, as determined via GFP expression, to generate histograms comparing tropism profiles (A) and Müller transduction efficiencies (B) of rAAV2, rShH10, and rAAV6 dsCAG-GFP. Transduction efficiencies were calculated based on the ratio of Müller cells infected relative to the total number of Müller cells in a 10 μm transverse retinal slice (n = 6). Error bars represent standard deviation among sample population.

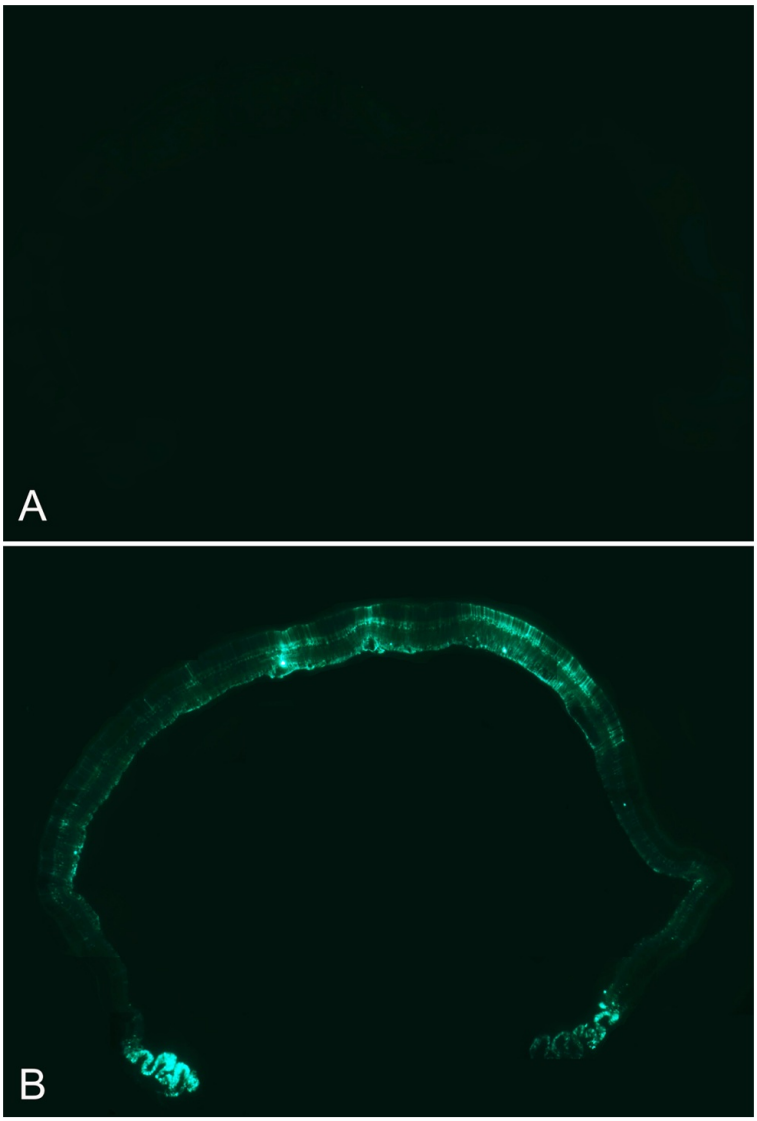

Figure 3b.4. rShH10 expression in the whole retina following intravitreal injection. Fluorescence microscopy of transverse retinal sections from rShH10 dsCAG-GFP and rAAV6 dsCAG-GFP injected animals 3 weeks post-injection reveals broadly spread expression by ShH10 (B), with the most prominent expression localized at the injection site. AAV6 (A) shows no visible expression.

Recombinant ShH10 (rShH10) led to diffuse expression throughout the retina with a *highly* specific transduction profile of approximately 94% Müller cells, 2% interneurons, and 4% retinal ganglion cells (Figures 3b.2, 3b.3, 3b.4). In comparison, the parent vector, AAV6, showed very low transduction of the retina, and the related AAV2 vector showed a less specific retinal tropism with a transduction profile of approximately 76% Müller cells, 3% interneurons, and 21% retinal ganglion cells (Figures 3b.2, 3b.3, 3b.4). Quantification of transduction efficiencies revealed that ShH10 was approximately 62% more efficient at infecting Müller cells relative to AAV2, infecting 22% vs. 14% of

total Müller cells respectively in transverse retinal slices (Figure 3b.3b). When we intravitreally injected ShH10 into adult murine retina, we again observed robust transduction of Müller cells, with a greater efficiency and specificity of transduction relative to AAV6 (Figure 3b.5).

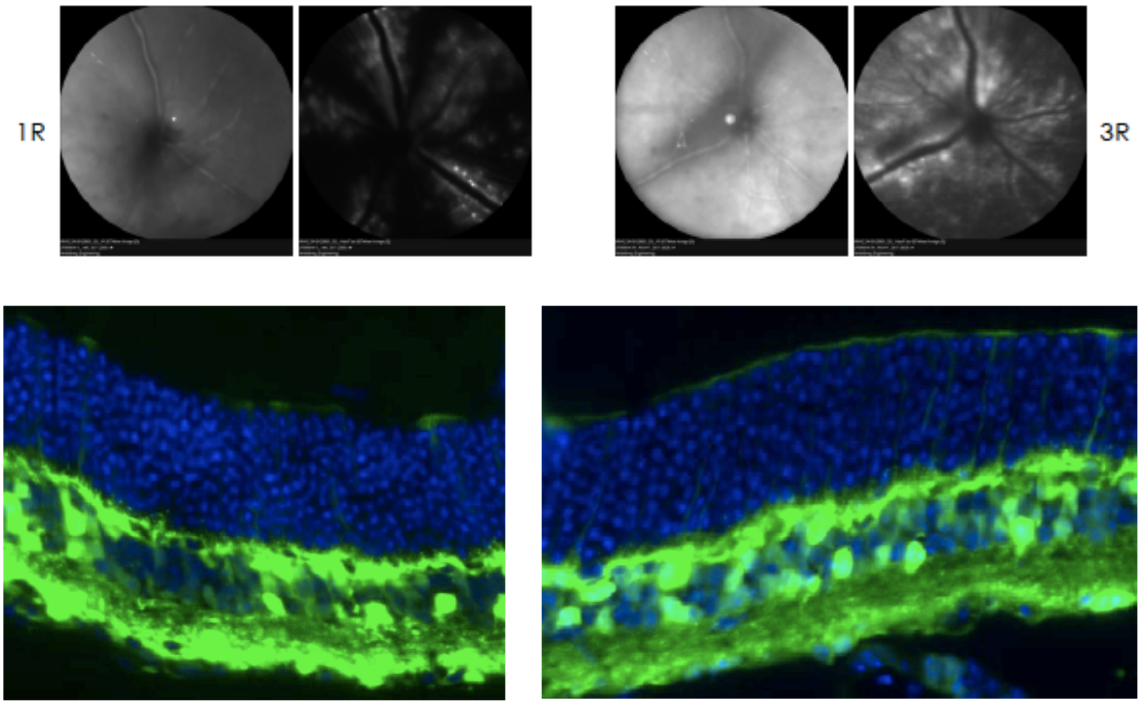

Figure 3b.5. rShH10 expression following intravitreal injection in the adult murine retina. Scanning laser ophthamoscope (SLO) imaging (top) of murine retina 1 week post-injection of 2.5×10^{10} viral particles (vector genomes) of dsCAG-GFP vectors with capsids from AAV6 (1R - left) and ShH10 (3R -right). Transverse retinal sections overlaid with DAPI staining (blue) reveal robust Müller cell expression in rShH10 injected eyes (bottom right) whereas AAV6 injected eyes show less Müller expression and more expression in RGC's (bottom left).

Temporal observation of ShH10 expression using fundus imaging, coupled with anti-laminin immunostaining of retinal flatmounts to visualize vasculature, also revealed a unique tropism for retinal astrocytes at earlier time points following injection (Figure 3b.6). Unlike Müller cells, retinal astrocytes are not derived from the retinal neuroepithelium, but serve some analogous roles in the retina including providing nutritional support to neurons, neurotransmitter metabolism, and ionic homeostasis [133]. They also serve as axonal glial sheaths for ganglion cells bodies and envelop the retinal vasculature, forming part of the blood-brain barrier. One week post-injection, fundus imaging revealed localized expression near those areas dense in retinal astrocytes, e.g. the optic nerve and along retinal vasculature (Figure 3b.6). Additionally, transverse retinal sections showed that areas underlying major vasculature bore strong Müller expression

(Figure 3b.6d). At later time points (2–3 weeks), expression became more evenly spread, but interestingly, those regions in proximity to vasculature ultimately maintained the strongest Müller cell expression (Figure 3b.4).

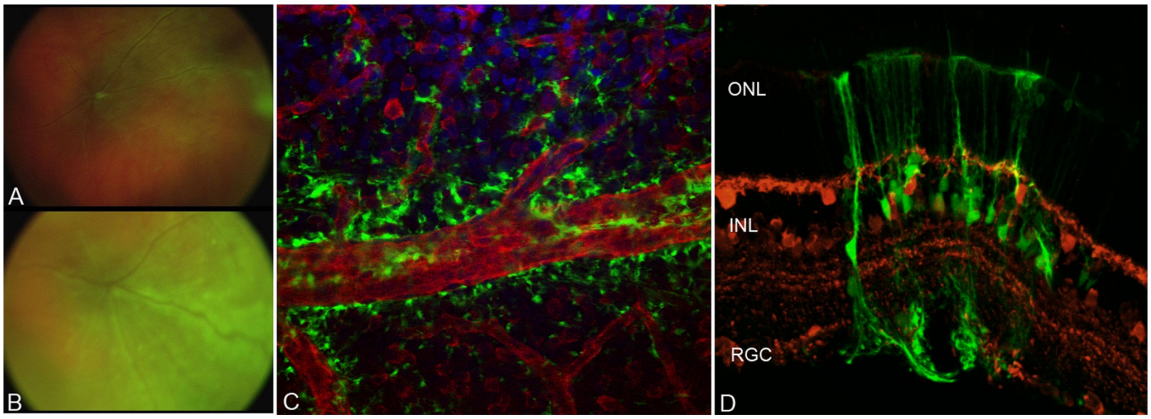

Figure 3b.6. Retinal astrocyte infectivity of ShH10. Fundus imaging of rShH10 dsCAG-GFP injected rats at one week (A) reveals a characteristic expression pattern localized near major vasculature and the optic nerve, which subsequently shows spreading after three weeks (B). Closer examination by flatmount (C) through laminin (red) and DAPI (blue) staining reveals a strong localization of GFP expression along the edges of retinal blood vessels, areas dense in retinal astrocytes. Transverse sections (D) stained for calbindin (red), a marker of RGCs and interneurons in the retina, illustrate a local region of expression within retinal astrocytes and Müller cells ensheathing a blood vessel.

Mutational analysis of ShH10

ShH10 is highly Müller cell selective, while AAV6 yields no detectable retinal expression upon intravitreal administration, yet intriguingly ShH10 differs from AAV6 at only four residues: I319V, N451D, D532N, and H642N (Supplemental Figure 3b.S1). To analyze the contributions of each of these mutations to ShH10's novel phenotype, single point mutants and all potential double mutants were generated from the AAV6 *cap* gene via site-directed mutagenesis. Each resulting variant was used to package rAAV-CMV-GFP and was purified via iodixanol gradient ultracentrifugation. To characterize the *in vitro* infectivity of these mutants, and in particular their glycan dependence in light of the substantial role proteoglycans and glycoproteins play in AAV transduction [66, 69, 128], we analyzed their relative transduction efficiencies on a panel of cell types: Pro5, a Pro5 mutant (Lec1) deficient in N-linked sialic acid, CHO, and a CHO derivative (pgsA) deficient in all glycosaminoglycans [152]. AAV6 exhibited a dependence on N-linked sialic acids for efficient transduction, as previous studies have indicated (Figure 3b.7) [69]. However, the N451D mutation decreased the viral dependence on N-linked sialic acids, and the D532N mutation increased the viral transduction in the absence of N-linked sialic acids (Figure 3b.7c). This D532N mutation, located near the HSPG binding domain of the AAV6 capsid [153], may enable the virus to utilize a transduction pathway

distinct from AAV6 (Figure 3b.8).

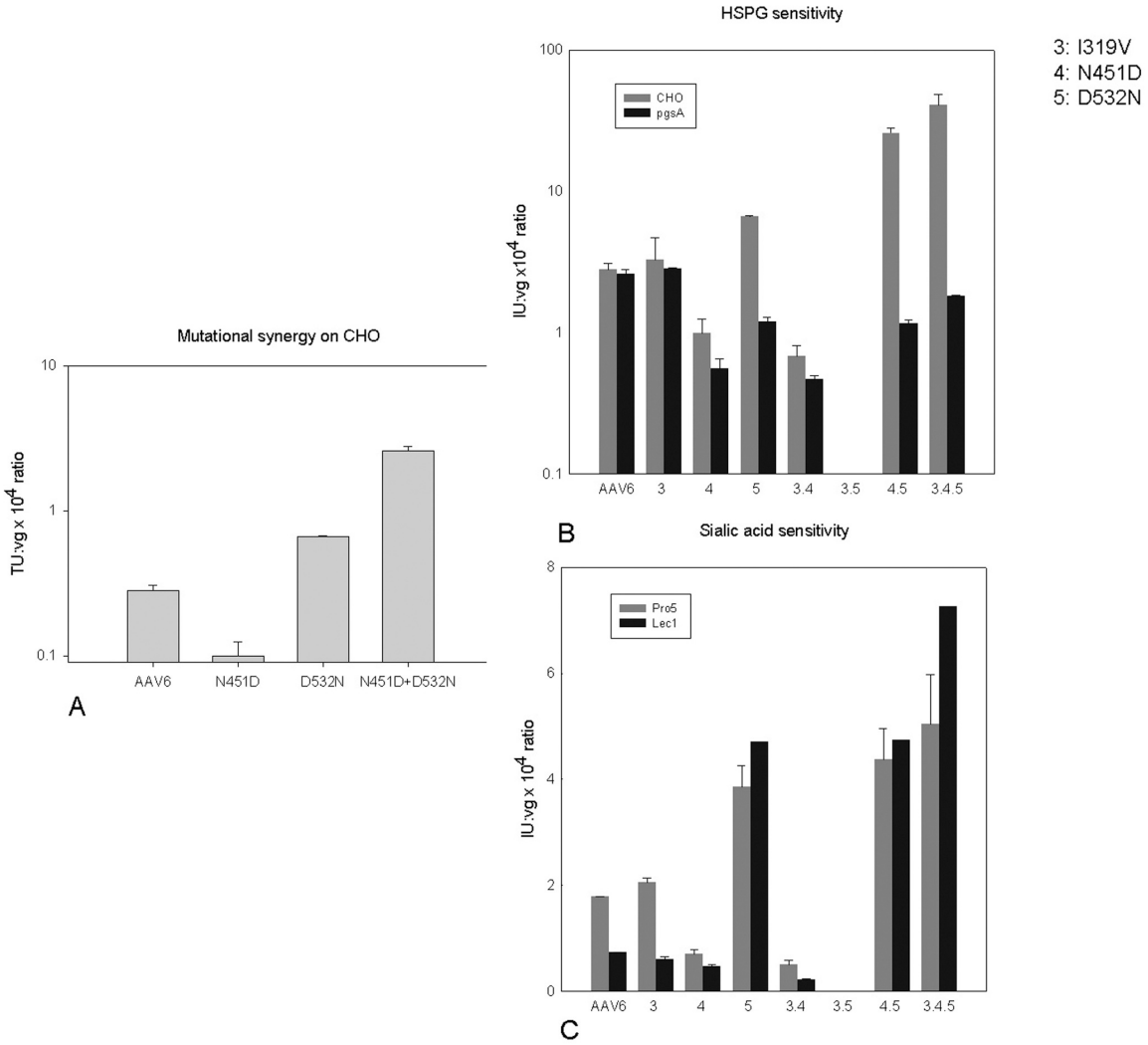

Figure 3b.7. In vitro characterization of ShH10. (A) CHO cell transduction by rAAV6, rAAV6 N451D, rAAV6 D532N, and rAAV6 N451D+D532N carrying CMV-GFP. (B) CHO/PgsA transduction demonstrating the HSPG dependence of various permutations of the mutations that comprise ShH10. (C) Pro5/Lec1 transduction examining sialic acid dependence of various permutations of the mutations that compose ShH10.

Whereas AAV6 does not utilize HSPG for transduction (Figure 3b.7b) [69], several of the ShH10 mutations confer a new dependence on HSPG. Intriguingly, AAV6 N451D exhibited lower transduction levels relative to AAV6 in CHO cells, but when coupled with the D532N mutation was more infective than either AAV6 or AAV6 D532N (Figure 3b.7a). Comparing infection efficiencies among the single point mutants between CHO and pgsA cells, cell lines containing and lacking HSPG respectively, AAV6 D532N was the only mutant to exhibit a substantial HSPG dependence, which became more pronounced when coupled with mutations I319V and N451D (Figure

3b.7b). The enhanced infectivity of ShH10 is thus likely due to a synergy between mutations that in part augments HSPG affinity as suggested by the heparin affinity chromatogram (Figure 3b.9). To determine whether AAV6 mutations that enhance infectivity also function *in vivo*, equal titer intravitreal injections of 5×10^9 genomic particles of recombinant vector mutants carrying dsCAG-GFP revealed that that only AAV6 N451D was sufficient to confer the intravitreal Müller tropism. This mutant was considerably more efficient than AAV6 on Müller cells, though only half as efficient as ShH10 (Figure 3b.3, 3b.8b).

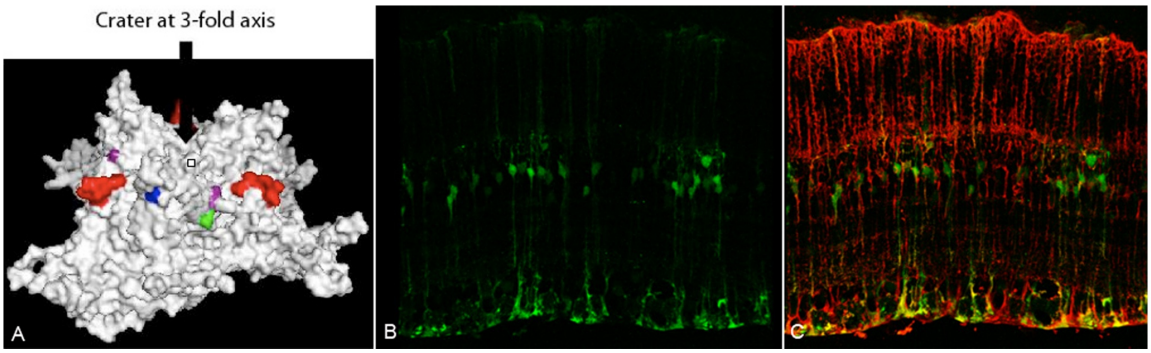

Figure 3b.8. rAAV6 N451D expression following intravitreal injection.
Confocal imaging of immunostained transverse retinal sections 3 weeks post-injection of rAAV6 N451D dsCAG-GFP (B, C). GFP expression analysis (B) and overlay with GS (C) reveal this mutant to be sufficient for an intravitreal Müller infection, though at a reduced efficiency relative to ShH10 (Figure 3b.1d,f). Mapping of this mutation onto the AAV6 capsid subunit VP3 (A) (blue) shows its location near the three-fold axis of symmetry of the assembled capsid. Three-dimensional models of the AAV6 VP3 subunit were generated using Swiss Model with the coordinates of AAV2 (Protein Databank accession no. 1LP3) supplied as a template and images were rendered in Pymol and Rasmol. Additionally, the D532N mutation (green) maps near the HSPG-binding domain (purple) [153].

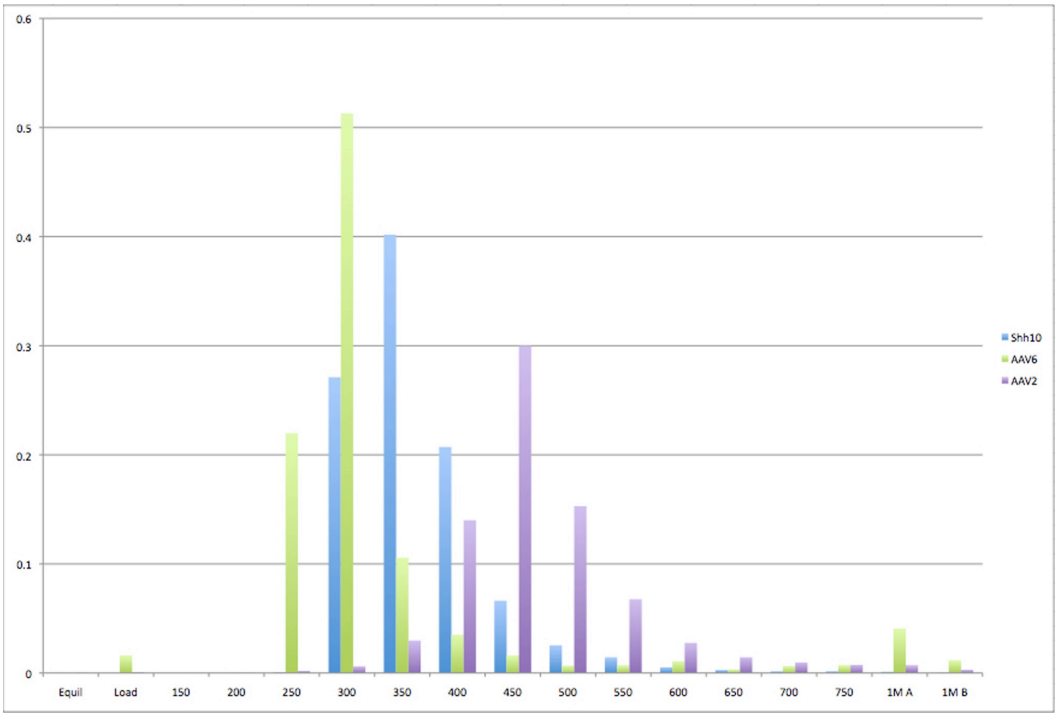

Figure 3b.9. Heparin binding affinity of ShH10, AAV2, and AAV6. Elution profile from a heparin column for ShH10, AAV2, and AAV6. Y-axis values represent the fraction of virus eluted, and the X-axis represents the concentration of NaCl in the eluant (mM).

Discussion:

Our results demonstrate that the selection on primary human astrocytes from our previous study [141]was sufficient to produce a variant that overcomes intraocular barriers to infection, apparently due to the cellular similarities between Müller glia and astrocytes. These similarities may be based on their shared cellular lineages, proteomic profiles, cellular polarity, and functionally analogous roles in the CNS [133, 135, 147, 148]. Interestingly, primary astrocytes may have even been more suitable as a selection model *in vitro* in lieu of directly selecting against primary Müller cells, as proteomic profiling studies of primary Müller cells in culture revealed a loss of cellular identity with significant shifts in expression that suggested a dedifferentiation into a fibroblast-like phenotype [154]. Characterizations of astrocytes in culture have pointed to fewer changes, thus making this cell type relatively closer to its initial *in vivo* state [155].

The *in vitro* evolution from our previous study selected for variants with the capacity to bind to the glial cell surface and traffic to the nucleus [141]. This may, in part, explain why the majority of variants were unable to overcome the additional extracellular barriers present in the retina *in vivo* [55]. However, one of the variants, ShH10, showed strong expression following intravitreal injection. Interestingly, sequence analysis (Supplemental Figure 3b.S1) reveals that ShH10 does not share mutations with the other evolved variants except for mutation H642N with variant ShH13, which has been shown

in our previous work to have an enhanced tropism for Müller cells upon subretinal injection [141]. However, interestingly, ShH13 shows no expression with intravitreal administration (data not shown).

Importantly, in beginning to mechanistically investigate viral infection in the retina, our previous studies have shown that AAV binding at the inner limiting membrane (ILM) is implicated in mediating transduction via intravitreal injection of AAV serotype 2, and to a lesser extent 8 and 9 [55]. The ILM is a meshwork of extracellular matrix proteoglycans located at the interface of the vitreous and the retinal ganglion cell (RGC) layer and Müller cell endfeet (Figure 3b.1), and it constitutes one of the first physical barriers encountered by intravitreally injected virus. Receptors such as HSPG and the 32 k laminin receptor that are abundant at this site may allow binding of AAV serotypes 2, 8, and 9, whereas AAV serotypes such as 1 and 5 that bind sialic acid, which is not found at the ILM, show no expression in the rat retina following intravitreal administration [55, 93, 146]. Once binding to the ILM occurs, AAV then needs to overcome additional diffusional and trafficking barriers in the retina to achieve efficient transduction. In this respect, although AAV6 can infect cells upon subretinal injection [141], its subretinal tropism is largely limited to retinal pigment epithelia (RPE) and photoreceptors, and it completely lacks the capacity to infect retinal cells upon intravitreal injection in rat retina (Figure 3b.2). However, in murine retina, AAV6 has a limited ability to infect intravitreally, likely due to differences between murine and rat ILM (Figure 3b.5). These results suggest two distinct obstacles in AAV6's inability to infect Müller cells intravitreally: a marginal capacity to first bind to the ILM via proteoglycan interactions and a limited ability to then overcome Müller cell-surface and/or intracellular barriers.

In first binding to the ILM, the presence of high levels of heparan sulfate in the proteoglycan matrix of the ILM may mediate viral accumulation at this site and act as a ‘sink’ [55]. Although this may sequester AAV particles, it may also effectively localize the virus and prevent it from being cleared from the vitreous via the trabecular meshwork, thereby facilitating subsequent transduction [156]. Although wild-type AAV6 does not depend on HSPG for infection [69], ShH10 exhibits a newly conferred HSPG dependence, allowing it to better bind and traverse the ILM (Figure 3b.7b). Preliminary results indicate that the D532N mutation (shown in green in Figure 3b.8a) may be responsible for this dependence, as the D532N mutant exhibits enhanced viral binding to heparin and significantly increased transduction of CHO cells (data not shown and Figures 3b.7a, 3b.9). This mutation lies next to the K531 residue (shown in purple in Figure 3b.8a) that has been shown to confer heparin binding to wild-type AAV6 [153]. The loss of negative charge in the D532N mutant may facilitate more efficient electrostatic interactions between K531 and the negatively charged sulfate groups present within HSPG. AAV2's higher HSPG affinity, but lower transduction efficiency, relative to ShH10's (Figure 3b.9) may then suggest a potential dueling role in achieving optimum transduction, as too high of an affinity may also encumber efficient viral penetration in the retina.

Once it traverses the ILM, ShH10 must bind Müller cells. Recent studies have implicated the epidermal growth factor receptor (EGFR), which is expressed on the surface of Müller cells, as a coreceptor for AAV6 transduction [157, 158]. However,

since AAV6 is largely refractory to intravitreal transduction and has a marginal ability to transduce Müller cells subretinally [141], ShH10's novel tropism may then partly result from an improved binding affinity for EGFR (or another co-receptor) to enable Müller cell binding and endocytosis.

Preliminary results suggest that the N451D mutation may partly be responsible for such potentially improved receptor interactions, as this substitution is sufficient to confer a limited Müller cell intravitreal infectivity (Figure 3b.8). The asparagine to aspartic acid mutation places a negative charge near the tip of the 3-fold axis of symmetry on the AAV capsid (Figure 3b.8a), an area implicated in receptor binding on the AAV2 capsid [128]. Intriguingly, the N451D mutation (shown in blue in Figure 3b.8a) alone decreased viral transduction of CHO and Pro5 cells (Figure 3b.7), but when this mutation is combined with the D532N change, viral transduction of CHO cells is synergistically improved. This synergism may then reflect an improved receptor/co-receptor relationship, with the D532N mutation negating the detrimental aspects of the N451D mutation while concomitantly enhancing binding to a primary proteoglycan receptor (i.e. HSPG).

ShH10 exhibited enhanced transduction of Müller cells underlying areas of retinal vasculature, suggesting that its infectivity of retinal astrocytes may also offer a possible mechanistic explanation for its tropism. Whether this is just a result of commonalities between these glial subtypes that allow for ShH10 permissivity in both or whether infection of one type may facilitate adjacent infection of the other through localized binding remains to be analyzed. Regardless, this property would be useful in infecting the activated Müller cells in neovascularized tissue to deliver neurotrophic factors to sites of vascular abnormalities[150].

Overall, efficient and selective intravitreal transduction of Müller cells by AAV may provide safer and more effective treatments for retinal degenerative conditions through secretion of neuroprotective factors, while also enabling basic investigations to gain a greater understanding of Müller cell physiology. For instance, the uncertain role of Müller cells in the visual cycle of cone photoreceptors can be examined *in vivo* through Müller-specific AAV-mediated RNAi-knockdown of factors implicated in 11-cis-retinol generation [159]. Likewise, in a similar approach, the undefined role of these cells in regulating the fluid dynamics of the retina could be further explored by specifically modulating Müller aquaporin (AQP) levels [160].

For future studies, the use of highly diverse AAV libraries coupled with *in vivo* selections could provide a more powerful approach to directly target specific cell types in the retina. For example, the targeting of engineered light gated channels to specific subpopulations of retinal cells, such as ON bipolar cells or ON/OFF retinal ganglion cells [161], may restore functional vision in individuals with a severely degenerated ONL by reestablishing downstream retinal circuitry. Likewise, targeted delivery to photoreceptors may enable additional strategies for neuroprotective therapy.

Chapter 4

Selective Secretion of hGDNF from Müller Cells via AAV-mediated Intravitreal Gene Delivery Leads to Functional Rescue in a Rat Model of Retinitis Pigmentosa

Preface:

This work was done in collaboration with Dr. Deniz Dalkara, a post-doctoral fellow in the Flannery and Schaffer Labs at UC Berkeley, as well as Dr. Kate Kolstad and Dr. Karen Guerin, former graduate students in the Flannery lab. Natalie Hoffman and Meike Visel provided technical assistance.

Abstract:

Retinitis pigmentosa (RP) and numerous other inherited retinal degenerative diseases are causally linked to a vast array of deleterious mutations that converge into a common photoreceptor degenerative phenotype. A pro-survival and anti-apoptotic therapeutic approach employing neurotrophic factors secreted from Müller cells would be a broad strategy to combat these disparate conditions. We have previously applied directed evolution to create a novel AAV variant (ShH10) capable of efficient, selective Müller cell transduction through intravitreal injection. Here, we employ this vector to explore the efficacy of selective secretion of hGDNF from Müller cells in a rat animal model of RP using an intraocular gene delivery approach. We observe large levels of hGDNF production in treated retinas and importantly, we see sustained functional and histological rescue at more than 5 months post injection, with an average approximate rescue of 50% in ERG a and b-wave amplitudes relative to untreated controls. Our findings demonstrate that Müller-secretion of hGDNF mediated through intravitreal vector administration is a safe and effective approach to treating RP in a rat animal model, showing promise as a strategy for treating inherited retinal degenerative diseases.

Introduction:

The vast genetic heterogeneity of inherited retinal degenerative diseases presents an enormous obstacle for the development of gene replacement or antisense strategies for treating these conditions. Retinitis pigmentosa, the most common inherited retinal dystrophy, exemplifies this challenge as over fifty loci are thought to be implicated in this disease [20, 162, 163]. In the opsin gene alone, which encodes a seven-pass transmembrane G-protein coupled receptor in the outer segment of photoreceptor cells, up to 150 mutations have been reported as causally contributing to the disease [20, 162, 163]. The most common autosomal-dominant mutations cause protein misfolding in the rhodopsin protein.

The molecular mechanisms underlying photoreceptor cell death from this misfolding is not well understood, although it is known that these proteins are retained within the endoplasmic reticulum (ER), triggering an Unfolded Protein Response (UPR) [164-166]. Initially, this cellular stress response reduces protein translation while specifically increasing the production of molecular chaperones in the ER to correct for deficiencies in protein folding [166]. However, when the ER is overwhelmed with misfolded protein aggregates, the UPR initiates a pro-apoptotic pathway, leading to cell death. The principal receptors involved in this response are PERK and Ire1 [167-169]. Whereas PERK is involved in mediating a translational block for new protein production, Ire1 binds with TRAF2, which activates the JNK signaling pathway and results in the activation of downstream caspases leading to apoptosis [169]. Additionally, the proapototic protein CHOP is known to be upregulated during ER stress, which downregulates the anti-apoptotic mitochondrial protein Bcl-2 [167, 168].

In this respect, a pro-survival and anti-apoptotic therapeutic strategy that counteracts these commonly shared stress response pathways in retinal degenerative conditions would be valuable in providing a broad treatment for RP and other conditions. Neurotrophic factors, such as glial-derived neurotrophic factor (GDNF) and basic-fibroblast growth factor (bFGF), have been shown in previous studies to have these properties [170-173]. Notably, subretinal viral delivery of hGDNF to photoreceptors in a S334-ter rat model of RP mitigated the progression of the disease as demonstrated by functional (ERG) and histological rescue [173].

However, for retinal gene therapy, the transduction of Müller glial cells would be the most advantageous in secreting neuroprotective factors. Müller cells transverse the entire thickness of the retinal tissue, ensheathing all retinal neurons in vertebrates. These cells serve numerous and significant physiological functions in the retina including but not limited to: metabolic support of neurons through the delivery of lactate and pyruvate, K^+ and water homeostasis through inward-rectifying potassium channels and aquaporin water channels respectively, free radical scavenging and oxidative protection through glutathione secretion, and neurotransmitter and photopigment uptake and recycling [147]. In many retinopathies, Müller cells naturally play an active role in mitigating retinal degeneration through the release of neurotrophic factors, such as bFGF, or by mediating

the effects of factors secreted from pathologically-stimulated microglia, such as GDNF, neurotrophin-3 (NT-3), nerve growth factor (NGF), and ciliary neurotrophic factor (CNTF) (Fig. 2) [147, 174]. Neuronal survival is thought to be regulated by two different receptors on the Muller cell surface upregulated during retinal degeneration: the high-affinity tyrosine kinase TrkC receptor and the low-affinity p75 neurotrophin receptor, which are implicated in mediating prosurvival or proapoptotic signals respectively [175]. Binding of NT-3 on TrkC receptors results in an increased release of bFGF from Müller glia while conversely, binding of NGF on p75 results in reduced bFGF release, ultimately contributing to increased photoreceptor apoptosis.

In regard to these glia-glia and glia-neuron networks and findings that suggest that the NGF pathway predominates over the NT-3 pathway during retinal degeneration, gene delivery of neurotrophic factors to Müller cells will help reinforce these survival pathways and prolong functional retinal lifespan. Secretion of neurotrophic factors by Müller cells would also reduce the occurrence of gliosis, a common result of retinal degeneration that leads to retinal scarring and further exacerbates losses of visual function. In addition to these strong points , targeting these cells holds two key benefits. Firstly, Müller cell accessibility from the vitreous allows for intravitreal injection of a gene delivery vehicle, an injection route that is advantageous relative to subretinal injection in terms of safety, simplicity, and diffusivity of expression. Secondly, as Müller cells survive during retinal degenerative conditions, they can mediate independent protection of the entire retina for a more extended period of time relative to a transduced damaged or dying neuron affected by one of these diseases.

We recently isolated an AAV variant derived from AAV6, named ShH10, that efficiently and specifically infects Müller cells from the vitreous. Here, we employ this variant for intravitreal gene delivery of hGDNF to Müller cells, achieving a significantly reduced rate of loss of visual function in an S334-4ter rat model of RP. These findings underscore the effectiveness of intravitreally targeting Müller cells to secrete neurotrophic factors as a therapy for treating RP. We anticipate this successful approach may help to provide a broad strategy for treating retinal degenerative conditions in humans.

Materials and Methods:

Generation of rAAV vectors Vectors were produced by the plasmid co-transfection method [141], and the resulting lysates were purified via iodixanol gradient ultracentrifugation as previously described [120]. This fraction was then passed through a heparin column, which was washed with 5 mL PBS and eluted with 5 mL of a 1 M NaCl solution. The resulting viral fractions were desalted and concentrated with Amicon Ultra-15 Centrifugal Filter Units to a final volume of 200 µl. Vector was then titered for DNase-resistant vector genomes by real time PCR relative to a standard.

Intraocular administration routes TgS334-4ter rats were used for all studies. All animal procedures were conducted according to the ARVO Statement for the Use of Animals and the guidelines of the Office of Laboratory Animal Care at the University of California, Berkeley. Before vector administration, rats were anesthetized with ketamine (72 mg/kg) and xylazine (64 mg/kg) by intraperitoneal injection. An ultrafine 30 1/2-gauge disposable needle was passed through the sclera, at the equator and next to the limbus, into the vitreous cavity. Injection of 5 µl, containing $1-5\times10^{12}$ vg/ml of AAV dsCAG-GFP or dsCAG-hGDNF, was made with direct observation of the needle in the center of the vitreous cavity.

Cyrosections Animals were humanely euthanized by CO_2 overdose and cervical dislocation. Eyes were enucleated, a hole was made in the cornea and eyes were fixed with 10% neutral buffered formalin overnight. The eyecups were washed in PBS and the cornea and lens were removed and then placed in 30% sucrose in PBS overnight. Eyes were then embedded in optimal cutting temperature embedding compound (OCT; Miles Diagnostics, Elkhart, IN) and oriented for 5-10µm thick transverse retinal sections.

Immunolabeling Tissue sections were rehydrated in PBS for 5 min, followed by incubation in a blocking solution of 1% BSA, 0.5% Triton X-100, and 2% normal donkey serum in PBS for 2–3 hours. Slides were then incubated with commercial monoclonal antibodies raised against glutamine synethetase in rabbit (Sigma G2781) at a 1:3000 dilution in blocking solution overnight at 4°C. The sections were then incubated with Cy3-conjugated secondary anti-rabbit (Molecular Probes) at a 1:1000 dilution in blocking solution for 2 hours at room temperature. The results were examined by fluorescence microscopy using an Axiophot microscope (Zeiss, Thornwood, NY) equipped with a Xcite PC200 light source and QCapturePro camera or a confocal microscope (LSM5; Carl Zeiss Microimaging).

Electroretinography Transgenic S334 line-3 rats at ages P45, P165 were dark-adapted for four hours, anesthetized, and pupils dilated. Animals were placed on a heating pad and contact lenses were positioned on the cornea of both eyes. Reference electrodes were inserted subcutaneously in the cheeks and a ground electrode was inserted in the tail. Electroretinograms were recorded (Espion ERG system; Diagnosys LLC, Littleton, MA) in response to seven light flash intensities ranging from -4 (cds/m^2) to 1 cds/m^2. Each stimulus was presented in series of three. Light flash intensity and timing were elicited from a computer controlled Ganzfeld flash unit. Data were analyzed with MatLab (v7.7; Mathworks, Natick, MA). After correction for oscillatory potentials and heartbeat artifacts, scotopic a-wave values were measured from the baseline to the minimum ERG peak while scotopic b-waves were measured from the minimum to maximum ERG peaks. Data were analyzed using Student's *t* test.

Histology At P90, rats were euthanized by CO_2 overdose and cardiac perfusion with 2.5% glutaraldehyde and 2% formaldehyde in PBS. The superior cornea was marked for orientation. Eyes were enucleated and cornea and lens were removed. Eye cups were

further fixed in 1% osmium tetroxide, dehydrated by incubation in increased ethanol concentrations and a final incubation in 100% propylene oxide. The dehydrated samples were embedded in an epon-araldite resin and heated overnight at 65°C. One-micrometer thin plastic sections of the eye were cut along the vertical meridian, through the optic nerve with a diamond blade. Sections were visualized using light microscopy.

ELISA Protein isolation buffer (50mM Tris-acetate, 65mM NaCl, 2mM MgCl2, 2mM EDTA, 1% protease inhibitors cocktail) and brief sonication was used to homogenize retinas from treated and control animals. ELISA was performed using the DuoSet Kit for human GDNF (R&D systems). A 96-well plate was coated overnight with the capture antibody diluted in PBS. After incubation, wells were washed 3 times in wash buffer (0.05% Tween-20 in PBS) then blocked for 3 hours at room temperature with 1% BSA in PBS. After 3 rinses, samples and standard were added in duplicate for 2 hours. Samples were washed and then incubated with the detection antibody. After the last series of washes, the substrate solution was added for 20 minutes. At the end of the incubation stop solution was directly added to the wells. The optical density of each well was determined immediately using a microplate reader set to 450nm. To correct for optical imperfections in the plate, 540 nm readings were subtracted from the readings at 450nm. The amount of GDNF present in samples was calculated from a hGDNF standard curve. Results are the average of duplicates.

Results:

Intravitreal injection of ShH10 Y445F in S334-4ter rat leads to selective transduction of Müller cells

Previous characterization of ShH10 revealed efficient and specific transduction of rat Müller cells in wild-type animals [176]. In order to achieve greater efficiencies in transduction, we further modified the variant by mutagenizing the surface-exposed tyrosine residue at position 445 to a phenylalanine. Surface exposed tyrosines on the AAV capsid can be phosphorylated within the cell and subsequently targeted via a ubiquitin-dependent pathway for proteosome-mediated degradation [92]. In light of this, studies have found that mutagenizing these residues leads to robust increases in retinal gene delivery [93]. Intravitreal injection of this recombinant ShH10 Y445F variant with a scCAG-GFP transgene in S334-4ter rats, an animal model of RP, revealed strong, selective expression in Müller cells throughout the retina (Figure 4.1).

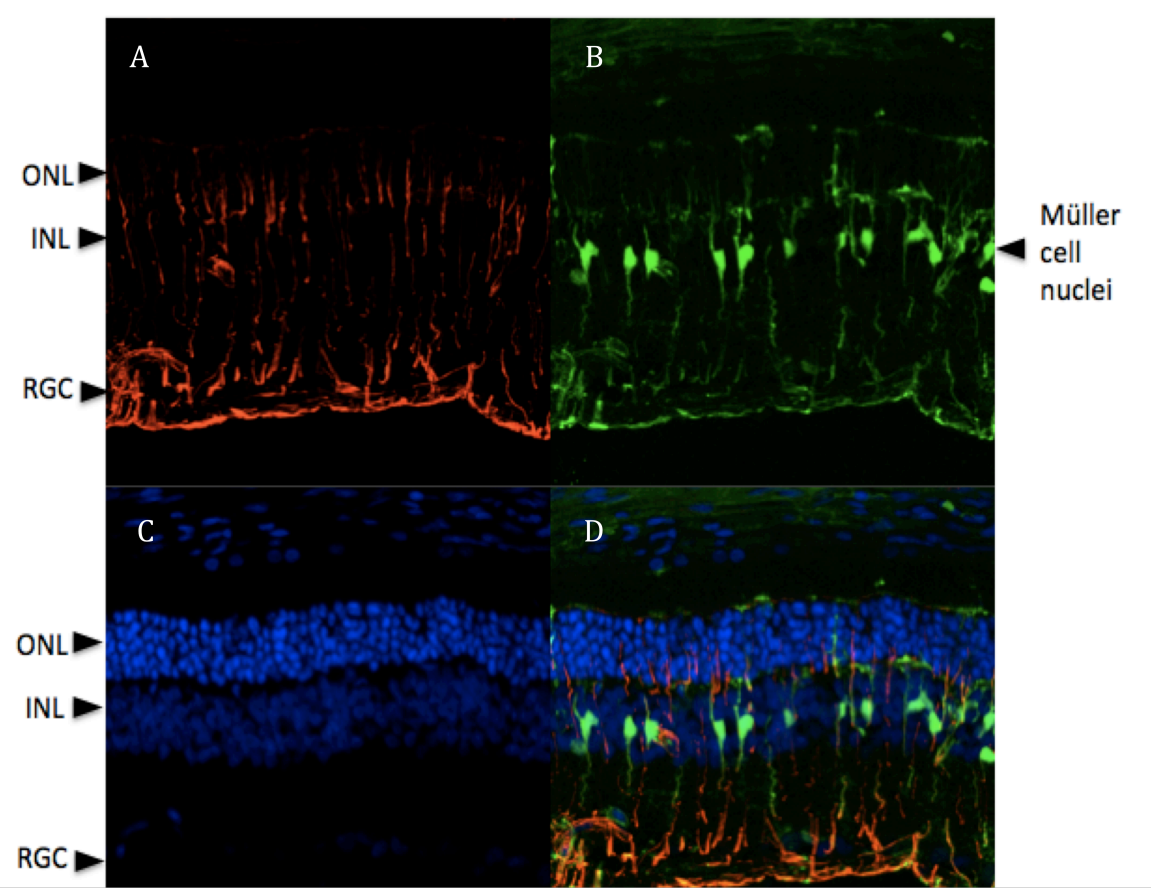

Figure 4.1 ShH10 Y445F scCAG-GFP drives strong expression in Müller cells when intravitreally injected in S334-4ter rats three weeks post injection. Overlay of GFP

expression (B) with glutamine synthase-staining (red) (A) and DAPI-staining (blue) (C) reveal selective GFP expression in Müller cells (D) in cryosections.

Intravitreal injection of ShH10 scCAG-GDNF leads to robust hGDNF secretion

Given the high specificity of our vector, we next cloned a self-complementary hGDNF transgene with the CAG promoter in order to promote the strongest secretion of hGDNF from Müller cells [84, 177]. The low level of off-target infectivity by ShH10 Y445F importantly allows us to employ strong, ubiquitous promoters to drive expression without the use of inefficient Müller-specific promoters such as CD44 or GFAP. Indeed, previous studies have indicated these promoters may even be cytotoxic as subretinal injection of AAV9 bearing an mGFAP promoter followed by a non-coding sequence led to reduced ERG a and b-waves one week post injection [13]. Additionally, fundus imaging of these animals revealed autofluorescence, indicative of toxicity, whereas a CBA.GFP transgene displayed no discernable toxicity. Although the exact mechanism by which this damage occurs is unknown, it may be that the saturation of Müller cells by these specific promoters hijacks essential transcriptional machinery for the cell.

ELISA measurements of retinal homogenates following intravitreal delivery of ShH10 scCAG.hDNF reveal robust secretion of hGDNF from Müller cells two months post injection (Figure 4.2). At more than 2.5 ng/mL , these levels of hGDNF are nearly 10-fold higher than those produced in previous studies that have achieved photoreceptor degeneration rescue through GDNF overproduction [172, 173].

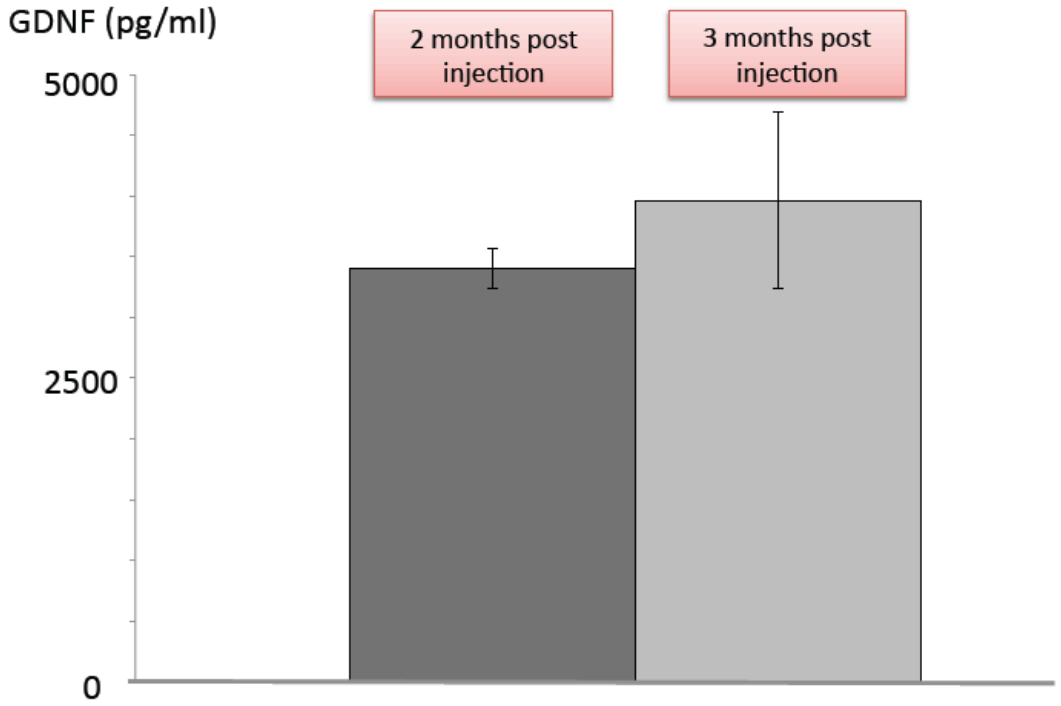

Figure 4.2 ELISA measurements of hGDNF protein expression levels in retinal homogenates two and three months following intravitreal delivery of ShH10 Y445F scCAG.hGDNF (n=7). All animals received hGDNF vector treatment in the right eye and no injection in the left eye.

Müller secretion of hGDNF leads to rescue of visual loss in S334-4ter rats

Attaining clinically-relevant levels of hGDNF expression in the retina, we next assessed visual function longitudinally for S334-4ter animals intravitreally injected at P15 with ShH10 Y445F scCAG-GDNF through electroretinography (ERG). The ERG is composed of two main components, the a-wave and the b-wave. The a-wave is the initial negative component of this response, reflecting the cessation of the dark current when photoreceptors are exposed to light stimuli. The larger, positive b-wave reflects a more complex summation of responses from ON bipolar cells and Müller cells.

One mouth post injection, we saw slight increases in a and b-wave amplitude overall relative to untreated eyes injected with PBS (Figure 4.3). Although the degree of visual loss is heterogeneous among animals, rescue is consistent between control and GDNF-injected eyes. Wild-type animals demonstrate a-wave amplitudes of approximately 455μV and b-wave amplitudes of 1370μV (Figure 4.3). Significantly, rescue is more pronounced three and five months post-injection, with a nearly two-fold increase in b-wave amplitude observed in one animal and an average approximate rescue of 50% amongst all animals (Figures 4.3, 4.4). Similar results were seen in measuring a-

wave amplitudes. Importantly, this rescue extends further than previous studies have shown.

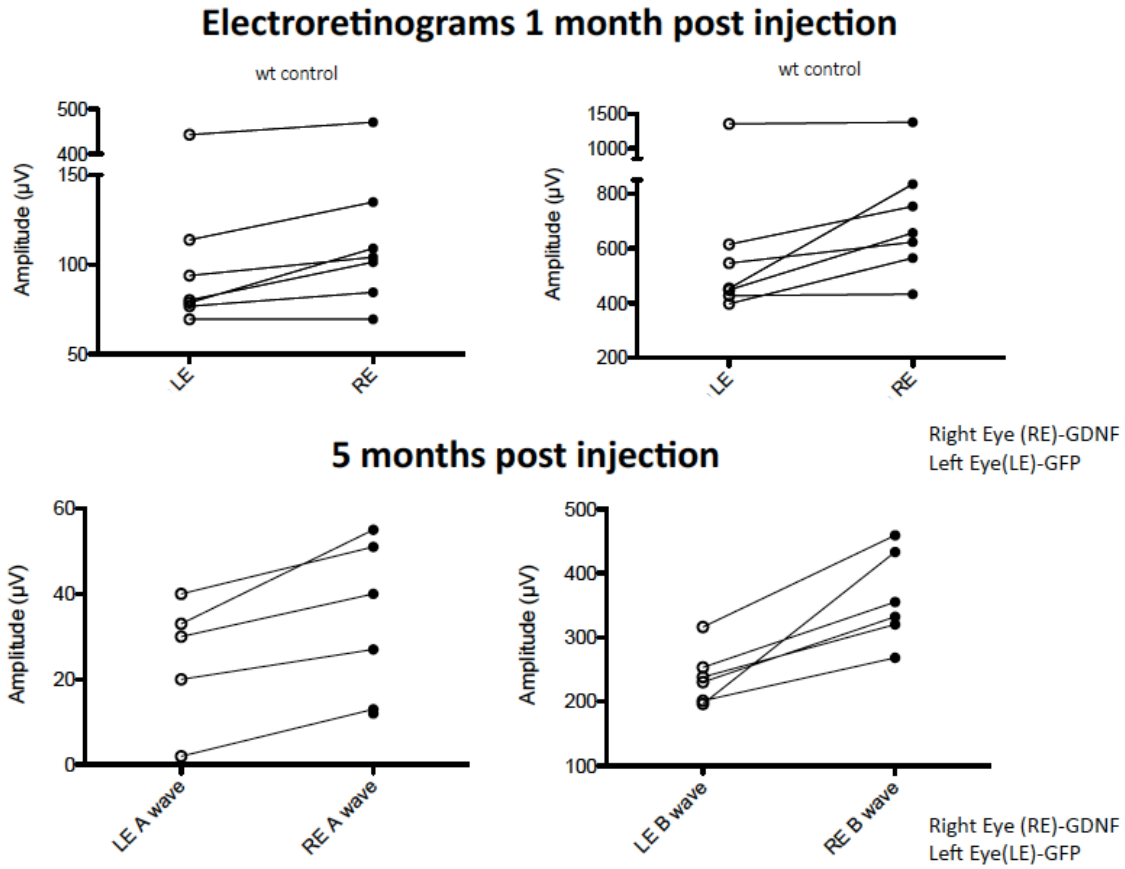

Figure 4.3 ERG a and b-wave plot in GDNF-treated (RE) and untreated eyes (LE) one month and five months post-injection. All animals received hGDNF vector treatment in the right eye and no injection in the left eye (n=6) at p15.

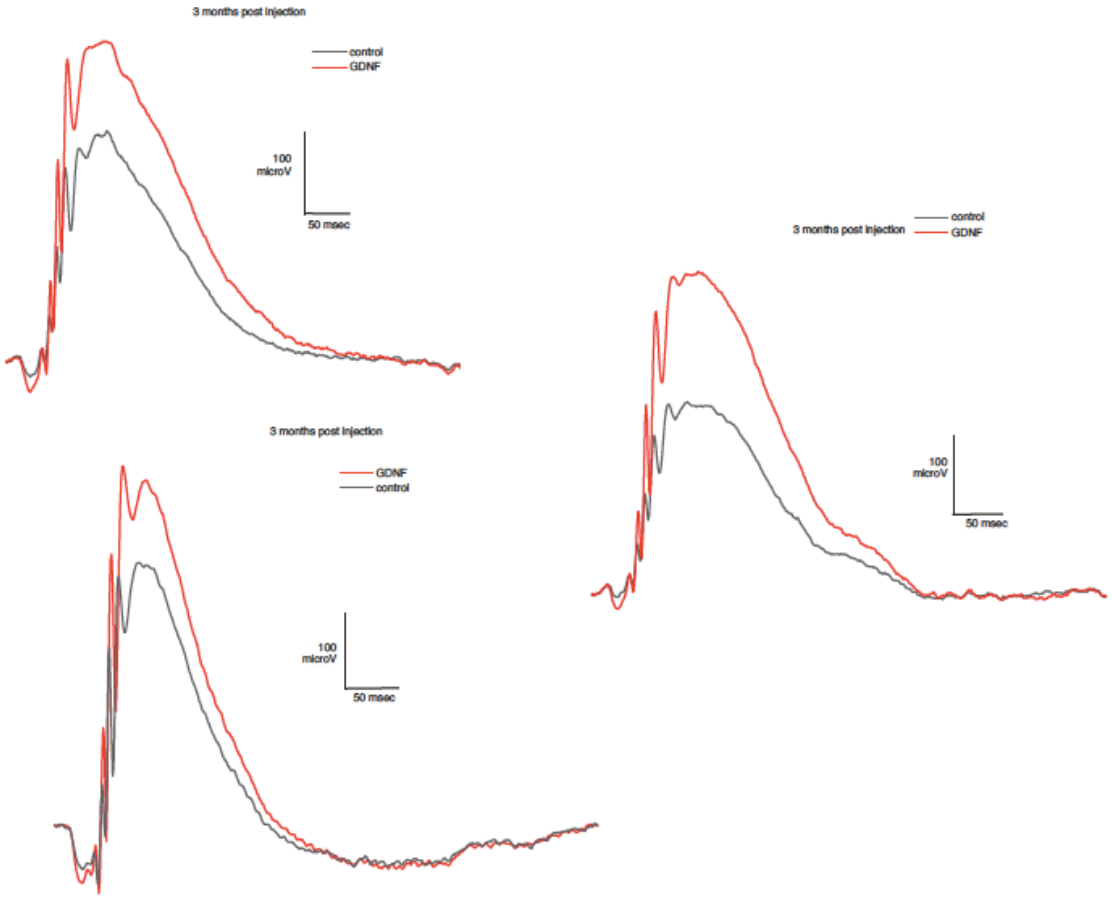

Figure 4.4 ERG recordings from three hGDNF-injected animals demonstrating the highest rescue three months post-injection. All animals received hGDNF vector treatment in the right eye and no injection in the left eye (n=6) at p15.

Histological examination of GDNF-injected and control retina corroborate these functional results (Figure 4.5-4.6). The ONL of treated eyes in the inferior retina are noticeably thicker than untreated eyes two months post injection, and the number of photoreceptor nuclei is greater as well in this region (data not shown). However, the superior retina shows similar results between control and injected eyes at this time point, most likely because this region degenerates more quickly due to a greater amount of light reaching this area. At three months post injection, the ONL is thicker and photoreceptor numbers are greater in both the inferior and superior regions of the retina in injected animals relative to control, likely because the therapeutic effect of GDNF is more pronounced given a larger window of time as seen in our ERG results (Figure 4.5).

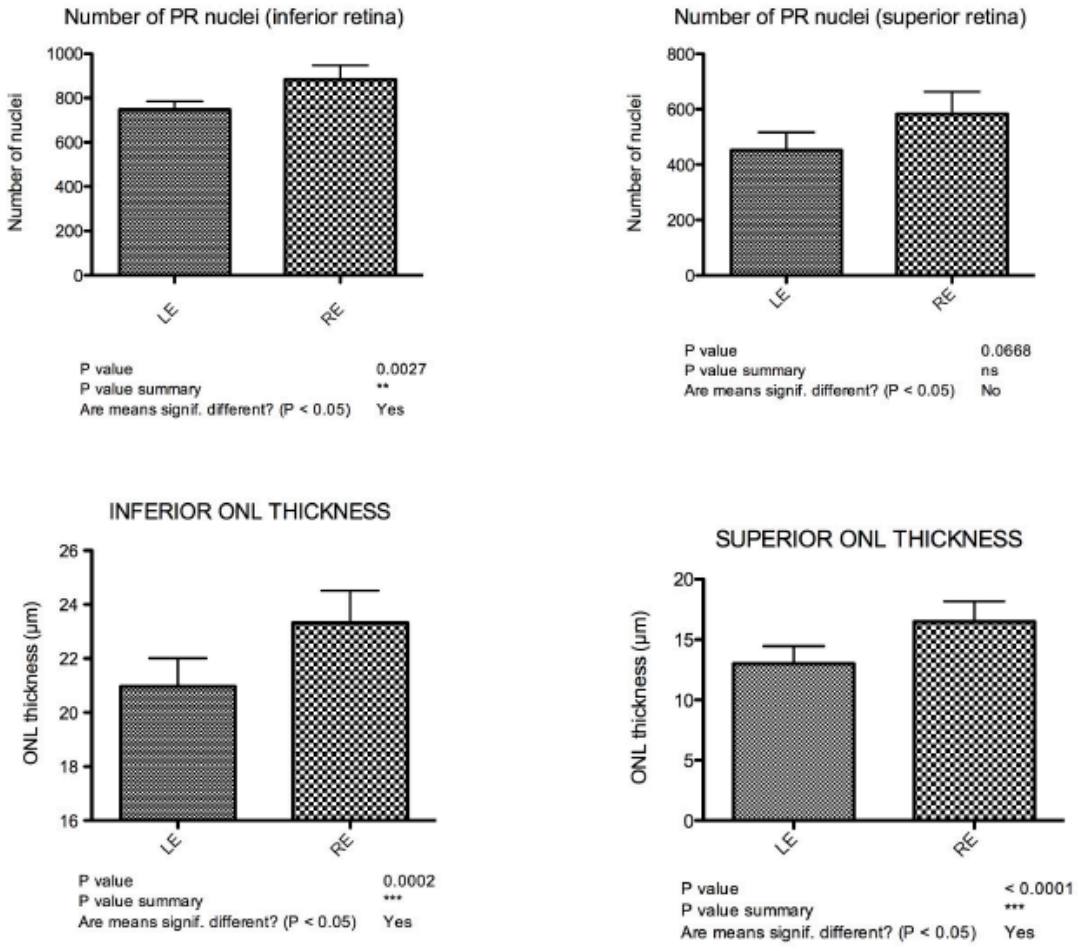

Figure 4.5 hGDNF treated retinas (RE) 3 months post injection show increases in ONL thickness and photoreceptor nuclei in the inferior and superior retina relative to control (LE).

Upon closer examination of transverse retinal sections, Müller cells appeared more hypertrophied in control eyes (Figure 4.6), a hallmark of the gliosis that accompanies severe retinal degeneration [174]. Additionally, photoreceptor outersegments, the region of the photoreceptor responsible for photon capture and phototransduction, were noticeably thicker in treated eyes relative to control, further corroborating the functional rescue we observed in ERG recordings.

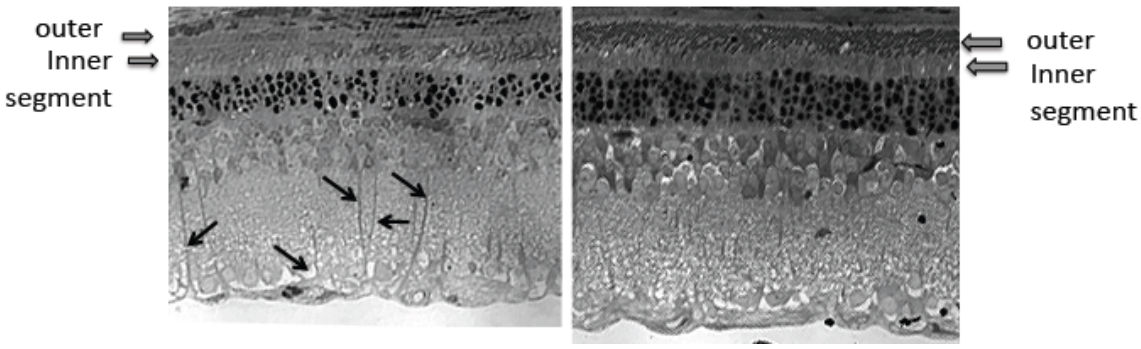

Figure 4.6 hGDNF treated retinas show increases in ONL and outer segment thickness and reduced glial hypertrophy relative to control. Representative plastic transverse sections of ShH10 Y445F scCAG-GDNF injected eyes (right) versus PBS injected eyes (left).

Discussion:

Our results demonstrate that selective expression of hGDNF from Müller cells through intravitreal targeting using a Müller-specific AAV vector leads to effective rescue in a rat model of retinitis pigmentosa. Functional and histological data indicate a greater survival of photoreceptors in treated animals and a reduced occurrence of retinal gliosis, demonstrating sustained rescue at more than five months post injection. Importantly, it is worth noting that though this rescue window in rats is ostensibly modest relative to human lifespan, this may translate into several years of functional rescue in humans where the time horizon of degeneration is far longer. The period of rescue we see in the study, longer than that observed in previous studies [173], underscores the utility of targeting Müller cells that allow for continuous neurotrophic secretion relative to degenerating neurons where secretion may taper off.

Although we see noticeable increases in ONL thickness and photoreceptor nuclei numbers in GDNF treated retinas, the relationship between functional rescue and histology is not proportional. This phenomenon was most noticeably seen in clinical trials involving CNTF secretion from transfected RPE cells sequestered within capsules that were surgically implanted into the vitreous of the eye [26, 29, 178]. Although retinas demonstrated greater ONL thicknesses relative to untreated eyes, ERG results were mixed, with reduced ERG responses in some instances. As ERG responses are a function of both total photoreceptor numbers and the health of individual photoreceptors, CNTF-treated photoreceptors may suffer from increased internal disorganization and / or more attenuated outer segments resulting in reduced photon-capture. Results from our study suggest that GDNF rescue may be mediated by both greater absolute numbers of photoreceptors as well as by more fully functional photoreceptors.

The different results between GDNF and CNTF most likely lies in the mechanism in which they mediate pro-survival and anti-apoptotic signals in neurons.

CNTF, a member of the IL-6 family of cytokines, acts through a heterotrimeric receptor complex composed of CNTF receptor α along with leukemia inhibitory factor receptor β and glycoprotein gp130 found both photoreceptors and Müller cells [27, 29]. On the other hand, GDNF is a member of the TGF-β family, signaling through binding and activation of the GFRα-1 and RET receptors that are only found on the Müller cell surface [179, 180]. Interestingly, GDNF has also been found to upregulate bFGF secretion from Müller cells, mediating an indirect pro-survival pathway for degenerating photoreceptors [175]. Thus, the targeting of Müller cells to secrete GDNF in our therapeutic approach ostensibly follows an autocrine-like pathway to effect rescue. Additional studies have also pointed to increases in synaptic efficiency in dopaminergic neurons through GDNF-treatment, resulting in augmented release of dopamine and glutamate [181, 182]. This may further contribute to functional rescue, specifically as seen in ERG b-wave recordings, through the strengthening of photoreceptor-bipolar cell synapses. This synergism provided by GDNF may in part explain its greater efficacy relative to CNTF for rescue, although much remains unknown as to the mechanisms underlying these differences.

In the present study, we employed a new glial-specific AAV variant to deliver hGDNF to Müller cells through a vitreal injection route, achieving sustained rescue in S334-4 RP rats. Future enhancements of this therapeutic approach could involve co-injection with vectors bearing bFGF in light of its shared role in photoreceptor rescue with GDNF [179]. In translating these results to the clinic, a critical limitation is the physiological differences between human and rat eyes, specifically a thicker ILM in humans that acts as a significant barrier to transduction. Studies in primates [144] have shown that intravitreally injected AAV2 forms a distinctive annular expression pattern around the fovea, an area consequently with the thinnest ILM in the retina. However, the use of directed evolutionary approaches with surface-exposed tyrosine mutagenesis, as employed in this study, potentially coupled with ILM-thinning protease treatment [55]may enable sufficient gains in intravitreal retinal transduction to promote rescue through neurotrophic secretion. We are in the process of examining the efficacy of this approach in canines and primates.

Chapter 5

Molecular Evolution of Adeno-associated Virus for Enhanced Intravitreal Photoreceptor Transduction

Preface:

This work was done in collaboration with Dr. Deniz Dalkara, a post-doctoral fellow in the Flannery and Schaffer Labs at UC Berkeley. Natalie Hoffman, Meike Visel, and Christin Hong provided technical assistance.

Abstract:

Adeno-associated viral (AAV) gene delivery to photoreceptors currently requires an invasive subretinal delivery route to achieve transduction. For targeting photoreceptors as a therapeutic strategy for treating retinal degenerative diseases, an intravitreal delivery route would be desirable in terms of safety, simplicity, and diffusivity of expression. However, natural AAV serotypes are incapable of transducing photoreceptors from the vitreous due to the enormous physiological barriers present in the retina, most significantly the inner limiting membrane and the overlying strata of neuronal and glial cell bodies and processes occluding photoreceptor cell accessibility. Here, we employed an *in vivo* directed evolutionary strategy in a Rho-GFP transgenic line of mice with a panel of three distinct AAV libraries to evolve variants capable of infecting photoreceptors from the vitreous. We successfully isolated a variant from our AAV2 peptide display library, named 7M8, capable of efficient intravitreal photoreceptor transduction. Additionally, surface-exposed tyrosine mutagenesis further increased 7M8 infectivity, surpassing levels achieved in a quadruple tyrosine mutant AAV2 vector. Our findings demonstrate that AAV is a highly versatile vector capable of substantial increases in infectivity from minor sequence changes as a result of an *in vivo* directed evolutionary approach.

Introduction:

Photoreceptors are the first neurons in the retina to receive and process visual information, converting visible electromagnetic radiation into hyperpolarized responses through phototransduction. The overwhelming majority of inherited retinal diseases result in the loss of these cells, either directly, such as in dominant mutations that affect rhodopsin protein folding, or indirectly, such as in recessive mutations that affect retinal recycling pathways in the retinal pigment epithelium (RPE) [34,162,183,184]. The convergence of these disparate diseases into a common neurodegenerative phenotype makes photoreceptors an attractive gene delivery target for gene replacement, antisense, and/or neurotrophic therapeutic strategies to lessen or even stop photoreceptor cell loss.

The use of viral vectors including lentivirus and adeno-associated virus (AAV) has met with success in transducing photoreceptors through subretinal administration for gene-based therapies[72,173,185]. Most recently, a recombinant AAV5 vector containing a human L-opsin gene successfully restored trichromatic color vision behavior in a dichromatic primate[186]. Additionally, delays in photoreceptor degeneration were achieved through the use of subretinally and intravitreally injected recombinant AAV vector bearing glial derived neurotrophic factor (hGDNF) in a transgenic rat model of retinitis pigmentosa (RP) [173]. Due to the significant advantages of vector transduction via intravitreal injection relative to subretinal injection, namely safety, simplicity, and diffusivity of expression, intravitreal-mediated gene delivery to photoreceptors would be ideal for gene therapeutic purposes. Unfortunately, naturally occurring serotypes of AAV are incapable of transducing photoreceptors form the vitreous due to the enormous physical barriers obstructing these cells[55]. The inner limiting membrane and the overlying strata of neuronal and glial cell bodies and processes results in a formidable diffusive obstacle for AAV particles, despite their small size.

Marginal success has been attained in increasing intravitreal photoreceptor gene delivery through mutagenizing tyrosine residues on the AAV capsid surface[93]. Tyrosine residues naturally target AAV particles for proteosome-mediated degradation via an ubiquitin-dependent pathway once they are endocytosed within the cell[92]. This process is initiated by tyrosine phosphorylation by the epidermal growth factor receptor protein tyrosine kinase (EGFR-PTK). Substitution with a phenylalanine residue allows AAV to abrogate this pathway, enabling greater efficiency of viral gene delivery to cell nuclei. In this regard, the Hauswirth lab achieved limited intravitreal photoreceptor transduction of murine photoreceptors through the use of an AAV2 Y444F vector[93]. These results suggest that AAV2 has the partial ability to reach the ONL from the vitreous and infect photoreceptors. In this respect, directed evolution of AAV capsid may enable increases in infectivity based on subtle sequence changes that allows virions to better surpass the ILM, evade sequestration within the RGC and INL layers, and / or overcome photoreceptor cellular barriers.

Due to the complexity of these physiological barriers, an *in vivo* screening methodology is critical for selecting for permissive variants. The recent creation of a transgenic line of mice bearing a rhodopsin-GFP fusion[187] has enabled this approach as selective expression of GFP in photoreceptor outer segments allows for the isolation of photoreceptors via fluorescence activated cell sorting (FACS). Thus, an evolutionary strategy involving direct vitreal injection of viral libraries followed by photoreceptor cell isolation and PCR rescue may enable the creation of permissive variants for intravitreal photoreceptor transduction. Here, we describe the results of this selection strategy through the use of three distinct AAV libraries: a novel AAV2 Y444F error prone library, an AAV2 heptamer insertion library, and a shuffled library composed of AAV serotypes 1-9. The successful creation of novel AAV vectors that transduce photoreceptors from the vitreous will result in the creation of new gene therapeutic strategies for combating a wide array of inherited retinal degenerative diseases.

Materials and Methods:

Library generation and viral production. Random mutagenesis libraries were generated by subjecting *cap* genes from AAV2 Y444F to error-prone PCR using CAP For and CAP Rev as forward and reverse primers, respectively, as previously described [120]. To generate the Y444F mutation on the AAV2 *cap* gene, as well as all subsequent tyrosine to phenylalanine mutations, a site directed mutagenesis kit was used (QuikChange® Lightning, Agilent Technologies). Peptide display libraries were generated similar to previous reports [118, 119]. Briefly, a unique *Avr*II was introduced into pSub2Cap2 between amino acid 587 and 588 by PCR mutagenesis. A random 21 nucleotide insert, 7mer For, was used to synthesize dsDNA inserts, along with the antisense primer 7mer Rev. The resulting dsDNA inserts were cloned into the *Avr*II site of pSub2Cap2 after digestion with *Nhe*I. A previously generated AAV library constructed by DNA shuffling of *cap* genes from AAV1, 2, 4–6, 8, and 9 was also used [121].

The rcAAV libraries and rAAV vectors expressing GFP under a CAG or Rho promoter were packaged as previously described [120, 121]. DNase-resistant genomic titers were obtained via quantitative PCR.

Library selection and evolution. The libraries were initially combined and two rounds of evolution were performed. One round of evolution consisted of initial library diversification followed by three selection steps. Briefly, in one round of selection, P30 rho-GFP mice were intravitreally injected with 2µL of PBS-dialyzed, iodixanol-purified library with a genomic titer of approximately $1x10^{12}$ vg/mL. All animal procedures were conducted according to the ARVO Statement for the Use of Animals and the guidelines of the Office of Laboratory Animal Care at the University of California, Berkeley. Before vector administration, mice were anesthetized with ketamine (72 mg/kg) and xylazine (64 mg/kg) by intraperitoneal injection. An ultrafine 30 1/2-gauge disposable needle was passed through the sclera, at the equator and next to the limbus, into the vitreous cavity. Injection of 2µl was made with direct observation of the needle in the center of the vitreous cavity.

One week post-injection, eyes were enucleated and retinas dissociated using a light,

papain protease treatment, followed by FACs isolation of photoreceptor populations. Successful virions were then PCR amplified from subsequent genomic extractions and further cloned and repackaged for injection. Following two rounds of evolution, the cap genes of fifty variants were sequenced to determine the most prominent and successful variants to have permissive mutations for intravitreal photoreceptor transduction.

***In vivo* characterization** P30 wild-type mice were used for characterization after library selection. Intravitreal injections were performed similarly as before. One to three weeks after vector injection, mice were humanely euthanized, the eyes were enucleated, a hole was introduced in the cornea, and tissue was fixed with 10% neutral buffered formalin for 2–3 hours. The cornea and lens were removed. The eyecups were washed in PBS followed by 30% sucrose in the same buffer overnight. Eyes were then embedded in optimal cutting temperature embedding compound (OCT; Miles Diagnostics, Elkhart, IN) and oriented for 10 μm thick transverse retinal sections. Tissue sections were rehydrated in PBS for 5 minutes followed by incubation in a blocking solution of 1% bovine serum albumin, 0.5% Triton X-100, and 2% normal donkey serum in PBS for 2–3 hours. Slides were incubated overnight at 4 °C with commercial rabbit monoclonal antibody raised against the GFP (Invitrogen, Carlsbad, CA) at 1:400 or mouse monoclonal antibody raised again AAV2 (A20) at 1:400. The sections were then incubated with Alexa 488–conjugated secondary anti-rabbit or anti-mouse antibody (Molecular Probes, Grand Island, NY) at 1:1000 in blocking solution for 2 hours at room temperature. The results were analyzed by fluorescence microscopy using an Axiophot microscope (Zeiss, Thornwood, NY) equipped with X-Cite PC200 light source and QCapture Pro camera, or by confocal microscopy (LSM5; Carl Zeiss Microimaging, Thornwood, NY).

***In Vitro* Transduction Analysis** Transduction studies using rAAV CAG-GFP were performed with 5×10^4 cells (CHO, pgsA, Pro5, and Lec1) in 6-well plates. Cells were transduced with rAAV GFP vectors at a gMOI of 10^3–10^5 (n = 3), and the percentage of GFP-expressing cells was determined by flow cytometry 4 days post-infection.

Results:

Library selection

Three different libraries with a diversity of approximately $1x10^7$ were employed for *in vivo* selection in transgenic rho-GFP mice. Besides the AAV2 heptamer insertion and AAV 1-9 shuffled libraries we've employed in previous studies, we created a tyrosine mutated error prone library (AAV2 Y444F EP) in light of the marginal success observed in previous studies for AAV2 Y444F in reaching photoreceptors from the vitreous. The libraries were initially combined and two rounds of evolution were performed. One round of evolution consisted of initial library diversification followed by three selection steps. Briefly, in one round of selection, P30 rho-GFP mice were intravitreally injected with 2μL of PBS-dialyzed, iodixanol-purified library with a genomic titer of approximately $1x10^{12}$ vg/mL. One week post-injection, eyes were enucleated and retinas dissociated using a light, papain protease treatment, followed by FACs isolation of photoreceptor populations (Figure 5.1). Successful virions were then PCR amplified from subsequent genomic extractions and further cloned and repackaged for injection.

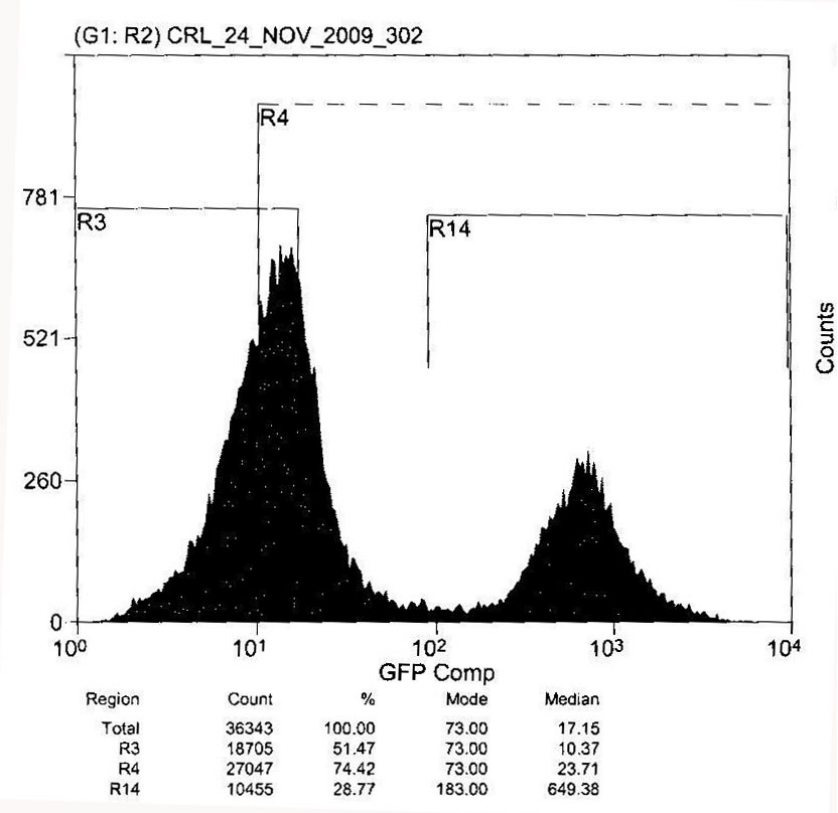

Region	Count	%	Mode	Median
Total	36343	100.00	73.00	17.15
R3	18705	51.47	73.00	10.37
R4	27047	74.42	73.00	23.71
R14	10455	28.77	183.00	649.38

Figure 5.1 Representative FACS plot of retinal dissociate from rho-GFP mice. The expression of a rhodopsin-GFP fusion allows for the segregation of photoreceptor cells populations (region R14) from retinal dissociate.

Following two rounds of evolution, the cap genes of fifty variants were sequenced to determine the most prominent and successful variants to have permissive mutations for intravitreal photoreceptor transduction (Table 5.1). Remarkably, all isolated clones derived from the AAV2 7mer peptide insertion library (Figure 5.2). Furthermore, nearly two thirds of them contained the same distinct 7mer motif (~^{588}LGETTRP~). Interestingly, the next most prominent variant (~^{588}NETITRP~) also contained a similar flanking motif consisting of a positively-charged arginine residue in between a polar threonine and a nonpolar proline residue (TRP).

Clone	Frequency (%)
~^{588}LGETTRP~	64
~^{588}NETITRP~	12
~^{588}KAGQANN~	6
~^{588}KDPKTTN~	4

Table 5.1 Sequencing of isolated variants from directed evolution reveals a high degree of convergence in viral libraries. All variants derived from the AAV2 7mer library, with 64% of variants containing the same 7mer motif (~^{588}LGETTRP~).

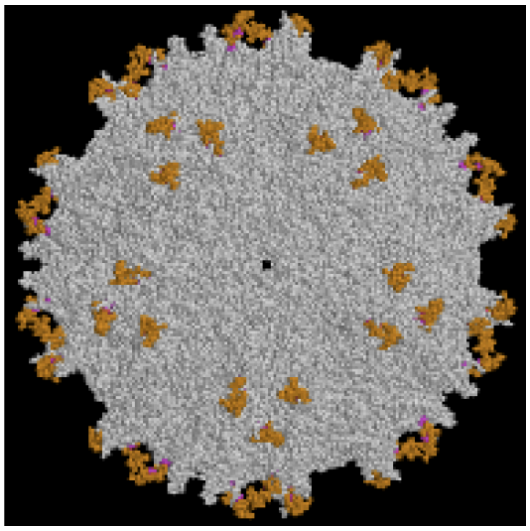

Figure 5.2. Representative three-dimensional capsid model of AAV2 containing a random heptamer (shown in orange) following amino acid 587. This area of the AAV2 capsid likely participates in cell-surface receptor binding.

***In vivo* characterization**

In light of the high degree of library convergence from our selection, we next cloned a recombinant form of AAV2 ~^{588}LGETTRP~ (nick named 7M8) and packaged the vector with a scCAG-GFP transgene to visualize its transduction profile. Three weeks following intravitreal injection in adult mice, we observed robust expression in numerous cell types including RGCs and Müller cells. Importantly, we observed transduction of photoreceptors in retinas injected with 7M8 as seen by GFP expression in ONL nuclei (red arrows) and in outer segments (Figure 5.3, blue arrows) whereas AAV2 showed no discernable photoreceptor expression. Although expression in Müller cells and RGCs is more prominent than in photoreceptors, this is likely because fewer viral copies made it into photoreceptors relative to other retinal cell types. Namely, our positive selection methodology directed virus towards greater infective efficiency, not necessarily specificity.

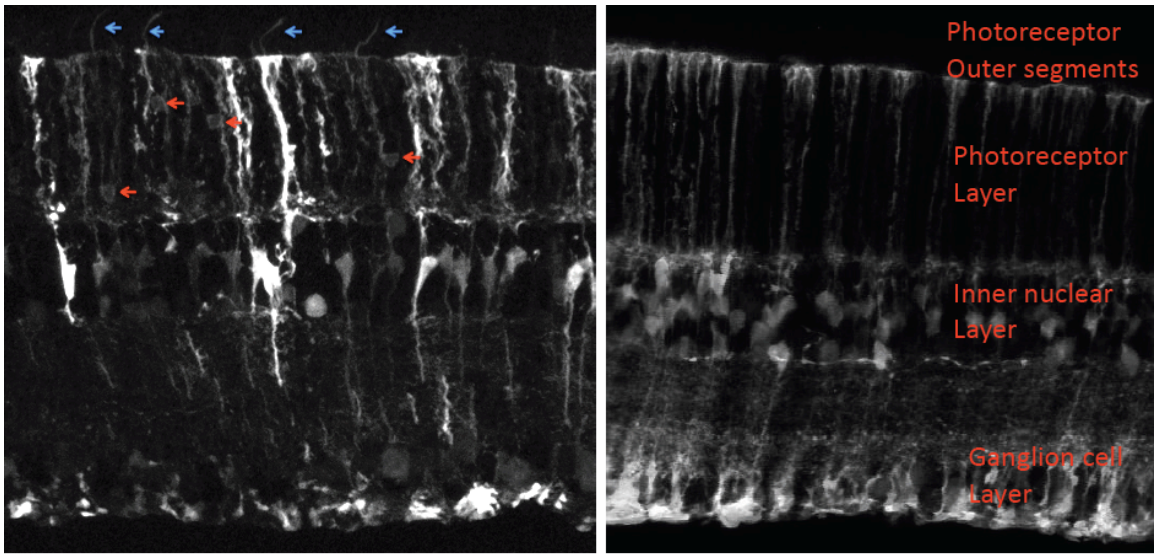

Figure 5.3 AAV2 7M8 variant (left) demonstrates greater levels of intravitreal photoreceptor transduction relative to AAV2 (right). Confocal microscopy of transverse

retinal sections three weeks after intravitreal injection of 3μL of $1x10^{12}$ vg/mL of AAV2 7M8 and AAV2 scCAG GFP in adult mice. Red arrows (top) denote photoreceptor nuclei and blue arrows (top) denote photoreceptor outer segments.

Tyrosine mutagenesis

In light of these impressive gains in photoreceptor transduction, we next sought to improve 7M8 transduction efficiency by combining a rational design approach to our previous blackbox approach. We reasoned that directed evolution enabled greater extracellular delivery of virus to the ONL as well as perhaps greater receptor-mediated endocytosis in photoreceptors. Since the photoreceptor infectivity of the 7M8 variant and a triple AAV2 tyrosine mutant (AAV2 Y444F, Y500F, Y730F) demonstrated similar levels of transduction (Figure 5.4), further improvements in an intracellular context through tyrosine mutagenesis may synergistically increase expression. Therefore, we mutagenized four surface exposed tyrosine residues to phenylalanines on the 7M8 capsid (Y273F, Y444F, Y500F, and Y730F). We further sought to increase specificity in expression through the use of the photoreceptor-specific rhodopsin promoter to better resolve transduction efficiencies.

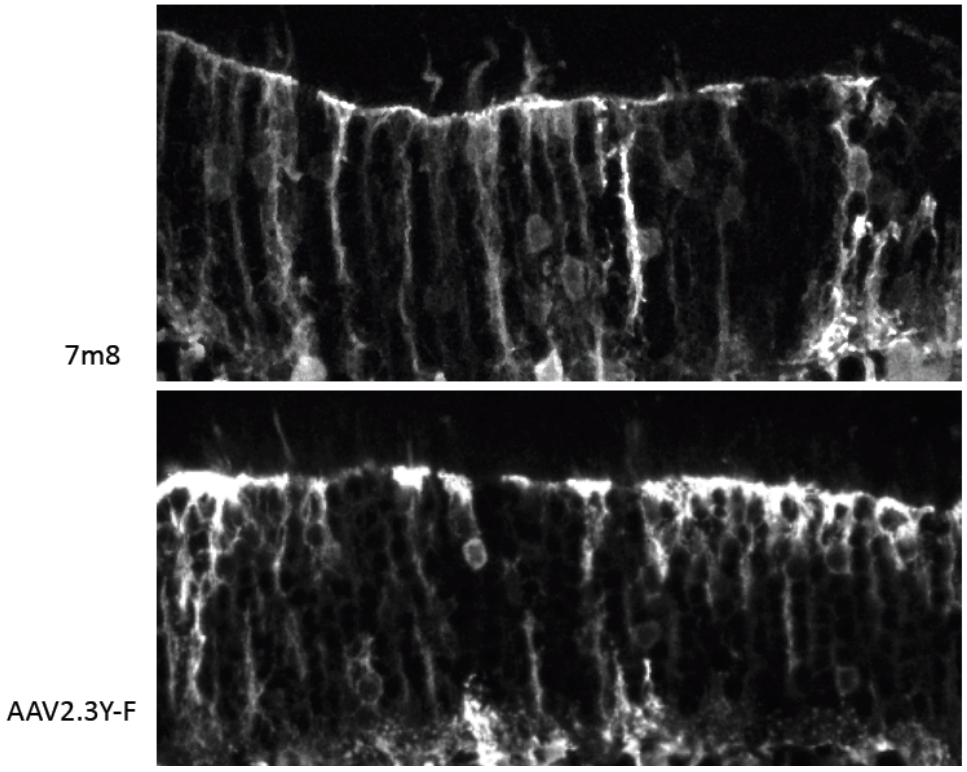

Figure 5.4 AAV2 7M8 (top) and a triple AAV2 tyrosine mutant (bottom) show similar levels of photoreceptor transduction. Confocal microscopy of transverse retinal sections

three weeks after intravitreal injection of 3μL of $1x10^{12}$ vg/mL of AAV2 7M8 and AAV2 Y444F, Y500F, Y730F scCAG GFP in adult mice. Close up of the outer limiting membrane highlights similar levels of GFP expression in photoreceptor nuclei and outer segments between the two viruses.

One month post-injection of 7M8 4Y, we qualitatively observed substantial increases in photoreceptor transduction relative to both 7M8, AAV2, and most notably AAV2 4Y injected eyes (Figures 5.3, 5.5). The differences in transduction efficiencies between 7M8 4Y and AAV2 4Y suggest two important considerations: tyrosine mutagenesis increases infectivity through a distinct mechanism relative to our peptide-insert variant's, and further, the combination of these two distinct pathways results in additive improvements in transduction. It is important to note that the Rho-GFP transgene used in these injections is a single-stranded construct, so results may be somewhat dampened relative to the more efficient self-complementary transgenes used in previous injections. However, this further underscores the robustness of the 7M8 4Y vector and further quantitative analysis using a 7M8 ssRho-GFP vector as a basis of comparison should corroborate these improvements.

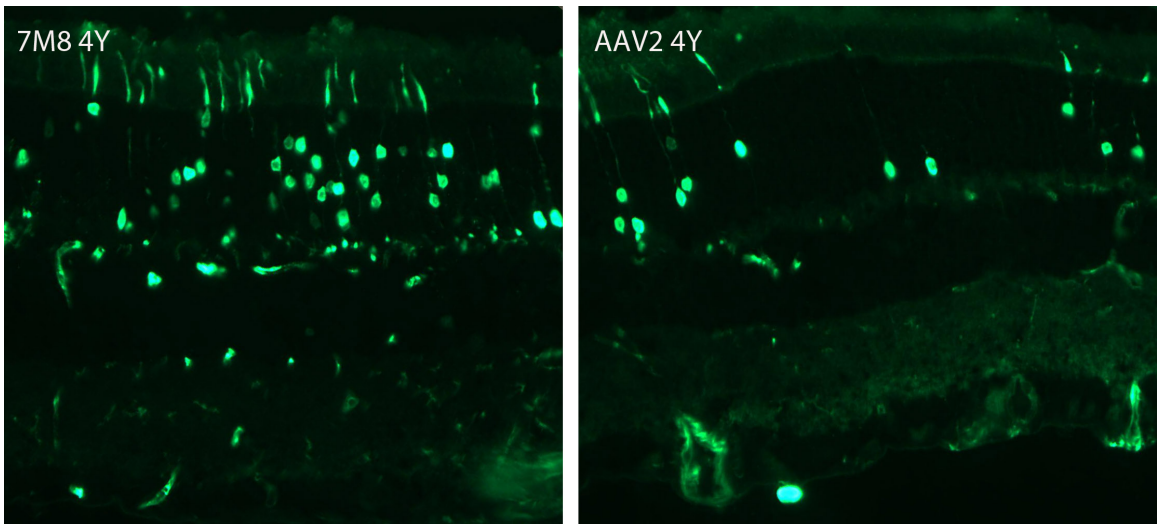

Figure 5.5 AAV2 7M8 4Y variant (left) demonstrates greater levels of intravitreal photoreceptor transduction relative to AAV2 4Y (right). Fluorescence microscopy of transverse retinal sections stained with anti-GFP one month after intravitreal injection of 3μL of $1\text{-}5x10^{12}$ vg/mL of AAV2 7M8 4Y and AAV2 4Y ssRho-GFP in adult mice.

Mechanism:

To examine AAV2 7M8's mechanism of transduction, we first assayed its glycan dependencies on a panel of different cell types *in vitro (*Figure 5.6). AAV2 and AAV2 7M8 transduction efficiencies in CHO cells and pgsA cells, which lack heparin sulfate production, reveal strong heparin dependencies for both viruses with a log drop in infectivity. Conversely, both viruses showed no sialic acid dependence as transduction efficiencies were similar between Pro5 cells and Lec1 cells, which are deficient in sialic acid production. Interestingly, amongst all cell types, AAV2 7M8 showed substantial increases in transduction relative to AAV2, with between ten to a hundred fold increase in infectivity.

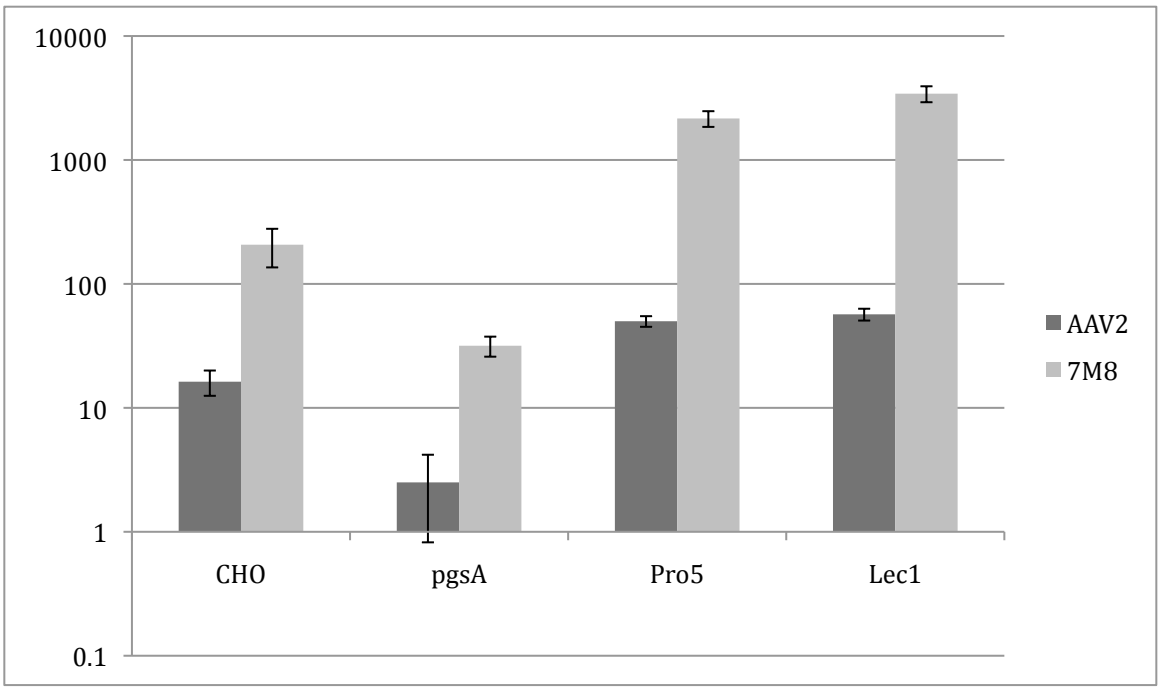

Figure 5.6. In vitro characterization of 7M8. CHO, PgsA, Pro5, and Lec1 cell transduction by rAAV2 and 7M8 carrying scCAG-GFP; Y-axis represents the ratio of TU :vg x10^4. (B) CHO/PgsA transduction demonstrating the HSPG dependence of AAV2 and 7M8. (C) Pro5/Lec1 transduction examining sialic acid dependence of AAV2 and 7M8.

When assaying heparin binding affinity (Figure 5.7), 7M8 actually demonstrates a sharper elution profile and a lower heparin affinity relative to AAV2, most likely because the inserted 7mer is localized near the AAV2 HSPG binding domain, occluding efficient binding. This lower heparin binding affinity is further confirmed through AAV capsid immunostaining using the anti-AAV2 A20 antibody (Figure 5.8). Notably, accumulation around the ILM, an area prominent in HSPGs, is less prominent in 7M8 injected eyes relative to AAV2. However, a more sensitive analysis of particle distribution past the

ILM will be needed to see whether the 7M8 variant more readily diffuses throughout the retina. In reconciling these observations with our *in vitro* data, 7M8's remarkably high infectivity most likely is a result of efficient binding to another, as yet undefined, cell surface receptor, or the result of greater efficiencies in intracellular viral trafficking and / or nuclear localization.

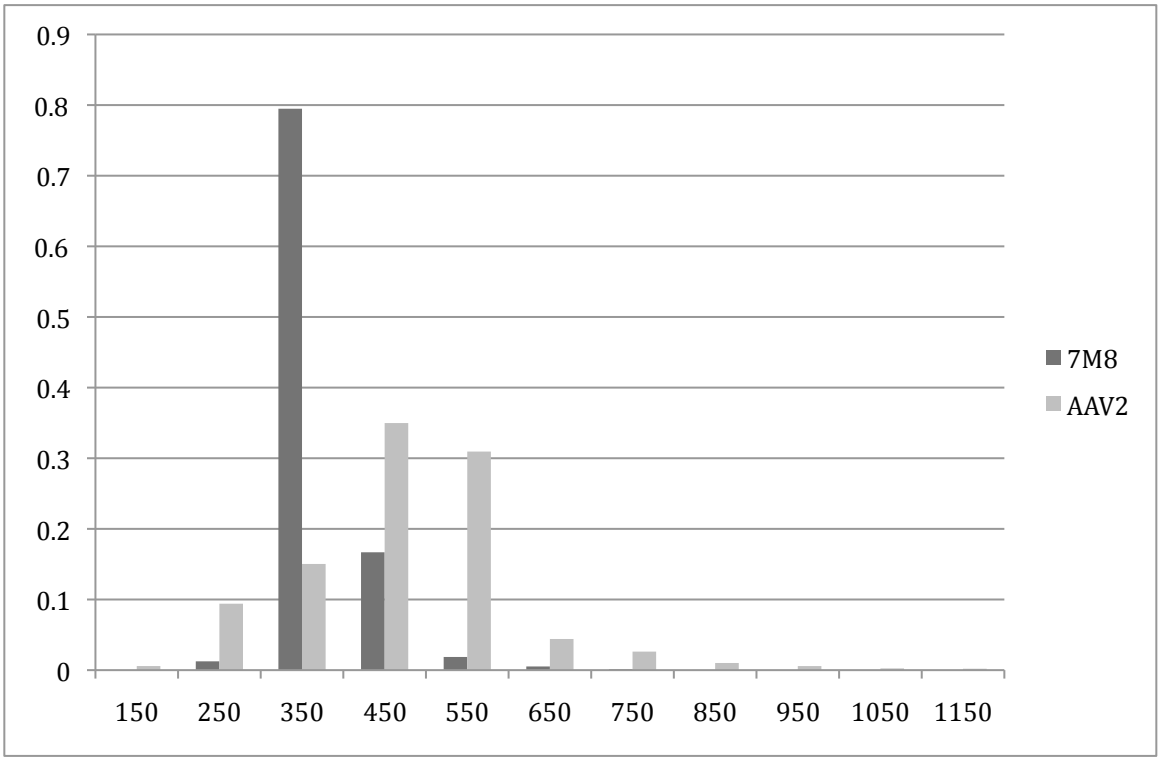

Figure 5.7. Heparin binding affinity of 7M8 and AAV2. Elution profile from a heparin column for 7M8 and AAV2. Y-axis values represent the fraction of virus eluted, and the X-axis represents the concentration of NaCl in the eluant (mM).

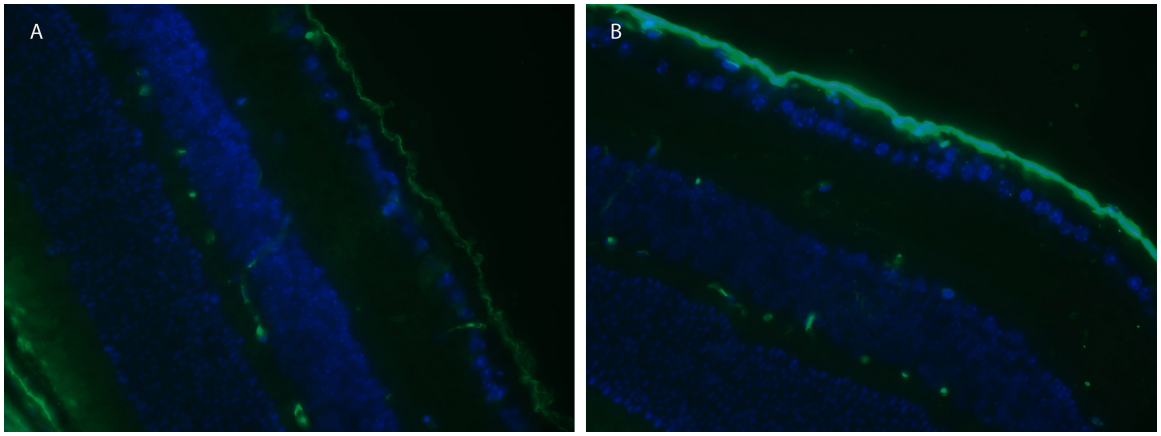

Figure 5.8. Immunostaining of AAV2 7M8 (a) and AAV2 (b) capsid proteins reveal stronger adherence of AAV2 to the ILM relative to AAV2 7M8. Fluorescence microscopy of immunostained transverse retinal sections using a mouse anti-AAV2 capsid antibody (A20) with secondary anti-mouse Alexa-488 conjugated antibodies. Sections were taken three days post injection of 3μL of $1x10^{12}$ vg/mL of AAV2 7M8 and AAV2.

Discussion

Our results demonstrate that our *in vivo* selection approach was sufficient to produce a variant that overcomes the substantial intravitreal barriers to photoreceptor infection. The remarkable degree of convergence from our initial starting libraries reflects the tremendous constraints imposed from our positive selection. Variants must not only surpass the ILM, but also through a tight extracellular matrix network formed between a meshwork of retinal cell bodies and processes to reach the ONL. Additionally, variants must bind to photoreceptor cell surface receptors and subsequently overcome intracellular barriers to transduction. The predominance of AAV2 based variants from our selection most likely is due to the critical importance of heparin-sulfate binding for surpassing the ILM in intravitreal AAV transduction. Our previous studies have shown that amongst natural AAV serotypes in the murine retina, only those which bind HSPG, such as AAV2, efficiently infect from the vitreous [55]. Thus, within our pool of libraries, variants based on heparin-binding templates held immediate advantage relative to other variants, easily out competing them in the first rounds of selection. In future studies, segregating library populations may thus be an effective way to achieve greater variant diversities based on other AAV serotypes with unique tropism profiles. For instance, AAV5's ability to efficiently and selectively infect photoreceptors from the subretinal space may make it a promising template for an error prone mutagenesis library.

Overall, our isolated peptide-insert variant 7M8 demonstrates significant transduction of photoreceptors, as well as all cell types within the retina (Figure 5.3). Further tyrosine-mutagenesis augments this ability while the use of a rhodopsin promoter successfully restricts expression to photoreceptors (Figure 5.5). In beginning to deduce 7M8's mechanism, the variant's reduced heparin affinity relative to AAV2 (Figure 5.6) may in part explain its unique properties. In first binding to the ILM, the presence of high levels of heparin sulfate in the proteoglycan matrix of the ILM may mediate viral localization at this site, preventing it from being cleared from the vitreous and thus facilitating intravitreal transduction (Figure 5.8) [55]. However, viral HSPG affinities may play a duel role in intravitreal transduction, as too high of an affinity may also encumber efficient viral penetration in the retina, similar to results seen in our previous mechanistic study of our AAV variant ShH10 [176]. Further possibilities for 7M8's increased infectivity, as it appears to not be limited to just photoreceptors, is that its 7mer insert may bind to a common cell surface receptor or more intriguingly, it may act as a nuclear localization signal within the cell. A protein BLAST search does not reveal any notable sequence matches, but the use of quantum dot labeling may reveal enhanced intracellular trafficking properties.

In this study, the successful isolation of a novel AAV variant that transduces photoreceptors from the vitreous serves as an important foundation in the development of new gene therapeutic strategies for combating a wide array of inherited retinal degenerative diseases. Additionally, the pan-retinal infective properties of 7M8 coupled with the use of promoters for cell-restrictive expression may make it a valuable vector for targeting other neurons in the retina. For example, gene delivery of synthetic light-sensitive channels, such as LiGluR, to ON-bipolar cells may allow for the artificial restoration of vision in ONL-depleted retinas. More broadly, further mechanistic dissection of 7M8 and other AAV variants isolated from *in vivo* selections may reveal common motifs that can be exploited to create a new generation of more efficient AAV vectors.

Chapter 6

Concluding Remarks

The results of this dissertation sought to address the need for broad, safe, and effective therapies for treating retinal degenerative diseases. Specifically, current therapies based on surgical or pharmacological intervention do not provide a simple, long-term treatment for progressive blinding diseases. However, the eye possesses unique properties that make it a great candidate for viral-mediated gene therapy. Its accessibility and seclusion in the body allow for localized delivery of vector without the need for systemic administration while the blood-brain barrier minimizes the risk of an immune response. Additionally, the eye's external accessibility allows for easy *in vivo* imaging and functional studies while the treatment of one eye alone allows the other eye to serve as an internal control.

However, current therapies based on AAV-mediated gene delivery, though promising, lack broad applicability and require the use of an invasive subretinal injection route, which limits the spread of vector and can cause damage through retinal tearing and detachment. These limitations were recently illustrated by Mancuso et al.'s gene therapy study for restoring trichromatic vision in primates. Although ultimately successful, delivery of the human L-opsin gene required three subretinal injections surrounding the cone-rich fovea, the area most critical for color and highly-resolved vision, to avoid retinal detachment[186].

To address the limitations posed by a subretinal injection route, we first identified natural barriers to intravitreal viral vector delivery and further developed pharmacological methods to overcome these barriers. Specifically, the inner limiting membrane (ILM) was identified as the main obstacle to efficient intravitreal gene delivery and mild digestion with a nonspecific protease substantially enhanced transduction in multiple cell types from the vitreous. We next evolved more efficient glial-permissive AAV vectors in the CNS and retina and employed them to intravitreally target Müller cells for GDNF secretion, resulting in functional and histological rescue in an animal model of retinitis pigmentosa. Additionally, we successfully evolved an AAV variant to target photoreceptors from the vitreous, which would enable an important new approach for treating retinal degenerative diseases using neurotrophic, gene replacement, and / or antisense strategies.

These results build upon previous improvements in AAV vectors that have made them more efficient gene delivery agents. These enhancements include the development of self-complementary transgenes[84], which overcomes the rate-limiting step of viral genome second-strand synthesis, as well as mutagenesis on surface-exposed capsid

tyrosines[92] to mitigate proteosomal degradation of virion particles. The use of directed evolution techniques provides an important element in AAV capsid engineering, and more broadly, protein engineering. The enormous complexity inherent in biological structures can create nearly insurmountable barriers for rational design approaches. Even a 20 amino acid sequence can have more unique permutations than the entirety of stars in the universe. Directed evolution allows one to draw a black box around the problem, shifting the focus from the minutia of mechanism to a broader end result. However, even this approach can be limited by library diversity, as diversities of trillions can look trivial relative to theoretical sequence permutations numbering in the trillions of trillions. The marriage of the two concepts thus becomes crucial, necessitating the use of rationally-designed templates as starting points for evolution as we have attempted in these studies, most notably in our semi-random peptide replacement library. Other recent AAV directed evolution studies have utilized a similar strategy, including the use of chimeric libraries to generate variants that cross the seizure-compromised blood-brain barrier [188]as well as the reengineering of the AAV2 receptor footprint with corresponding residues from other AAV serotypes to achieve selective, systemic gene transfer to muscle tissue[189]. Success in the development of new, more efficient AAV variants will thus rest on both a greater understanding of AAV biology, as well as the conception of novel libraries that exploit this understanding.

Importantly, the future of AAV-mediated gene therapy rests in translating results attained in animal studies to the clinic. The success of the LCA clinical trials, though directed towards a small segment of patients, may well presage the wider use of AAV for retinal gene therapy. The successful creation of AAV vectors that are efficient at transducing retina via intravitreal injection, as sought in this dissertation, will hasten this adoption. Although the vectors designed in this dissertation will face new and more significant obstacles in primate and human eyes, our results demonstrate an important proof of principle. Namely, minor sequence changes attained through directed evolution can result in significant increases in AAV transduction efficiency and specificity that can further be translated into more efficient gene therapies. We hope our results will provide an important foundation for tackling further hurdles in human retinal gene therapy.

References

1. Hageman GS, Johnson LV (1991) The photoreceptor-retinal pigmented epithelium interface. In: Heckenlively JR, Arden GB, editors. Principles and Practice of Clincial Electrophysiology of Vision. St. Louis: Mosby Year Book. pp. 53-68.
2. Dowling JE (2001) Neurons and networks; an introduction to behavioral neuroscience. Cambridge: Harvard University Press.
3. Hargrave PA, McDowell JH (1992) Rhodopsin and phototransduction. Int Rev Cytol 137B: 49-97.
4. Kolb H, Fernandez E, Schouten J, Ahnelt P, Linberg KA, et al. (1994) Are there three types of horizontal cell in the human retina? J Comp Neurol 343: 370-386.
5. Boycott BB, Wassle H (1991) Morphological Classification of Bipolar Cells of the Primate Retina. Eur J Neurosci 3: 1069-1088.
6. Mariani AP (1990) Amacrine cells of the rhesus monkey retina. J Comp Neurol 301: 382-400.
7. Kolb H, Linberg KA, Fisher SK (1992) Neurons of the human retina: a Golgi study. J Comp Neurol 318: 147-187.
8. Boycott BB, Hopkins JM (1981) Microglia in the retina of monkey and other mammals: its distinction from other types of glia and horizontal cells. Neuroscience 6: 679-688.
9. Trivino A, Ramirez JM, Salazar JJ, Ramirez AI, Garcia-Sanchez J (1996) Immunohistochemical study of human optic nerve head astroglia. Vision Res 36: 2015-2028.
10. Reichenbach A, Robinson SR (1995) The involvement of Muller cells in the outer retina. In: Djamgoz M, Archer SN, Vallerga S, editors. Neurobiology and clinical aspects of the outer retina. London: Chapman & Hall. pp. 395-416.
11. Jadhav AP, Roesch K, Cepko CL (2009) Development and neurogenic potential of Muller glial cells in the vertebrate retina. Prog Retin Eye Res 28: 249-262.
12. Franze K, Grosche J, Skatchkov SN, Schinkinger S, Foja C, et al. (2007) Muller cells are living optical fibers in the vertebrate retina. Proc Natl Acad Sci U S A 104: 8287-8292.
13. Kolstad KD (2009) Development and Assessment of Gene Therapies for Inherited Blinding Diseases. Berkeley: Univeristy of California, Berkeley. 210 p.
14. Williams R, Airey M, Baxter H, Forrester J, Kennedy-Martin T, et al. (2004) Epidemiology of diabetic retinopathy and macular oedema: a systematic review. Eye (Lond) 18: 963-983.
15. Geraldes P, Hiraoka-Yamamoto J, Matsumoto M, Clermont A, Leitges M, et al. (2009) Activation of PKC-delta and SHP-1 by hyperglycemia causes vascular cell apoptosis and diabetic retinopathy. Nat Med 15: 1298-1306.
16. Mozaffarieh M, Grieshaber MC, Flammer J (2008) Oxygen and blood flow: players in the pathogenesis of glaucoma. Mol Vis 14: 224-233.
17. Silvestri G (1997) Age-related macular degeneration: genetics and implications for detection and treatment. Mol Med Today 3: 84-91.
18. de Jong PT (2006) Age-related macular degeneration. N Engl J Med 355: 1474-1485.

19. Yang Z, Camp NJ, Sun H, Tong Z, Gibbs D, et al. (2006) A variant of the HTRA1 gene increases susceptibility to age-related macular degeneration. Science 314: 992-993.
20. Hartong DT, Berson EL, Dryja TP (2006) Retinitis pigmentosa. Lancet 368: 1795-1809.
21. Farrar GJ, Kenna PF, Humphries P (2002) On the genetics of retinitis pigmentosa and on mutation-independent approaches to therapeutic intervention. EMBO J 21: 857-864.
22. Fante RJ, Durairaj VD, Oliver SC (2010) Diabetic Retinopathy: An Update on Treatment. Am J Med 123: 213-216.
23. Stewart WC, Sine CS, LoPresto C (1996) Surgical vs medical management of chronic open-angle glaucoma. Am J Ophthalmol 122: 767-774.
24. Hubschman JP, Reddy S, Schwartz SD (2009) Age-related macular degeneration: current treatments. Clin Ophthalmol 3: 155-166.
25. Bressler NM (2009) Antiangiogenic approaches to age-related macular degeneration today. Ophthalmology 116: S15-23.
26. Sieving PA, Caruso RC, Tao W, Coleman HR, Thompson DJ, et al. (2006) Ciliary neurotrophic factor (CNTF) for human retinal degeneration: phase I trial of CNTF delivered by encapsulated cell intraocular implants. Proc Natl Acad Sci U S A 103: 3896-3901.
27. Wahlin KJ, Campochiaro PA, Zack DJ, Adler R (2000) Neurotrophic factors cause activation of intracellular signaling pathways in Muller cells and other cells of the inner retina, but not photoreceptors. Invest Ophthalmol Vis Sci 41: 927-936.
28. LaVail MM, Yasumura D, Matthes MT, Lau-Villacorta C, Unoki K, et al. (1998) Protection of mouse photoreceptors by survival factors in retinal degenerations. Invest Ophthalmol Vis Sci 39: 592-602.
29. Liang FQ, Aleman TS, Dejneka NS, Dudus L, Fisher KJ, et al. (2001) Long-term protection of retinal structure but not function using RAAV.CNTF in animal models of retinitis pigmentosa. Mol Ther 4: 461-472.
30. Emerich DF, Thanos CG (2008) NT-501: an ophthalmic implant of polymer-encapsulated ciliary neurotrophic factor-producing cells. Curr Opin Mol Ther 10: 506-515.
31. Chader GJ, Weiland J, Humayun MS (2009) Artificial vision: needs, functioning, and testing of a retinal electronic prosthesis. Prog Brain Res 175: 317-332.
32. Cideciyan AV, Aleman TS, Boye SL, Schwartz SB, Kaushal S, et al. (2008) Human gene therapy for RPE65 isomerase deficiency activates the retinoid cycle of vision but with slow rod kinetics. Proc Natl Acad Sci U S A 105: 15112-15117.
33. Hauswirth W, Aleman TS, Kaushal S, Cideciyan AV, Schwartz SB, et al. (2008) Phase I Trial of Leber Congenital Amaurosis due to RPE65 Mutations by Ocular Subretinal Injection of Adeno-Associated Virus Gene Vector: Short-Term Results. Hum Gene Ther.
34. den Hollander AI, Roepman R, Koenekoop RK, Cremers FP (2008) Leber congenital amaurosis: genes, proteins and disease mechanisms. Prog Retin Eye Res 27: 391-419.

35. Jacobson SG, Aleman TS, Cideciyan AV, Roman AJ, Sumaroka A, et al. (2009) Defining the residual vision in leber congenital amaurosis caused by RPE65 mutations. Invest Ophthalmol Vis Sci 50: 2368-2375.
36. Pathak A, Patnaik S, Gupta KC (2009) Recent trends in non-viral vector-mediated gene delivery. Biotechnol J 4: 1559-1572.
37. Naik R, Mukhopadhyay A, Ganguli M (2009) Gene delivery to the retina: focus on non-viral approaches. Drug Discov Today 14: 306-315.
38. Mallam JN, Hurwitz MY, Mahoney T, Chevez-Barrios P, Hurwitz RL (2004) Efficient gene transfer into retinal cells using adenoviral vectors: dependence on receptor expression. Invest Ophthalmol Vis Sci 45: 1680-1687.
39. Di Polo A, Aigner LJ, Dunn RJ, Bray GM, Aguayo AJ (1998) Prolonged delivery of brain-derived neurotrophic factor by adenovirus-infected Muller cells temporarily rescues injured retinal ganglion cells. Proc Natl Acad Sci U S A 95: 3978-3983.
40. Zou L, Yuan X, Zhou H, Lu H, Yang K (2001) Helper-dependent adenoviral vector-mediated gene transfer in aged rat brain. Hum Gene Ther 12: 181-191.
41. Greenberg KP, Geller SF, Schaffer DV, Flannery JG (2007) Targeted transgene expression in muller glia of normal and diseased retinas using lentiviral vectors. Invest Ophthalmol Vis Sci 48: 1844-1852.
42. Dinculescu A, Glushakova L, Min SH, Hauswirth WW (2005) Adeno-associated virus-vectored gene therapy for retinal disease. Hum Gene Ther 16: 649-663.
43. Buch PK, Bainbridge JW, Ali RR (2008) AAV-mediated gene therapy for retinal disorders: from mouse to man. Gene Ther 15: 849-857.
44. Surace EM, Auricchio A (2008) Versatility of AAV vectors for retinal gene transfer. Vision Res 48: 353-359.
45. Srivastava A, Lusby EW, Berns KI (1983) Nucleotide sequence and organization of the adeno-associated virus 2 genome. J Virol 45: 555-564.
46. Wu Z. AA, and Samulski R. (2006) Adeno-associated virus serotypes: vector toolkit for human gene therapy. Mol Ther 14: 316-327.
47. Ding W. ZL, Yan Z. and Engelhardt J. (2005) Intracellular trafficking of adeno-associated viral vectors. Gene Therapy 12: 873-880.
48. Bartlett K. WR, and Samulski R. (2000) Infectious entry pathway of adeno-associated virus and adeno-associated virus vectors. J Virol 74: 2777-2785.
49. Thomas C, Storm T., Huang Z., and Kay M. (2004) Rapid uncoating of vector genomes is the key to efficient liver transduction with pseudotyped adeno-associated virus vectors. J Virol 78: 3110-3122.
50. Nakazawa T, Matsubara A, Noda K, Hisatomi T, She H, et al. (2006) Characterization of cytokine responses to retinal detachment in rats. Mol Vis 12: 867-878.
51. Nakazawa T, Takeda M, Lewis GP, Cho KS, Jiao J, et al. (2007) Attenuated glial reactions and photoreceptor degeneration after retinal detachment in mice deficient in glial fibrillary acidic protein and vimentin. Invest Ophthalmol Vis Sci 48: 2760-2768.
52. Park TK, Wu Z, Kjellstrom S, Zeng Y, Bush RA, et al. (2009) Intravitreal delivery of AAV8 retinoschisin results in cell type-specific gene expression and retinal rescue in the Rs1-KO mouse. Gene Ther.

53. Aleman TS, Cideciyan AV, Sumaroka A, Windsor EA, Herrera W, et al. (2008) Retinal laminar architecture in human retinitis pigmentosa caused by Rhodopsin gene mutations. Invest Ophthalmol Vis Sci 49: 1580-1590.
54. Jacobson SG, Aleman TS, Sumaroka A, Cideciyan AV, Roman AJ, et al. (2009) Disease boundaries in the retina of patients with Usher syndrome caused by MYO7A gene mutations. Invest Ophthalmol Vis Sci 50: 1886-1894.
55. Dalkara D, Kolstad KD, Caporale N, Visel M, Klimczak RR, et al. (2009) Inner Limiting Membrane Barriers to AAV Mediated Retinal Transduction from the Vitreous. Mol Ther.
56. Jang JH, Lim KI, Schaffer DV (2007) Library selection and directed evolution approaches to engineering targeted viral vectors. Biotechnol Bioeng 98: 515-524.
57. Giver L, Gershenson A, Freskgard PO, Arnold FH (1998) Directed evolution of a thermostable esterase. Proc Natl Acad Sci U S A 95: 12809-12813.
58. Zhao H, Arnold FH (1999) Directed evolution converts subtilisin E into a functional equivalent of thermitase. Protein Eng 12: 47-53.
59. Arnold FH, Volkov AA (1999) Directed evolution of biocatalysts. Curr Opin Chem Biol 3: 54-59.
60. May O, Nguyen PT, Arnold FH (2000) Inverting enantioselectivity by directed evolution of hydantoinase for improved production of L-methionine. Nat Biotechnol 18: 317-320.
61. Maheshri N. KJ, Kaspar B., and Schaffer D. (2006) Directed evolution of adeno-associated virus yields enhanced gene delivery vectors. Nature Biotechnology 24: 198-204.
62. Excoffon KJ, Koerber JT, Dickey DD, Murtha M, Keshavjee S, et al. (2009) Directed evolution of adeno-associated virus to an infectious respiratory virus. Proc Natl Acad Sci U S A 106: 3865-3870.
63. Lebherz C, Maguire A, Tang W, Bennett J, Wilson JM (2008) Novel AAV serotypes for improved ocular gene transfer. J Gene Med 10: 375-382.
64. Mueller C, Flotte TR (2008) Clinical gene therapy using recombinant adeno-associated virus vectors. Gene Ther 15: 858-863.
65. Buning H, Perabo L, Coutelle O, Quadt-Humme S, Hallek M (2008) Recent developments in adeno-associated virus vector technology. J Gene Med 10: 717-733.
66. Goncalves MA (2005) Adeno-associated virus: from defective virus to effective vector. Virol J 2: 43.
67. Gao G, Vandenberghe LH, Alvira MR, Lu Y, Calcedo R, et al. (2004) Clades of Adeno-associated viruses are widely disseminated in human tissues. J Virol 78: 6381-6388.
68. Wu Z, Asokan A, Samulski RJ (2006) Adeno-associated virus serotypes: vector toolkit for human gene therapy. Mol Ther 14: 316-327.
69. Wu Z, Miller E, Agbandje-McKenna M, Samulski RJ (2006) Alpha2,3 and alpha2,6 N-linked sialic acids facilitate efficient binding and transduction by adeno-associated virus types 1 and 6. J Virol 80: 9093-9103.
70. Akache B, Grimm D, Pandey K, Yant SR, Xu H, et al. (2006) The 37/67-kilodalton laminin receptor is a receptor for adeno-associated virus serotypes 8, 2, 3, and 9. J Virol 80: 9831-9836.

71. Fisher SK, Lewis GP (2003) Muller cell and neuronal remodeling in retinal detachment and reattachment and their potential consequences for visual recovery: a review and reconsideration of recent data. Vision Res 43: 887-897.
72. Maguire AM, Simonelli F, Pierce EA, Pugh EN, Jr., Mingozzi F, et al. (2008) Safety and efficacy of gene transfer for Leber's congenital amaurosis. N Engl J Med 358: 2240-2248.
73. Harvey AR, Kamphuis W, Eggers R, Symons NA, Blits B, et al. (2002) Intravitreal injection of adeno-associated viral vectors results in the transduction of different types of retinal neurons in neonatal and adult rats: a comparison with lentiviral vectors. Mol Cell Neurosci 21: 141-157.
74. Candiello J, Balasubramani M, Schreiber EM, Cole GJ, Mayer U, et al. (2007) Biomechanical properties of native basement membranes. Febs J 274: 2897-2908.
75. Halfter W, Dong S, Dong A, Eller AW, Nischt R (2008) Origin and turnover of ECM proteins from the inner limiting membrane and vitreous body. Eye 22: 1207-1213.
76. Halfter W, Schurer B (1998) Disruption of the pial basal lamina during early avian embryonic development inhibits histogenesis and axonal pathfinding in the optic tectum. J Comp Neurol 397: 105-117.
77. Semina EV, Bosenko DV, Zinkevich NC, Soules KA, Hyde DR, et al. (2006) Mutations in laminin alpha 1 result in complex, lens-independent ocular phenotypes in zebrafish. Dev Biol 299: 63-77.
78. Mester V, Kuhn F (2000) Internal limiting membrane removal in the management of full-thickness macular holes. Am J Ophthalmol 129: 769-777.
79. Heegaard S, Jensen OA, Prause JU (1986) Structure and composition of the inner limiting membrane of the retina. SEM on frozen resin-cracked and enzyme-digested retinas of Macaca mulatta. Graefes Arch Clin Exp Ophthalmol 224: 355-360.
80. Grieger JC, Choi VW, Samulski RJ (2006) Production and characterization of adeno-associated viral vectors. Nat Protoc 1: 1412-1428.
81. Bartlett JS, Wilcher R, Samulski RJ (2000) Infectious entry pathway of adeno-associated virus and adeno-associated virus vectors. J Virol 74: 2777-2785.
82. Jurasek J, Johnson P, Olafson RW, Smillie LB (1971) An improved fractionation system for pronase on CM-sephadex. Can J Biochem 49: 1195-1201.
83. Van Vliet K, Blouin V, Agbandje-McKenna M, Snyder RO (2006) Proteolytic mapping of the adeno-associated virus capsid. Mol Ther 14: 809-821.
84. McCarty DM (2008) Self-complementary AAV vectors; advances and applications. Mol Ther 16: 1648-1656.
85. Schultz BR, Chamberlain JS (2008) Recombinant adeno-associated virus transduction and integration. Mol Ther 16: 1189-1199.
86. Allocca M, Mussolino C, Garcia-Hoyos M, Sanges D, Iodice C, et al. (2007) Novel adeno-associated virus serotypes efficiently transduce murine photoreceptors. J Virol 81: 11372-11380.
87. Auricchio A, Kobinger G, Anand V, Hildinger M, O'Connor E, et al. (2001) Exchange of surface proteins impacts on viral vector cellular specificity and transduction characteristics: the retina as a model. Hum Mol Genet 10: 3075-3081.

88. Weber M, Rabinowitz J, Provost N, Conrath H, Folliot S, et al. (2003) Recombinant adeno-associated virus serotype 4 mediates unique and exclusive long-term transduction of retinal pigmented epithelium in rat, dog, and nonhuman primate after subretinal delivery. Mol Ther 7: 774-781.
89. Pickard GE, Smeraski CA, Tomlinson CC, Banfield BW, Kaufman J, et al. (2002) Intravitreal injection of the attenuated pseudorabies virus PRV Bartha results in infection of the hamster suprachiasmatic nucleus only by retrograde transsynaptic transport via autonomic circuits. J Neurosci 22: 2701-2710.
90. Chai L, Morris JE (1999) Heparan sulfate in the inner limiting membrane of embryonic chicken retina binds basic fibroblast growth factor to promote axonal outgrowth. Exp Neurol 160: 175-185.
91. Chai L, Morris JE (1994) Distribution of heparan sulfate proteoglycans in embryonic chicken neural retina and isolated inner limiting membrane. Curr Eye Res 13: 669-677.
92. Zhong L, Li B, Mah CS, Govindasamy L, Agbandje-McKenna M, et al. (2008) Next generation of adeno-associated virus 2 vectors: point mutations in tyrosines lead to high-efficiency transduction at lower doses. Proc Natl Acad Sci U S A 105: 7827-7832.
93. Petrs-Silva H, Dinculescu A, Li Q, Min SH, Chiodo V, et al. (2009) High-efficiency transduction of the mouse retina by tyrosine-mutant AAV serotype vectors. Mol Ther 17: 463-471.
94. Kaludov N, Brown KE, Walters RW, Zabner J, Chiorini JA (2001) Adeno-associated virus serotype 4 (AAV4) and AAV5 both require sialic acid binding for hemagglutination and efficient transduction but differ in sialic acid linkage specificity. J Virol 75: 6884-6893.
95. Cho EY, Choi HL, Chan FL (2002) Expression pattern of glycoconjugates in rat retina as analysed by lectin histochemistry. Histochem J 34: 589-600.
96. Allocca M, Doria M, Petrillo M, Colella P, Garcia-Hoyos M, et al. (2008) Serotype-dependent packaging of large genes in adeno-associated viral vectors results in effective gene delivery in mice. J Clin Invest 118: 1955-1964.
97. Volterra A, Meldolesi J (2005) Astrocytes, from brain glue to communication elements: the revolution continues. Nat Rev Neurosci 6: 626-640.
98. Nedergaard M, Ransom B, Goldman SA (2003) New roles for astrocytes: redefining the functional architecture of the brain. Trends Neurosci 26: 523-530.
99. Sherwood CC, Stimpson CD, Raghanti MA, Wildman DE, Uddin M, et al. (2006) Evolution of increased glia-neuron ratios in the human frontal cortex. Proc Natl Acad Sci U S A 103: 13606-13611.
100. Nagele RG, Wegiel J, Venkataraman V, Imaki H, Wang KC (2004) Contribution of glial cells to the development of amyloid plaques in Alzheimer's disease. Neurobiol Aging 25: 663-674.
101. Nagai M, Re DB, Nagata T, Chalazonitis A, Jessell TM, et al. (2007) Astrocytes expressing ALS-linked mutated SOD1 release factors selectively toxic to motor neurons. Nat Neurosci 10: 615-622.
102. de Leeuw B, Su M, ter Horst M, Iwata S, Rodijk M, et al. (2006) Increased glia-specific transgene expression with glial fibrillary acidic protein promoters containing multiple enhancer elements. J Neurosci Res 83: 744-753.

103. Davidson BL, Stein CS, Heth JA, Martins I, Kotin RM, et al. (2000) Recombinant adeno-associated virus type 2, 4, and 5 vectors: transduction of variant cell types and regions in the mammalian central nervous system. Proc Natl Acad Sci U S A 97: 3428-3432.
104. Liu G, Martins IH, Chiorini JA, Davidson BL (2005) Adeno-associated virus type 4 (AAV4) targets ependyma and astrocytes in the subventricular zone and RMS. Gene Ther 12: 1503-1508.
105. Fitzsimons HL, Bland RJ, During MJ (2002) Promoters and regulatory elements that improve adeno-associated virus transgene expression in the brain. Methods 28: 227-236.
106. Wang Z, Wen XH, Ablonczy Z, Crouch RK, Makino CL, et al. (2005) Enhanced shutoff of phototransduction in transgenic mice expressing palmitoylation-deficient rhodopsin. J Biol Chem 280: 24293-24300.
107. Bainbridge JW, Smith AJ, Barker SS, Robbie S, Henderson R, et al. (2008) Effect of gene therapy on visual function in Leber's congenital amaurosis. N Engl J Med 358: 2231-2239.
108. Wang Z, Zhu T, Qiao C, Zhou L, Wang B, et al. (2005) Adeno-associated virus serotype 8 efficiently delivers genes to muscle and heart. Nat Biotechnol 23: 321-328.
109. Kaplitt MG, Leone P, Samulski RJ, Xiao X, Pfaff DW, et al. (1994) Long-term gene expression and phenotypic correction using adeno-associated virus vectors in the mammalian brain. Nat Genet 8: 148-154.
110. Harding TC, Dickinson PJ, Roberts BN, Yendluri S, Gonzalez-Edick M, et al. (2006) Enhanced gene transfer efficiency in the murine striatum and an orthotopic glioblastoma tumor model, using AAV-7- and AAV-8-pseudotyped vectors. Hum Gene Ther 17: 807-820.
111. Klein RL, Dayton RD, Tatom JB, Henderson KM, Henning PP (2008) AAV8, 9, Rh10, Rh43 vector gene transfer in the rat brain: effects of serotype, promoter and purification method. Mol Ther 16: 89-96.
112. Bartlett JS, Samulski RJ, McCown TJ (1998) Selective and rapid uptake of adeno-associated virus type 2 in brain. Hum Gene Ther 9: 1181-1186.
113. Taymans JM, Vandenberghe LH, Haute CV, Thiry I, Deroose CM, et al. (2007) Comparative analysis of adeno-associated viral vector serotypes 1, 2, 5, 7, and 8 in mouse brain. Hum Gene Ther 18: 195-206.
114. Peel AL, Klein RL (2000) Adeno-associated virus vectors: activity and applications in the CNS. J Neurosci Methods 98: 95-104.
115. Foust KD, Nurre E, Montgomery CL, Hernandez A, Chan CM, et al. (2009) Intravascular AAV9 preferentially targets neonatal neurons and adult astrocytes. Nat Biotechnol 27: 59-65.
116. Girod A, Ried M, Wobus C, Lahm H, Leike K, et al. (1999) Genetic capsid modifications allow efficient re-targeting of adeno-associated virus type 2. Nat Med 5: 1438.
117. Shi W, Arnold GS, Bartlett JS (2001) Insertional mutagenesis of the adeno-associated virus type 2 (AAV2) capsid gene and generation of AAV2 vectors targeted to alternative cell-surface receptors. Hum Gene Ther 12: 1697-1711.

118. Perabo L, Buning H, Kofler DM, Ried MU, Girod A, et al. (2003) In vitro selection of viral vectors with modified tropism: the adeno-associated virus display. Mol Ther 8: 151-157.
119. Muller OJ, Kaul F, Weitzman MD, Pasqualini R, Arap W, et al. (2003) Random peptide libraries displayed on adeno-associated virus to select for targeted gene therapy vectors. Nat Biotechnol 21: 1040-1046.
120. Maheshri N, Koerber JT, Kaspar BK, Schaffer DV (2006) Directed evolution of adeno-associated virus yields enhanced gene delivery vectors. Nat Biotechnol 24: 198-204.
121. Koerber JT, Jang JH, Schaffer DV (2008) DNA shuffling of adeno-associated virus yields functionally diverse viral progeny. Mol Ther 16: 1703-1709.
122. Li W, Asokan A, Wu Z, Van Dyke T, DiPrimio N, et al. (2008) Engineering and selection of shuffled AAV genomes: a new strategy for producing targeted biological nanoparticles. Mol Ther 16: 1252-1260.
123. Grimm D, Lee JS, Wang L, Desai T, Akache B, et al. (2008) In vitro and in vivo gene therapy vector evolution via multispecies interbreeding and retargeting of adeno-associated viruses. J Virol 82: 5887-5911.
124. Lai K, Kaspar BK, Gage FH, Schaffer DV (2003) Sonic hedgehog regulates adult neural progenitor proliferation in vitro and in vivo. Nat Neurosci 6: 21-27.
125. Zincarelli C, Soltys S, Rengo G, Rabinowitz JE (2008) Analysis of AAV serotypes 1-9 mediated gene expression and tropism in mice after systemic injection. Mol Ther 16: 1073-1080.
126. Duan D, Yue Y, Yan Z, Yang J, Engelhardt JF (2000) Endosomal processing limits gene transfer to polarized airway epithelia by adeno-associated virus. J Clin Invest 105: 1573-1587.
127. Lochrie MA, Tatsuno GP, Christie B, McDonnell JW, Zhou S, et al. (2006) Mutations on the external surfaces of adeno-associated virus type 2 capsids that affect transduction and neutralization. J Virol 80: 821-834.
128. Xie Q, Bu W, Bhatia S, Hare J, Somasundaram T, et al. (2002) The atomic structure of adeno-associated virus (AAV-2), a vector for human gene therapy. Proc Natl Acad Sci U S A 99: 10405-10410.
129. Shen X, Storm T, Kay MA (2007) Characterization of the relationship of AAV capsid domain swapping to liver transduction efficiency. Mol Ther 15: 1955-1962.
130. Nam HJ, Lane MD, Padron E, Gurda B, McKenna R, et al. (2007) Structure of adeno-associated virus serotype 8, a gene therapy vector. J Virol 81: 12260-12271.
131. Govindasamy L, Padron E, McKenna R, Muzyczka N, Kaludov N, et al. (2006) Structurally mapping the diverse phenotype of adeno-associated virus serotype 4. J Virol 80: 11556-11570.
132. Girod A, Wobus CE, Zadori Z, Ried M, Leike K, et al. (2002) The VP1 capsid protein of adeno-associated virus type 2 is carrying a phospholipase A2 domain required for virus infectivity. J Gen Virol 83: 973-978.
133. Abbott N (2006) The bipolar astrocyte: polzarized features of astrocytic glia underlying physiology, with particular reference to the blood-brain barrier. In:

Dermietzel E, editor. Blood-Brain Barriers: From Ontogeny to Artificial Interfaces. Weinheim: Wiley-VCH. pp. 189-208.
134. Cinaroglu A, Ozmen Y, Ozdemir A, Ozcan F, Ergorul C, et al. (2005) Expression and possible function of fibroblast growth factor 9 (FGF9) and its cognate receptors FGFR2 and FGFR3 in postnatal and adult retina. J Neurosci Res 79: 329-339.
135. Cahoy JD, Emery B, Kaushal A, Foo LC, Zamanian JL, et al. (2008) A transcriptome database for astrocytes, neurons, and oligodendrocytes: a new resource for understanding brain development and function. J Neurosci 28: 264-278.
136. Ding W, Zhang L, Yan Z, Engelhardt JF (2005) Intracellular trafficking of adeno-associated viral vectors. Gene Ther 12: 873-880.
137. Thomas CE, Storm TA, Huang Z, Kay MA (2004) Rapid uncoating of vector genomes is the key to efficient liver transduction with pseudotyped adeno-associated virus vectors. J Virol 78: 3110-3122.
138. Flannery JG, Zolotukhin S, Vaquero MI, LaVail MM, Muzyczka N, et al. (1997) Efficient photoreceptor-targeted gene expression in vivo by recombinant adeno-associated virus. Proc Natl Acad Sci U S A 94: 6916-6921.
139. Halbert CL, Rutledge EA, Allen JM, Russell DW, Miller AD (2000) Repeat transduction in the mouse lung by using adeno-associated virus vectors with different serotypes. J Virol 74: 1524-1532.
140. Xiao X, Li J, Samulski J (1996) Efficient long-term gene transfer into muscle tissue of immunocompetent mice by adeno-associated virus vector. J Virol 70: 8098-8108.
141. Koerber JT, Klimczak RR, Jang JH, Dalkara D, Flannery J, et al. (2009) Molecular evolution of adeno-associated virus for enhanced glial gene delivery. Mol Ther under review.
142. Park TK, Wu Z, Kjellstrom S, Zeng Y, Bush RA, et al. (2009) Intravitreal delivery of AAV8 retinoschisin results in cell type-specific gene expression and retinal rescue in the Rs1-KO mouse. Gene Ther 16: 916-926.
143. Ciulla TA, Rosenfeld PJ (2009) Antivascular endothelial growth factor therapy for neovascular age-related macular degeneration. Curr Opin Ophthalmol 20: 158-165.
144. Merigan WH, Scoles D, Hunter JJ, Masella B, Greenberg KP. Tracking transfection of macaque retinal ganglion cells with AAV2 viral vectors: In vivo imaging reveals differences between two promoters; 2008.
145. Balazs EA, Denlinger JL (1982) Aging changes in the vitreous. In: Liss AR, editor. Aging and human visual function. New York. pp. 45-57.
146. Hellstrom M, Ruitenberg MJ, Pollett MA, Ehlert EM, Twisk J, et al. (2009) Cellular tropism and transduction properties of seven adeno-associated viral vector serotypes in adult retina after intravitreal injection. Gene Ther 16: 521-532.
147. Bringmann A, Pannicke T, Grosche J, Francke M, Wiedemann P, et al. (2006) Muller cells in the healthy and diseased retina. Prog Retin Eye Res 25: 397-424.
148. Lupien CB, Salesse C (2007) Identification of genes specifically expressed by human Muller cells by use of subtractive hybridization. Mol Vis 13: 1828-1841.

149. Salmina A (2009) Neuron-glia interactions as therapeutic targets in neurodegeneration. J Alzheimers Dis 3: 485-502.
150. Dorrell MI, Aguilar E, Jacobson R, Yanes O, Gariano R, et al. (2009) Antioxidant or neurotrophic factor treatment preserves function in a mouse model of neovascularization-associated oxidative stress. J Clin Invest.
151. Li Q, Miller R, Han PY, Pang J, Dinculescu A, et al. (2008) Intraocular route of AAV2 vector administration defines humoral immune response and therapeutic potential. Mol Vis 14: 1760-1769.
152. Bame KJ, Lidholt K, Lindahl U, Esko JD (1991) Biosynthesis of heparan sulfate. Coordination of polymer-modification reactions in a Chinese hamster ovary cell mutant defective in N-sulfotransferase. J Biol Chem 266: 10287-10293.
153. Wu Z, Asokan A, Grieger JC, Govindasamy L, Agbandje-McKenna M, et al. (2006) Single amino acid changes can influence titer, heparin binding, and tissue tropism in different adeno-associated virus serotypes. J Virol 80: 11393-11397.
154. Hauck SM, Suppmann S, Ueffing M (2003) Proteomic profiling of primary retinal Muller glia cells reveals a shift in expression patterns upon adaptation to in vitro conditions. Glia 44: 251-263.
155. Bachoo RM, Kim RS, Ligon KL, Maher EA, Brennan C, et al. (2004) Molecular diversity of astrocytes with implications for neurological disorders. Proc Natl Acad Sci U S A 101: 8384-8389.
156. Sakurai E, Ozeki H, Kunou N, Ogura Y (2001) Effect of particle size of polymeric nanospheres on intravitreal kinetics. Ophthalmic Res 33: 31-36.
157. Chiorini JA, Weller M, Amornphimoltham P, Schmidt M, Gutkind JS. Epidermal growth factor receptor is a receptor for adeno-associated virus serotype 6; 2009. Mol Ther.
158. Limb GA, Salt TE, Munro PM, Moss SE, Khaw PT (2002) In vitro characterization of a spontaneously immortalized human Muller cell line (MIO-M1). Invest Ophthalmol Vis Sci 43: 864-869.
159. Wolf G (2004) The visual cycle of the cone photoreceptors of the retina. Nutr Rev 62: 283-286.
160. Goodyear MJ, Crewther SG, Junghans BM (2009) A role for aquaporin-4 in fluid regulation in the inner retina. Vis Neurosci 26: 159-165.
161. Lagali PS, Balya D, Awatramani GB, Munch TA, Kim DS, et al. (2008) Light-activated channels targeted to ON bipolar cells restore visual function in retinal degeneration. Nat Neurosci 11: 667-675.
162. Daiger SP, Bowne SJ, Sullivan LS (2007) Perspective on genes and mutations causing retinitis pigmentosa. Arch Ophthalmol 125: 151-158.
163. Hims MM, Diager SP, Inglehearn CF (2003) Retinitis pigmentosa: genes, proteins and prospects. Dev Ophthalmol 37: 109-125.
164. Ryoo HD, Domingos PM, Kang MJ, Steller H (2007) Unfolded protein response in a Drosophila model for retinal degeneration. EMBO J 26: 242-252.
165. Shinohara T, Mulhern ML, Madson CJ (2008) Silencing gene therapy for mutant membrane, secretory, and lipid proteins in retinitis pigmentosa (RP). Med Hypotheses 70: 378-380.
166. Kim I, Xu W, Reed JC (2008) Cell death and endoplasmic reticulum stress: disease relevance and therapeutic opportunities. Nat Rev Drug Discov 7: 1013-1030.

167. Wang XZ, Lawson B, Brewer JW, Zinszner H, Sanjay A, et al. (1996) Signals from the stressed endoplasmic reticulum induce C/EBP-homologous protein (CHOP/GADD153). Mol Cell Biol 16: 4273-4280.
168. Wang XZ, Ron D (1996) Stress-induced phosphorylation and activation of the transcription factor CHOP (GADD153) by p38 MAP Kinase. Science 272: 1347-1349.
169. Welihinda AA, Kaufman RJ (1996) The unfolded protein response pathway in Saccharomyces cerevisiae. Oligomerization and trans-phosphorylation of Ire1p (Ern1p) are required for kinase activation. J Biol Chem 271: 18181-18187.
170. Faktorovich EG, Steinberg RH, Yasumura D, Matthes MT, LaVail MM (1990) Photoreceptor degeneration in inherited retinal dystrophy delayed by basic fibroblast growth factor. Nature 347: 83-86.
171. Faktorovich EG, Steinberg RH, Yasumura D, Matthes MT, LaVail MM (1992) Basic fibroblast growth factor and local injury protect photoreceptors from light damage in the rat. J Neurosci 12: 3554-3567.
172. Frasson M, Picaud S, Leveillard T, Simonutti M, Mohand-Said S, et al. (1999) Glial cell line-derived neurotrophic factor induces histologic and functional protection of rod photoreceptors in the rd/rd mouse. Invest Ophthalmol Vis Sci 40: 2724-2734.
173. McGee Sanftner LH, Abel H, Hauswirth WW, Flannery JG (2001) Glial cell line derived neurotrophic factor delays photoreceptor degeneration in a transgenic rat model of retinitis pigmentosa. Mol Ther 4: 622-629.
174. Bringmann A, Reichenbach A (2001) Role of Muller cells in retinal degenerations. Front Biosci 6: E72-92.
175. Harada T, Harada C, Nakayama N, Okuyama S, Yoshida K, et al. (2000) Modification of glial-neuronal cell interactions prevents photoreceptor apoptosis during light-induced retinal degeneration. Neuron 26: 533-541.
176. Klimczak RR, Koerber JT, Dalkara D, Flannery J, Schaffer DV (2009) A novel evolved adeno-associated viral variant for efficient, targeted intravitreal transduction of Muller cells. PLoS One Under Review.
177. Yokoi K, Kachi S, Zhang HS, Gregory PD, Spratt SK, et al. (2007) Ocular gene transfer with self-complementary AAV vectors. Invest Ophthalmol Vis Sci 48: 3324-3328.
178. Kuno N, Fujii S (2010) Biodegradable intraocular therapies for retinal disorders: progress to date. Drugs Aging 27: 117-134.
179. Hauck SM, Kinkl N, Deeg CA, Swiatek-de Lange M, Schoffmann S, et al. (2006) GDNF family ligands trigger indirect neuroprotective signaling in retinal glial cells. Mol Cell Biol 26: 2746-2757.
180. Airaksinen MS, Saarma M (2002) The GDNF family: signalling, biological functions and therapeutic value. Nat Rev Neurosci 3: 383-394.
181. Bourque MJ, Trudeau LE (2000) GDNF enhances the synaptic efficacy of dopaminergic neurons in culture. Eur J Neurosci 12: 3172-3180.
182. Pothos EN, Davila V, Sulzer D (1998) Presynaptic recording of quanta from midbrain dopamine neurons and modulation of the quantal size. J Neurosci 18: 4106-4118.

183. Rolling F (2004) Recombinant AAV-mediated gene transfer to the retina: gene therapy perspectives. Gene Ther 11 Suppl 1: S26-32.
184. Reme CE, Grimm C, Hafezi F, Wenzel A, Williams TP (2000) Apoptosis in the Retina: The Silent Death of Vision. News Physiol Sci 15: 120-124.
185. Gruter O, Kostic C, Crippa SV, Perez MT, Zografos L, et al. (2005) Lentiviral vector-mediated gene transfer in adult mouse photoreceptors is impaired by the presence of a physical barrier. Gene Ther 12: 942-947.
186. Mancuso K, Hauswirth WW, Li Q, Connor TB, Kuchenbecker JA, et al. (2009) Gene therapy for red-green colour blindness in adult primates. Nature 461: 784-787.
187. Wensel TG, Gross AK, Chan F, Sykoudis K, Wilson JH (2005) Rhodopsin-EGFP knock-ins for imaging quantal gene alterations. Vision Res 45: 3445-3453.
188. Gray SJ, Blake BL, Criswell HE, Nicolson SC, Samulski RJ, et al. (2010) Directed evolution of a novel adeno-associated virus (AAV) vector that crosses the seizure-compromised blood-brain barrier (BBB). Mol Ther 18: 570-578.
189. Asokan A, Conway JC, Phillips JL, Li C, Hegge J, et al. (2010) Reengineering a receptor footprint of adeno-associated virus enables selective and systemic gene transfer to muscle. Nat Biotechnol 28: 79-82.

SUPPLEMENTARY MATERIAL

Supplemental data for Chapter 3a

Figure 3a.S1. Primary amino acid sequence alignment of AAV variants from chimeric AAV and AAV EP libraries along with parent serotypes. Distinct colors were used to shade each amino acid.

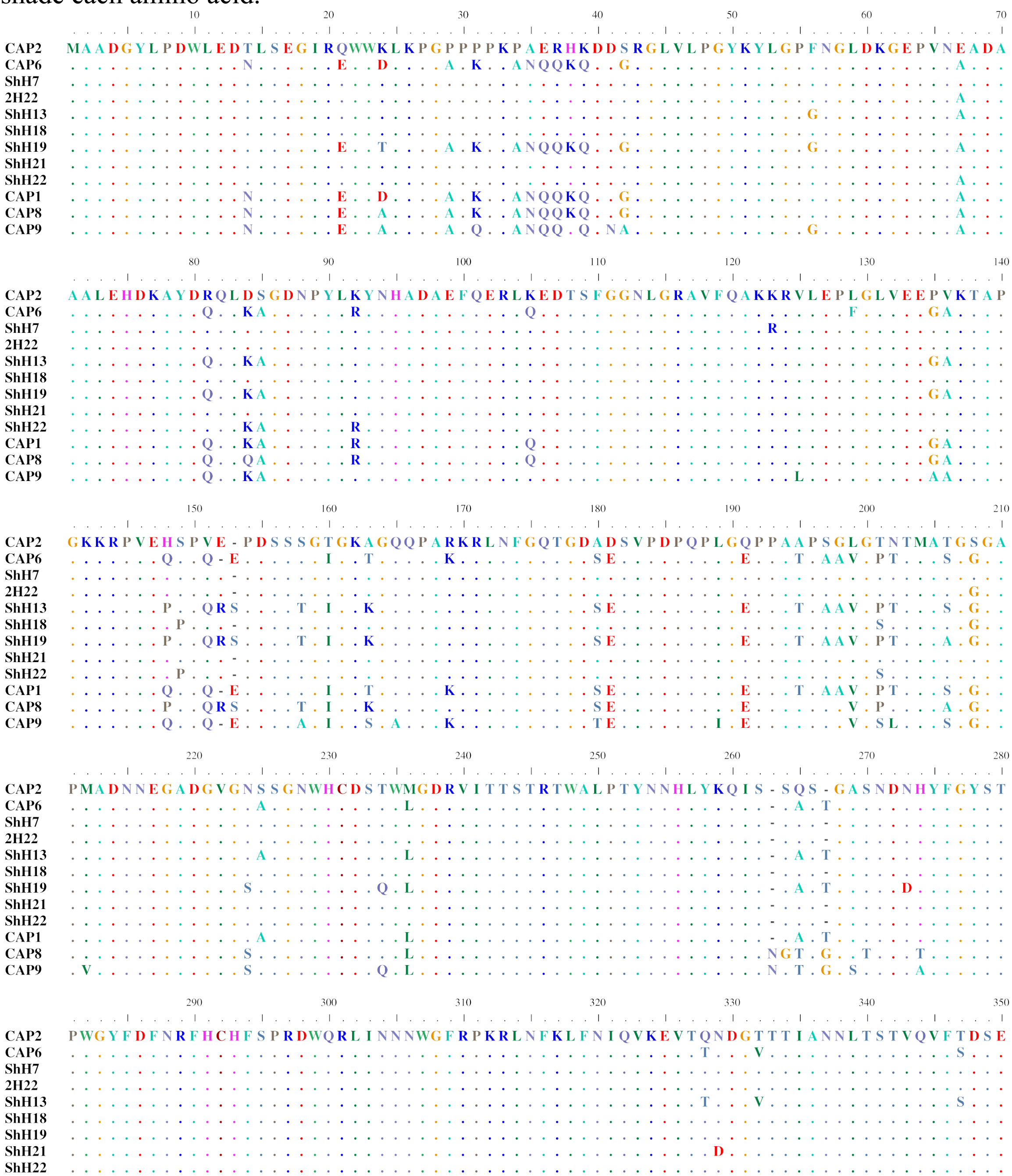

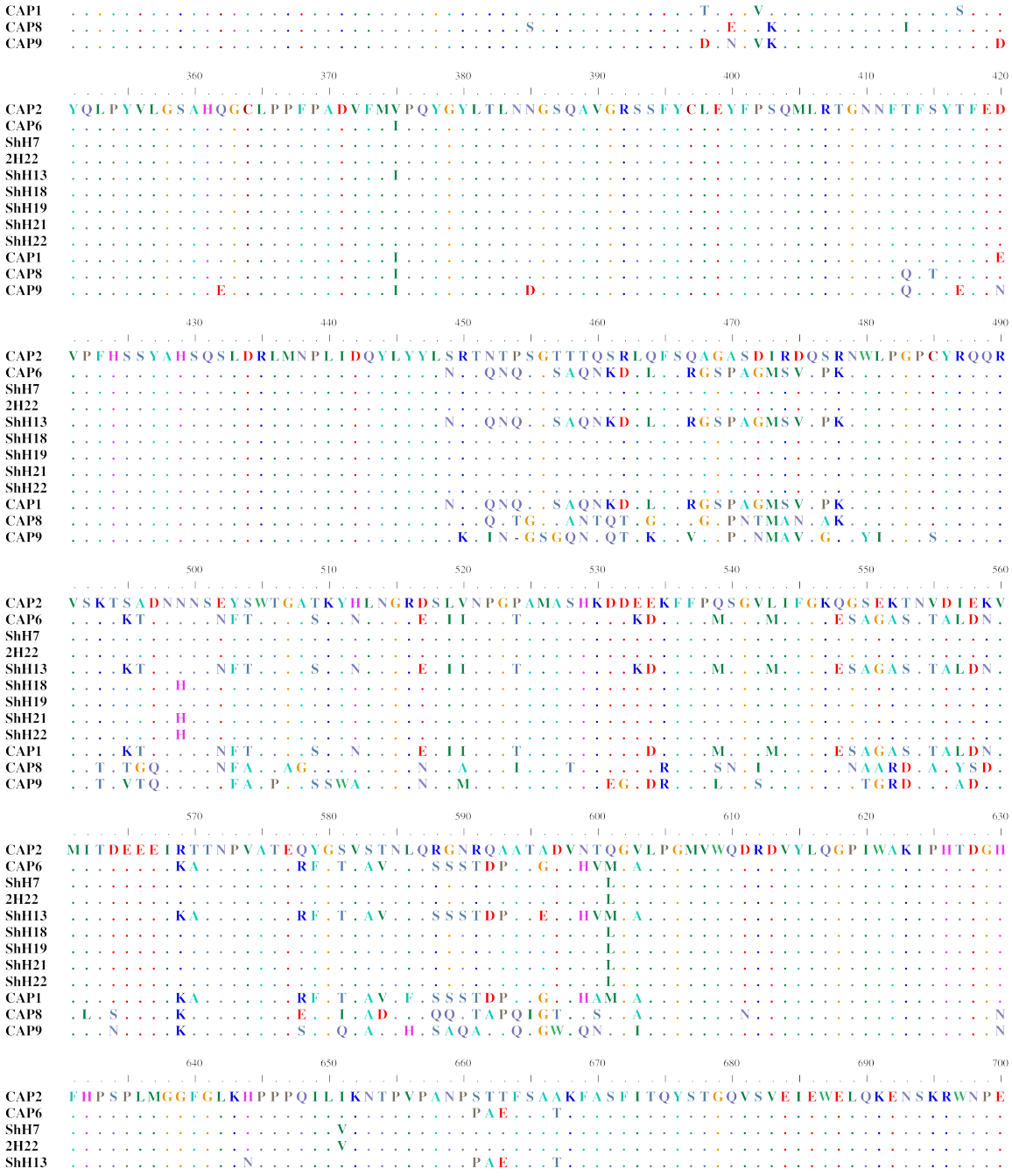
CAP1
CAP8
CAP9
360 370 380 390 400 410 420
CAP2 YQLPYVLGSAHQGCLPPFPADVFMVPQYGYLTLNNGSQAVGRSSFYCLEYFPSQMLRTGNNFTFSYTFED
CAP6
ShH7
2H22
ShH13
ShH18
ShH19
ShH21
ShH22
CAP1
CAP8
CAP9
430 440 450 460 470 480 490
CAP2 VPFHSSYAHSQSLDRLMNPLIDQYLYYLSRTNTPSGTTTQSRLQFSQAGASDIRDQSRNWLPGPCYRQQR
CAP6
ShH7
2H22
ShH13
ShH18
ShH19
ShH21
ShH22
CAP1
CAP8
CAP9
500 510 520 530 540 550 560
CAP2 VSKTSADNNNSEYSWTGATKYHLNGRDSLVNPGPAMASHKDDEEKFFPQSGVLIFGKQGSEKTNVDIEKV
CAP6
ShH7
2H22
ShH13
ShH18
ShH19
ShH21
ShH22
CAP1
CAP8
CAP9
570 580 590 600 610 620 630
CAP2 MITDEEEIRTTNPVATEQYGSVSTNLQRGNRQAATADVNTQGVLPGMVWQDRDVYLQGPIWAKIPHTDGH
CAP6
ShH7
2H22
ShH13
ShH18
ShH19
ShH21
ShH22
CAP1
CAP8
CAP9
640 650 660 670 680 690 700
CAP2 FHPSPLMGGFGLKHPPPQILIKNTPVPANPSTTFSAAKFASFITQYSTGQVSVEIEWELQKENSKRWNPE
CAP6
ShH7
2H22
ShH13

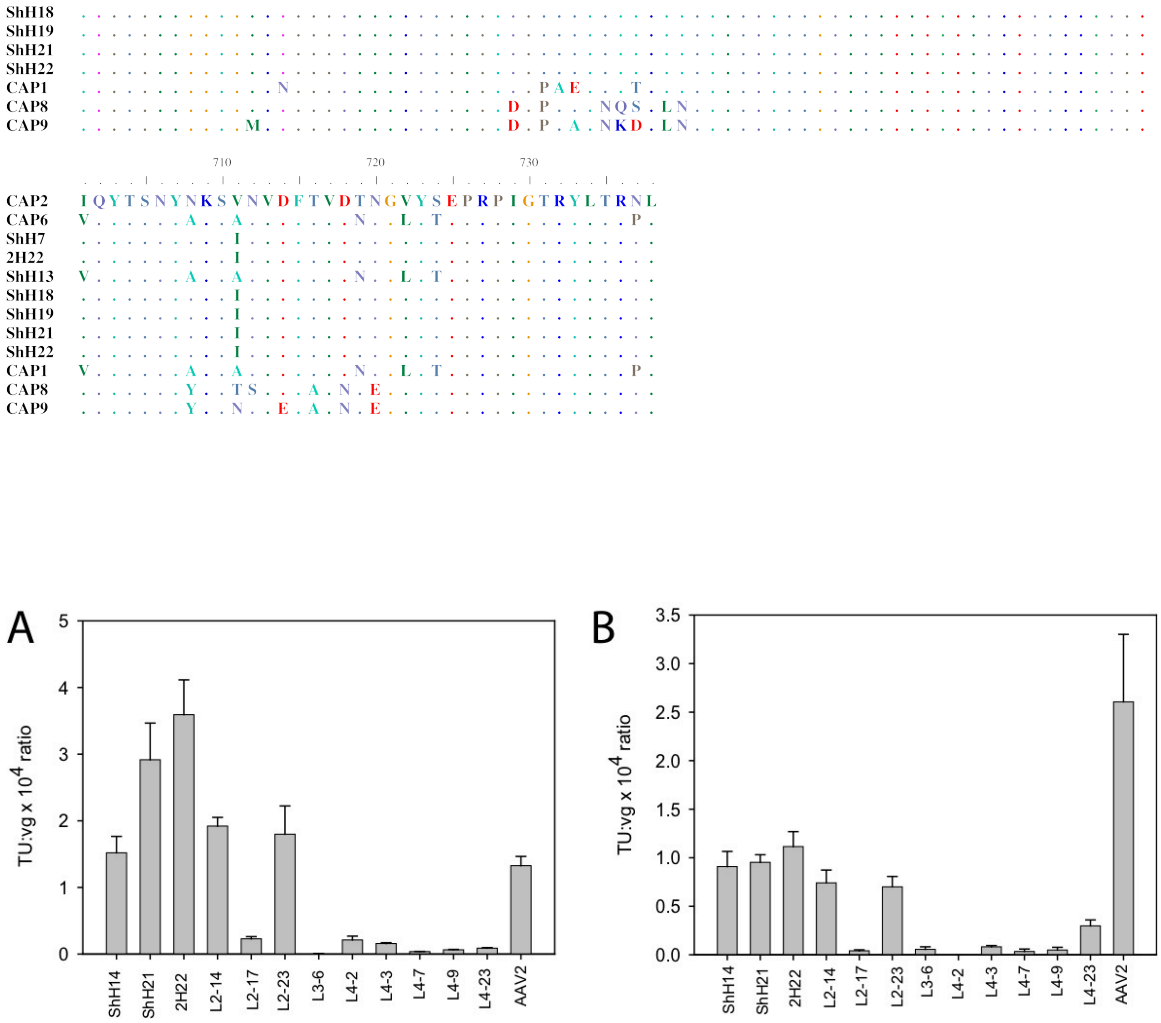

Figure 3a.S2. Transduction efficiencies of other AAV variants on primary human astrocytes (n = 3, error bars represent SD).

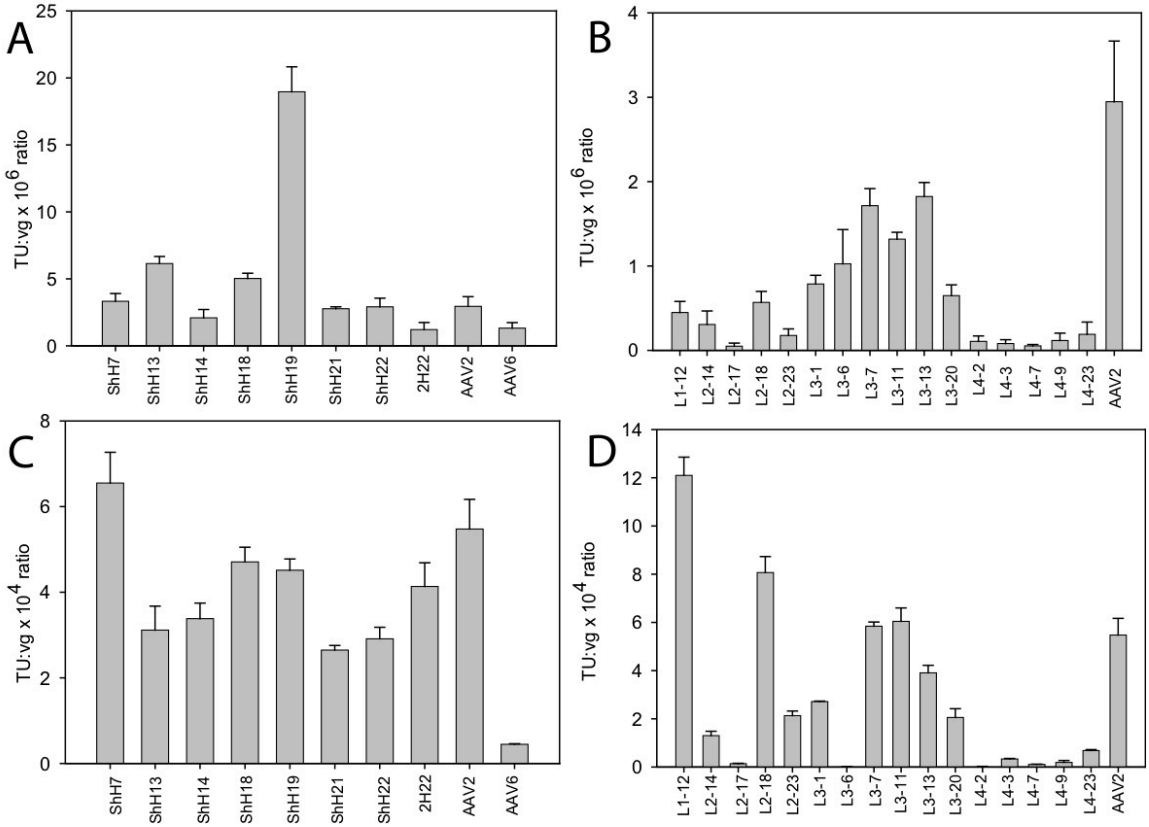

Figure 3a.S3. Transduction efficiencies of AAV variants on other glial cell lines. Tranduction of rat astrocytes with rAAV CMV-GFP clones from the both the chimeric (A) and random loop libraries (B) revealed significantly different trends compared to transduction of primary human astrocytes (n = 3, error bars represent SD). Tranduction of U87MG glioblastoma cells with rAAV CMV-GFP clones from the both the chimeric (C) and random loop libraries (D) revealed significantly different trends compared to transduction of primary human astrocytes (n = 3 and error bars represent SD).

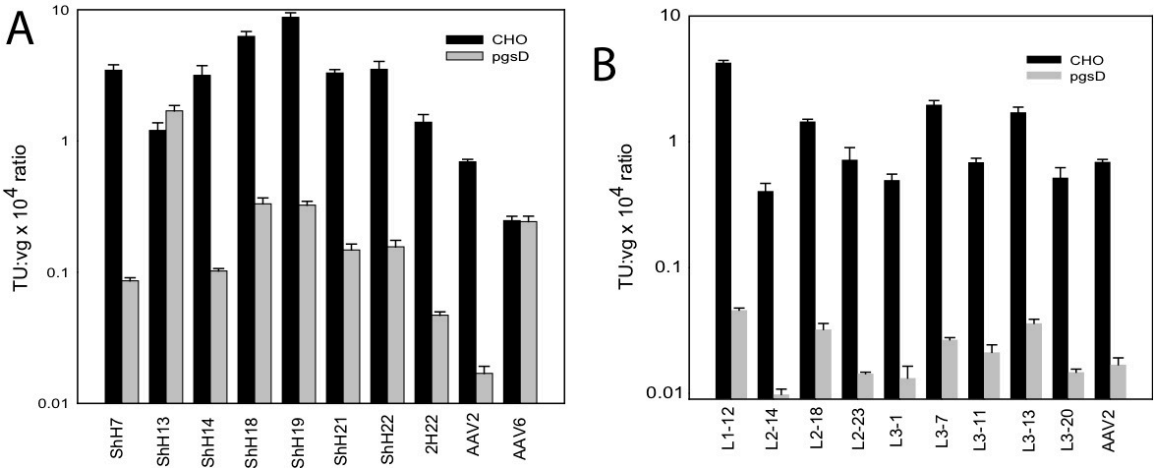

Figure 3a.S4. Heparan sulfate dependence of AAV variants. Transduction of parent CHO cell line and a CHO mutant deficient in heparan sulfate proteoglycan (HSPG) (psgD) demonstrated HSPG dependence of all AAV2-like variants from the chimeric (A) and random loop libraries (B) (n = 3, error bars represent SD).

Name	Sequence
CAP For	5'-CATGGGAAAGGTGCCAGACG-3'
CAP Rev	5'-CGCAGAGACCAAAGTTCAACTGA-3'
7mer For	5'-GGAGGGCTAGCA(NNK)$_7$GCTAGCAAAAGCGGGGGGAGAGTGAGG-3'
7mer Rev	5'-CCTCACTCTCCCCCCGCT-3'
Loop1 Rev	5'- AATTTGTTTGTAGAGGTGGTTGTTGTAGGTGGG-3'
Loop1 For	5'- AACAACCACCTCTACAAACAAATTTCCNNKNNKNNKNNKNNKNNKNN KNNKGACAATCACTACTTTGGCTACAGCACCC-3'
Loop2 Rev	5'- CAAGTAATACAGGTACTGGTCGATGAGAGG-3'
Loop2 For	5'- CGACCAGTACCTGTATTACTTGNNKNNKACTNNKNNKNNKRGCGGTNN KNNKNNKNNKNNKNNKCTTCWATTCTCTNNKNNKGGASCTNNKNNKA TRMGCNNKCAGTCTAGGAACTGGCTTCCTGGACCC-3'
Loop3 Rev	5'- CTTCCCAAAGATGAGAACCCCGCTCTGAGG-3'
Loop3 For	5'- GGGGTTCTCATCTTTGGGAAGNNKNNKDCTNNKNNKNNKRACNNKNN KMTTNNKNNKGTCATGATTACAGACGAAGAGG-3'
Loop4 Rev	5'- CTGGAGGTTGGTAGATACAGAACCATACTGCTCCG-3'
Loop4 For	5'- GGTTCTGTATCTACCAACCTCCAGNNKNNKNNKNNKNNKSCTNNKNNK NNKNNKGTGAACNNKCAAGGCGTTCTTCCAGGCATGG-3'

Table 3a.S1. Oligonucleotide sequences for construction of viral libraries.

Supplemental data for Chapter 3b

Figure 3b.S1 Sequence analysis of novel AAV variants. Sequence comparison between ShH10 and ShH13 along with parent AAV serotypes 2 and 6.